U. S. ARMY
TRANSPORTATION RESEARCH COMMAND
FORT EUSTIS, VIRGINIA

TRECOM TECHNICAL REPORT 64-23

AN EXPERIMENTAL INVESTIGATION INTO THE SHAPE OF THRUST-AUGMENTING SURFACES IN CONJUNCTION WITH COANDA-DEFLECTED JET SHEETS

(PART I)

Task 1D121401A14224
Grant DA TC-44-177-G1

December 1964

prepared by:

UNIVERSITY OF TORONTO
Institute for Aerospace Studies
Toronto 5, Ontario, Canada

DISCLAIMER NOTICE

When Government drawings, specifications, or other data are used for any purpose other than in connection with a definitely related Government procurement operation, the United States Government thereby incurs no responsibility nor any obligation whatsoever; and the fact that the Government may have formulated, furnished, or in any way supplied the said drawings, specifications, or other data is not to be regarded by implication or otherwise as in any manner licensing the holder or any other person or corporation, or conveying any rights or permission, to manufacture, use, or sell any patented invention that may in any way be related thereto.

* * *

DDC AVAILABILITY NOTICE

Qualified requesters may obtain copies of this report from

Defense Documentation Center
Cameron Station
Alexandria, Virginia 22314

* * *

This report has been released to the Office of Technical Services, U. S. Department of Commerce, Washington 25, D. C., for sale to the general public.

* * *

The findings and recommendations contained in this report are those of the contractor and do not necessarily reflect the views of the U. S. Army Mobility Command, the U. S. Army Materiel Command, or the Department of the Army.

HEADQUARTERS
U S ARMY TRANSPORTATION RESEARCH COMMAND
FORT EUSTIS, VIRGINIA 23604

This report has been reviewed by the U.S. Army Transportation Research Command and is considered to be technically sound. The report is published for the exchange of information and stimulation of ideas.

TASK 1D121401A14224
GRANT DA TC-44-177-G1
TRECOM TECHNICAL REPORT 64-23
December 1964

AN EXPERIMENTAL INVESTIGATION INTO THE SHAPE OF THRUST-AUGMENTING SURFACES IN CONJUNCTION WITH COANDA-DEFLECTED JET SHEETS (PART I)

UTIA Technical Note No. 70

Prepared by
University of Toronto
Institute for Aerospace Studies

for

U. S. ARMY TRANSPORTATION RESEARCH COMMAND
FORT EUSTIS, VIRGINIA

TABLE OF CONTENTS

		Page
	LIST OF ILLUSTRATIONS	v
	LIST OF SYMBOLS	xvii
	SUMMARY	1
1.	INTRODUCTION	2
2.	THE PROBLEM	3
3.	THE TEST RIG	4
	3.1 Its Variables	5
	3.2 The Air Supply	5
	3.3 The Balance Systems	6
4.	ISENTROPIC, INCOMPRESSIBLE THEORY OF THE THRUST AUGMENTATION RIG	8
	4.1 Momentum Box Theory	8
	4.2 The Momentum Equation	11
	4.3 The Continuity Equation	14
	4.4 Theoretical Lift on the Coanda Surface	17
5.	PROCEDURE	19
	5.1 Procedure Independent of the Pressure Ratio or Coanda Surface Used	19
	5.2 The Three-Inch Coanda Surface	20
	5.3 The Two-Inch Quadrant	21
	5.4 The Four-Inch Quadrant	21
	5.5 Effect of Pressure Ratio	21
	5.6 The Non-Dimensionalized Measured Forces	22
	5.7 Definition of Thrust Augmentation	22
	5.8 Effect of Diffuser Angles	23

TABLE OF CONTENTS (CONT'D.)

		Page
6.	DISCUSSION OF RESULTS	24
	6.1 The Linear Relationship of α and β	24
	6.2 The Secondary Flow Entrance	25
	6.2.1 Favorable Pressure Gradient	26
	6.2.2 Blockage of the Secondary Flow	26
	6.2.3 Secondary Flow Velocity Profile	26
	6.3 Thrust Augmentation	27
	6.3.1 The Deflection of the Secondary Flow	27
	6.3.2 Lift on the Coanda Surface	28
	6.3.3 Thrust Augmentation at Low Pressure Ratios	29
	6.3.4 Change in Pressure Ratio with Constant Throttle Setting	29
	6.3.5 Lift on the External Flaps	30
	6.3.6 Drag on the External Flaps, D_F	30
	6.3.7 Lift on the Nozzle Fairing, L_N	31
	6.3.8 Lengthening of the Diffuser	31
	6.4 Suggestions for the Increase of Thrust Augmentation	31
7.	CONCLUSIONS	35
	BIBLIOGRAPHY	37
	DISTRIBUTION	

LIST OF ILLUSTRATIONS

Figure		Page
1	The Thrust Augmentation Test Rig and Setup	38
2a	Coanda Surfaces (2- and 3-Inch Radii) and the Nozzle Fairing	39
2b	The Thrust-Augmenting Surfaces, Quadrants, and Nozzle	40
3	Schematic Diagram Illustrating the Fifteen Independent Variables	41
4	Diagram Indicating the Variables of the Momentum Boxes	42
5	Proposed Design of the Secondary Flow Channel	43
6	Configuration of the External Flaps in Respect to the Four-Inch Coanda Surface Where $\alpha - \beta = 20^{\circ}$ and $d = 3.25$ Inches	44
7	Configurations of the Top External Flap for $\alpha = 60^{\circ}$ with the Four-Inch Quadrant	45
8	Variation of the Non-Dimensional Forces, $F/m \cdot \sqrt{T}$, with the Non-Dimensional Channel Width, d/t, with a Coanda Surface Radius, $R = 2.0$ in., for a Pressure Ratio of $P_t/P_a = 1.50$	45
a	$\alpha = 50^{\circ}$, $\beta = 0^{\circ}$	45
b	$\alpha = 50^{\circ}$, $\beta = 10^{\circ}$	45
9	Variation of the Non-Dimensional Forces, $F/m \cdot \sqrt{T}$, with the Non-Dimensional Channel Width, d/t, with a Coanda Surface Radius, $R = 2.0$ in., for a Pressure Ratio of $P_t/P_a = 1.50$	46

LIST OF ILLUSTRATIONS (CONT'D)

Figure		Page
a	$\alpha = 50^{\circ}$, $\beta = 20^{\circ}$	46
b	$\alpha = 60^{\circ}$, $\beta = 20^{\circ}$	46
10	Variation of the Non-Dimensional Forces, $F/m \cdot T$, with the Non-Dimensional Channel Width, d/t, with a Coanda Surface Radius, $R = 2.0$ in., for a Pressure Ration of $P_t/P_a = 1.50$	47
a	$\alpha = 70^{\circ}$, $\beta = 20^{\circ}$	47
b	$\alpha = 70^{\circ}$, $\beta = 30^{\circ}$	47
11	Variation of the Non-Dimensional Forces, $F/m \cdot T$, with the Non-Dimensional Channel Width, d/t, with a Coanda Surface Radius, $R = 2.0$ in., for a Pressure Ratio of $P_t/P_a = 1.50$	48
	$\alpha = 70^{\circ}$, $\beta = 40^{\circ}$	48
	$\alpha = 90^{\circ}$, $\beta = 50^{\circ}$	48
12	Variation of the Non-Dimensional Forces, $F/m \cdot T$, with Flap Angles with a Coanda Surface Radius, $R = 2.0$ in., for a Pressure Ratio of $P_t/P_a = 1.50$	49
a	$\alpha = 50^{\circ}$,	49
b	$\alpha = 70^{\circ}$,	49
13	Variation of the Non-Dimensional Forces, $F/m \cdot T$, with Flap Angles with a Coanda Surface Radius, $R = 2.0$ in., for a Pressure Ratio of $P_t/P_a = 1.50$	50

LIST OF ILLUSTRATIONS (CONT'D.)

Figure		Page
a	$\alpha = 90^{\circ}$	50
b	$\beta = 20^{\circ}$	50
14	Variation of Non-Dimensional Forces with the Secondary Flow Entrance Angle, α, Corresponding to the Relationship: $\alpha-\beta = 40 \pm 2^{\circ}$ with a Coanda Surface Radius, R = 2.0 in.	51
15	Variation of the Non-Dimensional Forces, $F/m \cdot \sqrt{T}$, with the Non-Dimensional Channel Width, d/t, with a Coanda Surface Radius, R = 3.0 in., for a Pressure Ratio of $P_t/P_a = 1.50$	52
a	$\alpha = 0^{\circ}$, $\beta = 20^{\circ}$	52
b	$\alpha = 30^{\circ}$, $\beta = 0^{\circ}$	52
16	Variation of the Non-Dimensional Forces, $F/m \cdot \sqrt{T}$, with the Non-Dimensional Channel Width, d/t, with a Coanda Surface Radius, R = 3.0 in., for a Pressure Ratio of $P_t/P_a = 1.50$	53
a	$\alpha = 0^{\circ}$, $\beta = 0^{\circ}$	53
b	$\alpha = 24^{\circ}$, $\beta = 0^{\circ}$	53
17	Variation of the Non-Dimensional Forces, $F/m \cdot \sqrt{T}$, with the Non-Dimensional Channel Width, d/t, with a Coanda Surface Radius, R = 3.0 in., for a Pressure Ratio of $P_t/P_a = 1.50$	54
a	$\alpha = 30^{\circ}$, $\beta = 30^{\circ}$	54
b	$\alpha = 40^{\circ}$, $\beta = 0^{\circ}$	54

LIST OF ILLUSTRATIONS (CONT'D.)

Figure		Page
18	Variation of the Non-Dimensional Forces, $F/m \cdot \sqrt{T}$, with the Non-Dimensional Channel Width, d/t, with a Coanda Surface Radius, R = 3.0 in., for a Pressure Ratio of $P_t/P_a = 1.50$	55
a	$\alpha = 50^\circ$, $\beta = 30^\circ$	55
b	$\alpha = 60^\circ$ $\beta = 30^\circ$	55
19	Variation of the Non-Dimensional forces, $F/m \cdot \sqrt{T}$, with the Non-Dimensional Channel Width, d/t, with a Coanda Surface Radius, R = 3.0 in., for a Pressure Ratio of $P_t/P_a = 1.50$ in.	56
a	$\alpha = 60^\circ$, $\beta = 60^\circ$	56
b	$\alpha = 70^\circ$, $\beta = 30^\circ$	56
20	Variation of the Non-Dimensional Forces $F/m \cdot \sqrt{T}$, with the Non-Dimensional Channel Width, d/t, with a Coanda Surface Radius, R = 3.0 in., for a Pressure Ratio of $P_t/P_a = 1.50$	57
a	$\alpha = 70^\circ$, $\beta = 40^\circ$	57
b	$\alpha = 70^\circ$, $\beta = 50^\circ$	57
21	Variation of the Non-Dimensional Forces, $F/m \cdot \sqrt{T}$, with the Non-Dimensional Channel Width, d/t, with a Coanda Surface Radius, R = 3.0 in., for a Pressure Ratio of $P_t/P_a = 1.50$	58
a	$\alpha = 70^\circ$, $\beta = 60^\circ$	58
b	$\alpha = 80^\circ$, $\beta = 40^\circ$	58
22	Variation of the Non-Dimensional Forces, $F/m \cdot \sqrt{T}$, with the Non-Dimensional Channel Width, d/t, with a Coanda Surface Radius, R = 3.0 in., for a Pressure Ratio of $P_t/P_a = 1.50$.	59

LIST OF ILLUSTRATIONS (CONT'D.)

ure		Page
—	$\alpha = 80^\circ$, $\beta = 50^\circ$	59
	$\alpha = 80^\circ$, $\beta = 60^\circ$	59
	Variation of the Non-Dimensional Forces, $F/m \cdot \sqrt{T}$, with the Non-Dimensional Channel Width, g/t, with a Coanda Surface Radius, R = 3.0 in., for a Pressure Ratio of $P_t/P_a = 1.50$	60
	$\alpha = 90^\circ$, $\beta = 60^\circ$	60
	$\beta = 0^\circ$	60
	Variation of the Non-Dimensional Forces, $F/m \cdot \sqrt{T}$, with Flap Angles with a Coanda Surface Radius, R = 3.0, for a Pressure Ratio of $P_t/P_a = 1.50$	61
	$\beta = 30^\circ$	61
	$\beta = 60^\circ$	61
	Variation of the Non-Dimensional Forces, $F/m \cdot \sqrt{T}$, with Flap Angles with a Coanda Surface Radius, R = 3.0 in., for a Pressure Ratio of $P_t/P_a = 1.50$	62
	$\alpha = 70^\circ$	62
	$\alpha = 80^\circ$	62
	Variation of Non-Dimensional Forces with the Secondary Flow Entrance Angle, α, Corresponding to the Relationship: $\alpha - \beta = 30 \pm 2^\circ$ with a Coanda Surface Radius, R = 3.0 in.	63
	Variation of the Non-Dimensional Forces, $F/m \cdot \sqrt{T}$, with the Non-Dimensional Channel Width, d/t, with a Coanda Surface Radius, R = 4.0 in., for a Pressure Ratio of $P_t/P_a = 1.50$	54

LIST OF ILLUSTRATIONS (CONT'D.)

Figure		Page
a	$\alpha = 20^{\circ}$, $\beta = 0^{\circ}$	64
b	$\alpha = 40^{\circ}$, $\beta = 30^{\circ}$	64
28	Variation of the Non-Dimensional Forces, $F/m \cdot \sqrt{T}$, with the Non-Dimensional Channel Width, d/t, with a Coanda Surface Radius, R = 4.0 in., for a Pressure Ratio of $P_t/P_a = 1.50$	65
a	$\alpha = 40^{\circ}$, $\beta = 20^{\circ}$	65
b	$\alpha = 40^{\circ}$, $\beta = 10^{\circ}$	65
29	Variation of the Non-Dimensional Forces, $F/m \cdot \sqrt{T}$, with the Non-Dimensional Channel Width, d/t, with a Coanda Surface Radius, R = 4.0 in., for a Pressure Ratio of $P_t/P_a = 1.50$	66
a	$\alpha = 50^{\circ}$, $\beta = 30^{\circ}$	66
b	$\alpha = 60^{\circ}$, $\beta = 40^{\circ}$	66
30	Variation of the Non-Dimensional Forces, $F/m \cdot \sqrt{T}$, with the Non-Dimensional Channel Width, d/t, with a Coanda Surface Radius, R = 4.0 in., for a Pressure Ratio of $P_t/P_a = 1.50$	67
a	$\alpha = 70^{\circ}$, $\beta = 50^{\circ}$	67
b	$\alpha = 70^{\circ}$, $\beta = 60^{\circ}$	67
31	Variation of the Non-Dimensional Forces, $F/m \cdot \sqrt{T}$, with the Non-Dimensional Channel Width, d/t, with a Coanda Surface Radius, R = 4.0 in., for a Pressure Ratio of $P_t/P_a = 1.50$	68

LIST OF ILLUSTRATIONS (CONT'D.)

Figure		Page
a	$\alpha = 80^\circ$, $\beta = 60^\circ$	68
b	$\alpha = 90^\circ$, $\beta = 70^\circ$	68
32	Variation of the Non-Dimensional Forces, $F/m \cdot \sqrt{T}$, with Flap Angles with a Coanda Surface Radius, R = 4.0 in., for a Pressure Ratio of $P_t/P_a = 1.50$	69
a	$\alpha = 40^\circ$	69
b	$\alpha = 70^\circ$	69
33	Variation of the Non-Dimensional Forces, $F/m \cdot \sqrt{T}$, with Flap Angles with a Coanda Surface Radius, R = 4.0 in., for a Pressure Ratio of $P_t/P_a = 1.50$	70
a	$\alpha = 90^\circ$	70
b	$\beta = 30^\circ$	70
34	Variation of Non-Dimensional Forces with the Secondary Flow Entrance Angle, α, Corresponding to the Relationship: $\alpha-\beta = 20^\circ \pm 2^\circ$ with a Coanda Surface Radius, R = 4.0 in.	71
35	Variation of the Non-Dimensional Forces, $F/m \cdot \sqrt{T}$, with the Non-Dimensional Channel Width, d/t, with a Coanda Surface Radius, R = 4.0 in., for a Pressure Ratio of $P_t/P_a = 1.89$	72
a	$\alpha = 20^\circ$, $\beta = 0^\circ$	72
b	$\alpha = 40^\circ$, $\beta = 20^\circ$	72
36	Variation of the Non-Dimensional Forces, $F/m \cdot \sqrt{T}$, with the Non-Dimensional Channel Width, d/t, with a Coanda Surface Radius, R = 4.0 in., for a Pressure Ratio of $P_t/P_a = 1.89$	73

LIST OF ILLUSTRATIONS (CONT'D.)

Figure		Page
a	$\alpha = 50^{\circ}$, $\beta = 30^{\circ}$	73
b	$\alpha = 60^{\circ}$, $\beta = 40^{\circ}$	73
37	Variation of the Non-Dimensional Forces, $F/m \cdot \sqrt{T}$, with the Non-Dimensional Channel Width, d/t, with a Coanda Surface Radius, $R = 4.0$ in., for a Pressure Ratio of $P_t/P_a = 1.89$	74
a	$\alpha = 70^{\circ}$, $\beta = 50^{\circ}$	74
b	$\alpha = 70^{\circ}$, $\beta = 60^{\circ}$	74
38	Variation of the Non-Dimensional Forces, $F/m \cdot \sqrt{T}$, with the Non-Dimensional Channel Width, d/t, with a Coanda Surface Radius, $R = 4.0$ in., for a Pressure Ratio of $P_t/P_a = 1.89$	75
a	$\alpha = 80^{\circ}$, $\beta = 60^{\circ}$	75
b	$\alpha = 90^{\circ}$, $\beta = 70^{\circ}$	75
39	Variation of the Non-Dimensional Forces, $F/m \cdot \sqrt{T}$, with Flap Angles with a Coanda Surface Radius, $R = 4.0$ in., for a Pressure Ratio of $P_t/P_a = 1.89$	76
a	$\alpha = 40^{\circ}$	76
b	$\alpha = 70^{\circ}$	76
40	Variation of the Non-Dimensional Forces, $F/m \cdot \sqrt{T}$, with Flap Angles with a Coanda Surface Radius, $R = 4.0$ in., for a Pressure Ratio of $P_t/P_a = 1.89$	77
a	$\alpha = 90^{\circ}$	77
b	$\beta = 30^{\circ}$	77

LIST OF ILLUSTRATIONS (CONT'D.)

Figure		Page
41	Variation of Non-Dimensional Forces with the Secondary Flow Entrance Angle, α, Corresponding to the Relationship: $\alpha-\beta = 20^{\circ}\pm2^{\circ}$ with a Coanda Surface Radius, R = 4.0 in.	78
42	Variation of the Non-Dimensional Forces, $F/m\cdot\sqrt{T}$, with the Non-Dimensional Channel Width, d/t, with a Coanda Surface Radius, R = 4.0 in., for a Pressure Ratio of $P_t/P_a = 2.00$	79
a	$\alpha = 20^{\circ}$, $\beta = 0^{\circ}$	79
b	$\alpha = 40^{\circ}$, $\beta = 20^{\circ}$	79
43	Variation of the Non-Dimensional Forces, $F/m\cdot\sqrt{T}$, with the Non-Dimensional Channel Width, d/t, with a Coanda Surface Radius, R = 4.0 in., for a Pressure Ratio of $P_t/P_a = 2.00$	80
a	$\alpha = 50^{\circ}$, $\beta = 30^{\circ}$	80
b	$\alpha = 60^{\circ}$, $\beta = 40^{\circ}$	80
44	Variation of the Non-Dimensional Forces, $F/m\cdot\sqrt{T}$, with the Non-Dimensional Channel Width, d/t, with a Coanda Surface Radius, R = 4.0 in., for a Pressure Ratio of $P_t/P_a = 2.00$	81
a	$\alpha = 70^{\circ}$, $\beta = 40^{\circ}$	81
b	$\alpha = 70^{\circ}$, $\beta = 50^{\circ}$	81
45	Variation of the Non-Dimensional Forces, $F/m\cdot\sqrt{T}$, with the Non-Dimensional Channel Width, d/t, with a Coanda Surface Radius, R = 4.0 in., for a Pressure Ratio of $P_t/P_a = 2.00$	82

LIST OF ILLUSTRATIONS (CONT'D.)

Figure		Page
a	$\alpha = 80^\circ$, $\beta = 60^\circ$	82
b	$\alpha = 90^\circ$, $\beta = 70^\circ$	82
46	Variation of the Non-Dimensional Forces, $F/m \cdot \sqrt{T}$, with Flap Angles with a Coanda Surface Radius, R = 4.0 in., for a Pressure Ratio of $P_t/P_a = 2.00$	83
a	$\alpha = 40^\circ$	83
b	$\alpha = 70^\circ$	83
47	Variation of the Non-Dimensional Forces, $F/m \cdot \sqrt{T}$, with Flap Angles with a Coanda Surface Radius, R = 4.0 in., for a Pressure Ratio of $P_t/P_a = 2.00$	84
a	$\alpha = 90^\circ$	84
b	$\alpha = 30^\circ$	84
48	Variation of Non-Dimensional Forces with the Secondary Flow Entrance Angle, α, Corresponding to the Relationship: $\alpha-\beta = 20^\circ \pm 2^\circ$ with a Coanda Surface Radius, R = 4.0 in.	85
49	Variation of the Non-Dimensional Forces, $F/m \cdot \sqrt{T}$, with Flap Angles with a Coanda Surface Radius, R = 4.0 in., for a Pressure Ratio of $P_t/P_a = 1.50$	86
a	$\phi = 0^\circ$, $\alpha = 60^\circ$, $\beta = 40^\circ$, $d/t = 26$	86
b	$\phi = -1^\circ$, $\alpha = 60^\circ$, $\beta = 40^\circ$, $d/t = 26$	86
50	Variation of the Non-Dimensional Forces, $F/m \cdot \sqrt{T}$, with Flap Angles with a Coanda Surface Radius, R = 4.0 in., for a Pressure Ratio of $P_t/P_a = 1.50$	87

LIST OF ILLUSTRATIONS (CONT'D.)

Figure		Page
a	$\phi = -2^\circ$, $\alpha = 60^\circ$, $\beta = 40^\circ$, $d/t = 26$	87
b	$\gamma-\phi = 6^\circ$, $\alpha = 60^\circ$, $\beta = 40^\circ$, $d/t = 26$	87
51	Secondary Flow Velocity and Pressure Profiles Across the Entrance, A_2, with $\alpha = 60^\circ$, $\beta = 40^\circ$, $d/t = 26$ and $R = 4.0$ in. for a Pressure Ratio of 1.50	88
a	Secondary Flow Velocity, ft/sec	88
b	Secondary Flow Pressure, lb/ft^2	88
52	Velocity Profile for $\alpha = 60^\circ$, and $\beta = 40^\circ$ with a Four-Inch Quadrant and a Pressure Ratio of 1.50	89
a	Velocity Profile at the Diffuser Entrance	89
b	Velocity Profile at the Diffuser Exit	89

LIST OF SYMBOLS

angle between the horizontal and the tangent to the lip of the top exterior flap originating from the top of the quadrant near the end of the nozzle.

the angle of the top exterior flap from its vertical position.

the angle of the lowest exterior flap from its vertical position.

the angle of the interior flap (attached to the Coanda surface) from the vertical.

the angle of the center exterior flap from the vertical (in all cases it was vertical).

density (see subscripts for the corresponding station).

$\overline{V^2}/(\overline{V})^2$, ratio of the mean of the velocity squared to the mean velocity squared.

pressure difference across the primary flow over the Coanda surface.

vertical distance from the top of the quadrant to the exit of the nozzle.

width of the channel above the diffuser between the interior and exterior flaps.

distance from the quadrant to the lip of the top exterior flap along the tangent defining the angle, α .

horizontal distance from the top of the quadrant to the exit of the nozzle.

length of the top exterior flap (not including the top exterior flap's lip).

primary mass flow (subscripts for other stations than 1. (m_1)).

[redacted] flow cross-sectional areas (see Fig. 4).

$= A_1/A_2$ $\qquad A'_{12} = A_1/A'_2$.

$A_{32} = A_3/A_2$ $\qquad A'_{32} = A_3/A'_2$.

M — length of the interior flap.

N — length of the bottom exterior flap.

p — static pressure at certain stations (see subscripts for stations).

P_a — ambient atmospheric pressure.

P_t — total pressure of primary flow.

R — radius of Coanda surface or quadrant.

t — thickness of the exit of the subsonic nozzle.

T or T_T — total temperature of the primary flow.

V — velocity at certain stations (see subscripts for the corresponding stations).

$\overline{V^2} \equiv 1/A \int_A V^2 \cdot dA$, — mean velocity squared at a certain station.

$\overline{V} \equiv 1/A \int_A V \cdot dA$, — mean velocity at a certain station.

L_F — lift or vertical force on the three external flaps (augmenting surfaces).

L_B — lift or vertical force on the entire thrust augmenting rig.

L_N — lift or vertical force on the nozzle fairing.

$L_T = L_B + L_N$.

D_F — drag or horizontal force on the three external flaps.

D_B — drag or horizontal force on the entire thrust augmenting rig.

Subscripts

1	station at the exit of the subsonic nozzle (primary flow).
2	station at the secondary flow entrance (Fig. 4).
3	station at the exit of the thrust augmentation rig.
a	ambient or atmospheric conditions.
c	Coanda surface exposed to the primary flow.
s	free surface of the primary and entrained secondary flow flowing over the Coanda surface.
i	isentropic conditions (unshrouded).

SUMMARY

It is known that by means of additional surfaces, the thrust of a jet or jet sheet can be enhanced (thrust augmentation). This especially applies to Coanda-deflected jet sheets because of the inherent stronger entrainment into curved flow surfaces.

The flow from a two-dimensional subsonic nozzle was deflected by quadrants. A composite thrust-augmenting surface was added, and the effect of its shape on thrust augmentation was studied at various nozzle pressure ratios and radii of the quadrants.

This investigation yielded a maximum thrust augmentation of 1.21 for several optimum configurations, which was governed primarily by the relative magnitude and direction of the momentum of the secondary (entrained) flow in relation to the primary (nozzle) flow momentum. Thrust augmentation decreased with increasing nozzle pressure ratio but was independent of the quadrant radius. Some of the observed results were predicted theoretically. Suggestions for possibly introducing higher thrust augmentation are offered.

1. INTRODUCTION

The Coanda effect is believed to have a wide range of possible applications for V/STOL aircraft. For instance, it may be used for turning two-dimensional or annular jet sheets (replacing closed ducts), for instantaneous thrust and lift control (by means of shrouds, for example) during transition from hovering to forward flight, for stability and control purposes, or for focusing annular jets.

For all the above applications of the Coanda effect, two basic problems arise:

(a) how to turn the jet sheet at the minimum possible loss in jet momentum, and

(b) whether, where additional surfaces are feasible (in analogy, e.g., with straight ejectors), thrust augmentation is possible.

This experimental study deals with the question of augmenting the thrust of Coanda-deflected jet sheets by means of additional (secondary) surfaces.

2. THE PROBLEM

It is known that the free surface of a Coanda-deflected jet sheet entrains more ambient air (about twice as much) as this surface would entrain if it were straight. A higher rate of entrainment causes:

(a) faster mixing, which should lead to a reduction of the required mixing length and ducts.

(b) increased secondary flow velocities and consequently reduced static pressures on secondary surfaces, which, if properly arranged, can augment the basic jet momentum thrust.

It is the object of this experimental investigation to find out more about the shape of thrust augmenting surfaces for optimum thrust augmentation. To facilitate configurational changes, especially of the thrust augmenting surfaces, and to be able to use existing equipment, a two-dimensional test setup was chosen.

3. THE TEST RIG

The thrust augmentation rig (Fig. 1) consists of a Coanda surface (quadrant) and a series of adjustable flaps (the thrust augmenting surfaces; see also (Fig. 3). The two-dimensional jet sheet ejected from the primary flow nozzle is turned through 90 deg by means of a surface (see Fig. 2). The flaps are used to provide boundaries for the mixing of the primary with the secondary air flow and to control the air flow direction. Both quadrants and flaps are mounted between glass sidewalls to ensure two-dimensionality. The glass sidewalls are 8 in. apart. Since the nozzle exit is 1/8-in. thick, the aspect ratio of the primary flow (jet sheet) is initially 64 while the aspect of the diffuser averages out to be only about 2. Since a minimum aspect ratio of about 100 would be desirable in order to keep wall the frictional forces on the side wall glass plates, the observed thrust augmentations should, in our case here, be substantially less than those which would be obtained with a primary flow-to-nozzle aspect ratio of 100 or more.

Three Coanda surfaces or quadrants of radii, two, three, and four inches, were employed. The internal flap which is attached directly to the Coanda surface remained vertical throughout the experiment, except for the case where it was varied for the sole purpose of studying the effect of the change of diffuser angles on the lift force.

As can be seen in Fig. 1, a pit, 5 by 2 feet wide and 2-1/2 feet deep, was dug at the exit of the augmentation rig so that any ground effect was eliminated. By using two bent metal sheets, the exit flow was divided into two parts and then diverted to either side of the augmentation rig.

A flexible sheet of metal, also 8 inches wide, was attached to the top and center external flaps in such a manner that the surface exposed to the secondary flow was curved with its two ends tangent to the top and center flaps.

3.1 ITS VARIABLES

There are fifteen possible variables associated with the experimental equipment (Fig. 3). Not only can a total of five angles be altered (α, β, γ, δ, and ϕ) along with eight linear dimensions (L, M, N, l, a, R, d, and t), but also the temperature and pressure ratio (T_t/T_a and p_t/p_a respectively) can be varied.

Of these fifteen independent variables shown in Fig. 3, those variables considered to be most directly related to the diffuser and secondary flow entrance angles (four angles and two linear dimensions) as well as the pressure ratio are listed below:

(a) α - the angle between the tangent to the lip of the top exterior flap originating from the top of the quadrant (near the end of the nozzle) and the horizontal.

(b) β - the angle of the top exterior flap from its vertical position.

(c) γ - the angle of the lowest exterior flap from the vertical position.

(d) ϕ - the angle of the interior flap (attached to the Coanda surface) from the vertical.

(e) R - the radius of the Coanda surface or quadrant.

(f) d - the width of the channel (distance between the interior and center exterior flaps).

(g) P_T/P_a - the ratio of the primary flow total pressure to the ambient atmospheric pressure.

Of the above seven variables, the first and major portion of the experiment involved the variation of α, β, and d while ϕ and γ remained constant at zero and six degrees respectively for the two-, three- and four-inch-radius Coanda surfaces.

3.2 The Air Supply

A small gas turbine engine (Blackburn and General Aircraft Turbomeca Palouste 500), housed in a soundproof

room and remotely controlled, was used as a compressed air source for these tests. The compressed air, bled off the engine compressor, could be delivered at temperatures of up to 230 deg centigrade, at pressure ratios of up to 3.7, and at a weight flow of up to 2.7 lb/sec. A large water cooler reduced the air temperature to about 10°C (50°F). This cooled air was ducted to the settling chamber and the subsonic nozzle by means of eight-inch-diameter piping.

The mass flow was measured by a U-tube water manometer, which indicated the pressure difference across an orifice plate situated in an eight-inch pipe through which the primary flow flowed to the settling chamber. The total pressure of the primary flow was indicated on a mercury manometer board connected to a pressure probe located in the settling chamber.

3.3 The Balance Systems

The weight of the thrust augmentation rig (see Fig. 1) was suspended primarily by a balance with a fixed fulcrum (which gives a constant lift for small deflections of the test rig), and the remaining small portion of the rig's weight was suspended by a strain gauge balance system, the deflections of the lever arm, causing a small change in lift, are included. The measurements of the horizontal (drag, D_B) and vertical (lift, L_B) forces on the thrust augmentation rig by means of the strain gauge balance were made possible by the physical separation of the Coanda surface and the nozzle. During the experiment, this gap defined by the horizontal distance, ℓ , and the vertical distance, a , was kept constant at $\ell = 1/4$ in. and $a = 1/10$ in. with the engine off. The linkages of the strain gauge system allowed the drag forces and the mutually perpendicular components of the lift to be measured independently of each other. The strains associated with these forces are measured on an SR-4 strain indicator (type N), and the actual forces can be obtained directly from the calibration of the balance.

Furthermore, force measurements on the thrust augmenting surface alone were made possible by avoiding any rigid physical connection between it and the two glass plates. The three exterior flaps were supported solely by a frame connected to another strain gauge system mounted rigidly to the frame of the thrust augmentation rig. Again, as with the main strain gauge balance, both the mutually perpendicular lift, L_F, and drag, D_F, forces were measured on another SR-4 strain indicator.

All the strain gauge electrical bridge networks were arranged so that they were self-compensating with respect to external temperature changes.

The nozzle top surface is faired in, and the pressure on this fairing was measured with six flush static pressure taps (Fig. 2a) connected to a water manometer board, giving the lift on the nozzle, L_N, assuming ambient atmospheric pressure on the bottom surface of the nozzle. A subsonic nozzle, seven inches in length, was used in order to reduce the blockage effect of the settling tank on the secondary flow along the nozzle top fairing. The thickness of the exit slot of the nozzle was one-eighth of an inch. Thus the exit slot area of the nozzle was one square inch, since its width was eight inches.

4. ISENTROPIC, INCOMPRESSIBLE THEORY OF THE THRUST AUGMENTATION RIG

There are two main principles of thrust augmentation associated with this experiment. The first is to efficiently entrain a relatively large amount of ambient air into the primary flow and thereby increase the mass flow, m_3, and decrease the exit velocity, V_3. Thus the exit momentum $(m_3 \cdot V_3)$ is increased, assuming that frictional effects cause relatively low energy losses.

The second aspect of this thrust augmentation rig is that the vectorial difference between the outlet and inlet momentum in the direction perpendicular to the initial direction of the primary flow can be increased by varying the shape of the external flap combination.

Thus the vertical reaction force or lift can be increased to a value greater than the reaction force from a simple unshrouded subsonic nozzle.

4.1 MOMENTUM BOX THEORY

Figure 4 illustrates a general form of the thrust augmentation rig with the angles of the flow streamlines defined at the entrance and exit areas. The primary flow variables have the subscript 1, and the inlet station considered is at the throat of the nozzle (of area A_1). The secondary flow variables, denoted by the subscript 2, include the velocity, V_2, at the entrance area, A_2, located between the nozzle exit and the lip of the top exterior flap. The angle of entrance of the secondary flow streamlines to the vertical is ϵ. The secondary flow entrance, A_2', as shown in Fig. 4, has identical notations except that a prime mark is used. It is assumed that at point X on the nozzle, the secondary flow velocity over the nozzle approaches zero (from a maximum value at the exit of the nozzle) Thus the vertical reaction force, F_V', will include the lift over the nozzle. It is furthermore assumed that a normal to the exit area, A_3, is parallel to the vertical streamlines of the uniform outlet velocity, V_3; and the uniform static pressure at the exit is assumed to equal the ambient atmospheric pressure.

Let F'_V and F'_H be the resultant vertical (y-direction) and horizontal (x-direction) internal wall reaction forces respectively. Thus the vertical lift on the thrust augmentation rig as well as on the nozzle is ideally

$$F'_V = \rho_3(\bar{V}_3)^2 + (p_3 - p_a)A_3$$

$$- \int_{A'_2} [\rho'_2(V'_2)^2 \cos(\epsilon' - \alpha')\cos\epsilon' + (p'_2 - P_a) \cdot \cos\alpha']dA'_2 \quad (4\text{-}1a)$$

while

$$-F'_H = \int_{A_1} [\rho_1 V_1^2 + (p'_1 - P_a)]dA_1$$

$$+ \int_{A'_2} [\rho_2(V'_2)^2 \cos(\epsilon' - \alpha)\sin\epsilon' + (p'_2 - P_a)\sin\alpha']\cdot dA'_2 \,. \quad (4\text{-}1b)$$

The above equations can be simplified by defining a term, $\lambda = [\overline{V^2}/(\bar{V})^2]$, the ratio of the mean square velocity $\overline{V^2} = 1/A \int_A V^2 dA$ to the square of the mean value $\bar{V} = 1/A \int_A V dA$. By integrating the properties of the flow over the cross-sectional A'_2, Bernoulli's equation becomes $(\bar{p}'_2 - P_a) = -\rho_2/2 \cdot \lambda_2(\bar{V}'_2)^2$, where the mean pressure is defined in general by $\bar{p} = 1/A \int_A p\, dA$. Further, the values for $\cos\alpha'$, $\sin\alpha'$, $\cos\epsilon'$ and $\sin\epsilon'$ within the integrals can be averaged as shown below for instance for the case of $\cos\alpha'$.

$$\overline{\cos\alpha'} = \frac{1}{\int_{A'_2}(p'_2 - P_a)dA'_2} \int_{A'_2} (\cos\alpha')(p'_2 - P_a)dA'_2$$

$$= \frac{1}{-\frac{\rho_2}{2}\lambda'_2(\bar{V}'_2)^2 A'_2} \int_{A'_2} -\frac{\rho_2}{2}(V'_2)^2 \cos\alpha' \, dA'_2 \qquad (4\text{-}2)$$

As the flow becomes more non-uniform, the term λ rises above unity, its minimum value for a uniform velocity profile. Making use of the above expressions and assuming the exit and secondary flows to be incompressible, it can be shown that

$$F'_V = \rho \left[(\bar{V}_3)^2 A_3 + \frac{1}{2} \lambda'_2 (\bar{V}'_2)^2 \overline{\cos \alpha'} A'_2 \right.$$

$$\left. - \int_{A'_2} (V'_2)^2 \cos(\epsilon' - \alpha') \cos \epsilon' \, dA'_2 \right] \qquad (4\text{-}3a)$$

while

$$-F'_H = \rho_1 \lambda_1 (\bar{V}_1)^2 A_1 + (\bar{p}_1 - p_a) A_1 - \frac{\rho}{2} \lambda'_2 (\bar{V}'_2)^2 \overline{\sin \alpha'} A'_2$$

$$+ \int_{A'_2} \rho (V'_2)^2 \cos(\epsilon' - \alpha') \sin \epsilon' \, dA'_2 \, . \qquad (4\text{-}3b)$$

For the condition of $\alpha' = \epsilon'$ (as for instance along area A'_2), the last term in Eq. (4-3a) becomes

$$\int_{A'_2} (V'_2)^2 \cos \alpha' \, dA'_2$$

which then can be reduced to

$$\overline{\cos \alpha'} \int_{A'_2} (V'_2)^2 dA'_2 = \overline{\cos \alpha'} \, \lambda'_2 (\bar{V}'_2)^2 A'_2 \, . \qquad (4\text{-}4)$$

Combining now the last two equations furnishes

$$\overline{\cos \alpha'} = \frac{1}{\lambda'_2 (\bar{V}'_2)^2 A'_2} \int_{A'_2} (V'_2)^2 \cos \alpha' \, dA'_2$$

which is the same expression as that previously given as Eq. (4-2). The equation for the vertical lift, F_V' can then be greatly simplified and becomes

$$F_V' = \rho\left[\bar{V}_3^2 A_3 - \frac{1}{2}\lambda_2' \overline{\cos\alpha'}\,(\bar{V}_2')^2 A_2'\right] . \qquad (4\text{-}5a)$$

This equation expresses the fact that F_V' becomes a maximum when the inlet momentum along the vertical y-coordinate is zero for both the primary and secondary flow. This condition is fulfilled for the secondary flow if ϵ' (and α') approach 90 deg. However, in general, the angle ϵ' is not large. (It was found that the secondary flow streamlines near the nozzle follow the contour of the nozzle while the flow near the lip of the exterior flap follows the lip contour. Thus, the flow near the nozzle has a high value of ϵ', which is desirable, while most of the flow near the lip approaches under a relatively low angle ϵ').

The object of this experiment was to increase ϵ' or ϵ as much as possible, while keeping the secondary flow inlet momentum as large as possible. If one assumes that the inlet momentum (of primary and secondary flow) remains constant for given values of α and d/t, independently of β (see Fig. 3), then increasing ϵ to an optimum value could, it seems, be achieved by varying the angle, β, of the top exterior flap.

For the condition $\alpha' = \epsilon'$, the horizontal reaction force component F_H' can be obtained as

$$-F_H' = \rho_1\left[\lambda_1(\bar{V}_1)^2 A_1\right] + \frac{1}{2}\rho\lambda_2' \overline{\sin\alpha'}\,(\bar{V}_2')^2 A_2' \qquad (4\text{-}5b)$$

assuming that the term $(\bar{p} - p_a)A_1$ is small enough to be neglected.

4.2 The Momentum Equation for Ideal Fluid Flows

According to BLASIUS's THEOREM, the resultant force of an ideal flow acting on a two-dimensional body is always perpendicular to the free stream direction, or, the resultant force (thrust or drag) in the direction of the free stream is zero. To make an analysis possible of the otherwise very complex real flow model under experimental

investigation in this study, ideal and incompressible fluid flow is assumed. Applying BLASIUS THEOREM to the ideal fluid flow through a straight (not curved) duct, the momentum equation (zero thrust or drag) reduces to

$$\rho \int_{A'_2} (V'_2)^2 \cos(\epsilon' - \alpha') dA'_2 + (\bar{p}'_2 - P_a)A'_2$$

$$+ \rho_1 \bar{V}_1^2 A_1 + (\bar{p}_1 - P_a)A_1 = \rho A_3 \bar{V}_3^2 \qquad (4\text{-}6)$$

assuming that $\bar{p}_3 = P_a$. If the duct is curved, as it is in the configuration here under investigation, Eq. (4-6) still applies for the above stated assumptions. External (wall) forces solely force the flow to change its direction but do not induce any velocity or pressure changes of the primary and secondary flows at inlet or of the mixed flow at the outlet cross section.

Since A'_2 is many times larger than A_1 and assuming that the average static pressure of the primary flow is approximately equal to that of the secondary flow, the term $(\bar{p}_1 - P_a)A_1$ is, in the following discussion, omitted since it is considered negligible in comparison with $(\bar{p}'_2 - P_a)A'_2$. Consequently, the outlet momentum equals

$$\rho \cdot A_3 \cdot \bar{V}_3^2 = \rho_1 \cdot A_1 \cdot \bar{V}_1^2$$

$$+ \rho \left[\int_{A'_2} (V'_2)^2 \cos(\epsilon' - \alpha') \cdot dA'_2 - \frac{1}{2}(\bar{V}'_2)^2 \cdot \lambda'_2 \cdot A'_2 \right]. \qquad (4\text{-}7)$$

Substituting Eq. (4-7) in Eq. (4-3), the following expression is obtained:

$$F_y = \rho_1 \cdot A_1 \bar{V}_1^2$$

$$+ \rho \left[\int_{A'_2} [(V'_2)^2 \cdot \cos(\epsilon' - \alpha') - (V'_2)^2 \cdot \cos(\epsilon' - \alpha') \cdot \cos(\epsilon')] \cdot dA'_2 \right.$$

$$\left. - \frac{\lambda'_2}{2} \cdot (V'_2)^2 \cdot A'_2 + \frac{\lambda'_2}{2} (V'_2)^2 \cdot A'_2 \cdot \cos \alpha' \right] . \qquad (4\text{-}8)$$

Consequently, the amount of thrust augmentation, ϕ, defined as the ratio of the vertical measured lift, L_T, (corresponding to F_V') to the isentropic thrust of the unshrouded nozzle, $(\rho_1 \cdot V_1^2 \cdot A_1)_i$, would be ideally

$$\frac{L_T}{(\rho_1 \cdot \overline{V_1^2} \cdot A_1)_i} =$$

$$\frac{\int_{A_2'} (V_2')^2 \cdot \cos(\epsilon' - \alpha') \cdot [1 - \cos \epsilon'] \cdot dA_2' - \frac{1}{2} \lambda_2' \cdot (\overline{V_2'})^2 (1 - \overline{\cos \alpha'}) A_2'}{(\frac{\rho_2}{\rho_1}) \qquad (A_1 \cdot \overline{V_1^2})_i} \qquad (4\text{-}9)$$

assuming that the isentropic thrust $(\rho_1 \cdot \overline{V_1^2} \cdot A_1)_i$ equals the measured primary flow momentum, $\rho_1 \cdot \overline{V_1^2} \cdot A_1$.

Comparing the momentum term, $\int_{A_2'} (V_2')^2 \cdot \cos(\epsilon' - \alpha') \cdot [1 - \cos \epsilon'] \cdot dA_2'$, with the pressure term, $\lambda_2' (\overline{V_2'})^2 \cdot 1/2 \cdot (1 - \cos \alpha') \cdot A_2'$, it can be seen that $\cos(\epsilon' - \alpha')$ corresponds to $1/2$ while $(1 - \cos \epsilon')$ corresponds to $(1 - \cos \alpha')$. As long as $\cos(\epsilon' - \alpha')$ is greater than $1/2$ or $|\epsilon' - \alpha'|$ is less than 60 deg, then the flow should enter at the largest angle of ϵ' possible, even at the cost of decreasing $(\cos \alpha')$ in order that the highest value of augmentation is obtained.

If ideal conditions were present such that a maximum amount of mass flow was entrained for a given area and average velocity (that is, the streamlines are parallel to the normal vector of the entrance area, or if $\alpha' = \epsilon'$), then

$$\phi = 1 + (\frac{\rho}{\rho_1}) \cdot \frac{\overline{V_2}^2}{V_1} \cdot \frac{\lambda_2'}{\lambda_1} \cdot \frac{A_2'}{A_1} \cdot [\frac{1}{2}(1 - \overline{\cos \epsilon'})]. \qquad (4\text{-}10)$$

Under the above conditions, maximization occurs upon maximizing λ_2' (the non-uniformity of the velocity profile at the secondary flow entrance area) as well as ϵ'. In causing λ_2' to increase the total momentum, composed of both the momentum terms $(\rho \cdot \overline{V_2'^2} \cdot A_2')$ and the pressure contributions

$([P_a - \overline{p_2'}] \cdot A_2')$ are augmented. Furthermore, if ϵ' is made larger, the vectorial difference between the outlet and inlet dynamic momentum is increased in the outlet momentum's direction. Thus it can be seen that the thrust augmentation is simply caused by the change in the total momentum's magnitude and direction of the entrained (secondary) flow. (If $\alpha' = \epsilon' = 0^o$, then $\Phi = 1.0$ even if λ_2' is large.)

Since it is desired that the secondary or entrained flow undergo the greatest change in total momentum, it would seem advantageous that through mixing, the primary flow should lose the largest possible amount of momentum to the secondary flow. This would lead to a uniform exit velocity profile or $\lambda_3 = 1.0$, assuming that the static pressure at the exit is equal to the ambient pressure.

The degree of momentum transfer and the loss of energy are major factors in thrust augmentation. Since entrainment relies on viscosity, and since viscosity induces frictional losses, the kinetic energy of the exit flow cannot equal that of the primary flow. Defining a mixing efficiency as the ratio of the kinetic energy of the exit to primary flow,

$$\eta_{mix} \equiv (m_3/m_1) \cdot (\overline{V}_3/\overline{V}_1)^2 \cdot \lambda_3/\lambda_1 \ . \qquad (4\text{-}11)$$

The efficiency of this experiment was found to be approximately 20 per cent. Of course, the lower the mixing efficiency, the lower is the entrained mass flow and exit momentum.

4.3 The Continuity Equation

Consider the continuity and momentum equations:

$$\rho_1 \cdot V_1 \cdot A_1 + \rho \int_{A_2'} \overline{V_2'} \cdot \cos(\epsilon' - \alpha') \cdot dA_2' = \rho \cdot \overline{V}_3 \cdot A_3 \qquad (4\text{-}12)$$

$$\rho \cdot A_3 \cdot \overline{V_3^2} = \rho_1 \cdot A_1 \cdot \overline{V_1^2} + \rho \left[\int_{A_2'} (V_2')^2 \cos(\epsilon' - \alpha') \cdot dA_2' - \lambda_2'/2 \cdot (\overline{V_2'})^2 A_2' \right] \qquad (4\text{-}7)$$

From Eq. (4-12),

$$(\bar{V}_2)^2 = \frac{1}{\cos_2^2(\epsilon'-\alpha')}\left[A'_{32}\,\bar{V}_3 - \frac{\rho_1}{\rho}\,A'_{12}\cdot\bar{V}_1\right]^2 \qquad (4\text{-}13)$$

where the average values of $\cos(\epsilon'-\alpha')$ are defined as:

$$\overline{\cos_1(\epsilon'-\alpha')} \equiv \frac{1}{\lambda'_2(\overline{V'_2})^2\cdot A'_2}\cdot\int_{A'_2}(V'_2)^2\cdot\cos(\epsilon'-\alpha')\cdot dA'_2$$

$$\overline{\cos_2(\epsilon'-\alpha')} \equiv \frac{1}{\overline{V'_2}\cdot A'_2}\int_{A'_2}(V'_2)\cdot\cos(\epsilon'-\alpha')\cdot dA'_2 . \qquad (4\text{-}14)$$

Combining Eqs. (4-13) with (4-7) gives Eq. (4-15).

$$\lambda_3\cdot(\bar{V}_3)^2 = \frac{\rho_1}{\rho}\cdot A_{13}\cdot(\bar{V}_1)^2\cdot\lambda_1 + \lambda''_2$$

$$\lambda'_{23}\left[(A'_{32})^2\cdot(\bar{V}_3)^2 + (A'_{12})^2\cdot(\bar{V}_1)^2\left(\frac{\rho_1}{\rho}\right)^2 - 2\,\frac{\rho_1}{\rho}\,A'_{32}\cdot A'_{12}\cdot V_3\cdot V_1\right] \qquad (4\text{-}15)$$

where

$$\lambda''_2 = \lambda'_2\,\frac{\overline{\cos_1(\epsilon'-\alpha')}-\frac{1}{2}}{\cos_2^2(\epsilon'-\alpha')} \qquad (4\text{-}16)$$

or

$$(\bar{V}_3)^2[\lambda_3 - \lambda''_2 A_{32}] + (\bar{V}_3)[2\cdot\lambda''_2\cdot A'_{12}\cdot\bar{V}_1\cdot(\rho_1/\rho)]$$

$$-(\bar{V}_1)^2[\lambda_1\cdot A_{13}\cdot(\rho_1/\rho) + \lambda''_2\cdot A'_{23}\cdot A'_{12}(\rho_1/\rho)^2] = 0 . \qquad (4\text{-}17)$$

If $\cos_1(\epsilon'-\alpha')$ and $\cos_2(\epsilon'-\alpha')$ are approximately equal, then λ_2'' has a maximum value of about $\lambda_2'/2$ for the case where $\epsilon' = \alpha'$. Solving Eq. (4.17),

$$\frac{\bar{V}_3}{\bar{V}_1} = \sqrt{\frac{(\rho_1/\rho)\cdot A_{13}}{\lambda_3 - A'_{32}\cdot\lambda_2''}} - \frac{\lambda_2''\cdot A_{12}\cdot(\rho_1/\rho)}{\lambda_3 - A'_{32}\cdot\lambda_2''} \quad . \tag{4-18}$$

For $\lambda_3 = 1.0$, Eq. (4-12) yields

$$(\rho/\rho_1)\cdot\frac{V'_2}{\bar{V}_1}\frac{A'_2}{A_1} = \frac{1}{\cos_2(\epsilon'-\alpha')}\left[\frac{\rho}{\rho_1}\cdot\frac{\bar{V}_3}{\bar{V}_1}\cdot A_{31} - 1\right]$$

$$= \frac{1}{\cos_2(\epsilon'-\alpha')}\left\{\sqrt{\frac{(\rho/\rho_1)A_{31}}{1 - A'_{32}\cdot\lambda_2''}} - \left[\frac{\lambda_2''\cdot A'_{32}}{1 - A'_{32}\cdot\lambda_2''} + 1\right]\right\}. \tag{4-19}$$

Assuming that the shape of A_2' is chosen such that its normal is parallel to the corresponding local velocity vector (that is, $\epsilon' = \alpha'$), the value of thrust augmentation, Φ, equals (from Eq. 4-10)

$$\Phi = 1 + \left[\frac{\rho}{\rho_1}\cdot\frac{\bar{V}'_2}{\bar{V}_1}(A'_{21})\right]^2\cdot\left[\frac{\lambda'_2}{\lambda_1}\,\frac{1}{2}(1-\overline{\cos\epsilon'})\cdot\frac{\rho_1}{\rho}\cdot A'_{12}\right]$$

$$= 1 + \left[\sqrt{\frac{(\rho/\rho_1)(A_{21})}{1 - A'_{32}\cdot\lambda_2''}} - \frac{\lambda_2''\cdot A'_{32}}{1 - A'_{32}\cdot\lambda_2''} + 1\right]^2\cdot\left[\frac{\lambda'_2}{\lambda_1}\cdot\frac{1}{2}(1-\overline{\cos\epsilon'})\cdot\frac{\rho_1}{\rho}\cdot A'_{12}\right] \tag{4-20}$$

where

$$(\lambda_2'') = \frac{\lambda'_2}{2} \quad .$$

For a given optimum physical configuration and suitably high values of ϵ' and α', it would seem to be desirable for the shape of A_2' (as defined above) to approach a straight line, as indicated in Fig. 4 by A_2'', causing the effective value of A_2' to become smaller.

The product $A_{32}' \cdot \lambda_2''$, in Eq. (4-20), cannot exceed unity in order that Φ be a real number. However, if $A_{32}' \cdot \lambda_2''$ approaches unity, Φ is also increased. If $\lambda_2'' = \lambda_2'/2$, then the maximum value of A_{32}' is $2/\lambda_2'$ for $\epsilon' = \alpha'$. However, the larger $|\epsilon' - \alpha'|$ becomes, the larger λ_2' and/or A_{32}' must be, to compensate for any loss in thrust augmentation.

In conjunction with A_{32}' being large, A_{21}' should be small, or A_2' (or A_2) should be as small as possible. Furthermore, it would be preferable for the primary flow to be incompressible.

In conclusion, it can be said that a positive contribution to thrust augmentation can be obtained only if at least a portion of the entrained air enters the system at an angle different from the exit flow angle. Also, the entrance area of the entrained flow should be as small as possible while the inlet momentum of the entrained flow should naturally be high.

If the momentum box is extended to include also the complete primary air supply unit (as, e.g., in an airborne self-contained vehicle) and if the inlet momentum of the flow into this unit is assumed to be parallel to and in the same direction as the outlet momentum ($\rho_s \cdot \vec{V}_s \cdot A_s$), then this inlet momentum must be subtracted from the resulting lift force of the thrust augmentation rig. Another case is the possibility of having the inlet momentum of the primary flow enter the air supply unit at right angles or even in the opposite direction to the final outlet momentum, and thus potentially optimizing the resultant thrust augmentation.

In addition, the flow over a Coanda surface entrains almost as much as a free jet entrains on both unbounded surfaces.

4.4 Theoretical Lift on the Coanda Surface

The major portion of the total lift is contributed by the Coanda surface. If one could define the primary flow

accurately as it flows around the Coanda surface, then, theoretically, the pressure difference across it, Δp, could be obtained by equating it to the centrifugal force, $\rho_1 \cdot t \cdot \overline{V_1^2}/R$. Thus the pressure on the Coanda surface, p_C, would be equal to the static pressure, p_s, on the free surface of the primary flow jet sheet minus the pressure difference, $\Delta p = p_s - p_C$, which is ideally constant for a given nozzle, quadrant, and pressure ratio. Assuming ambient atmospheric pressure below the Coanda surface of radius R, the lift on the quadrant becomes

$$R(P_a - p_C) = R(P_a - [p_s - \Delta p]) = R(P_a - p_s) + \rho_1 \cdot t \cdot \overline{V_1^2}$$

$$= \rho_1 \cdot t \cdot \overline{V_1^2} + \rho \cdot (R/2) \cdot V_s^2 \qquad (4\text{-}21)$$

where p_C is the pressure on the Coanda surface and $(P_a - p_s) = 1/2 \cdot \rho \cdot V_s^2$. Since R is 32 times the value of t for the 1/8-in. nozzle and 4.0-in. quadrant, it would seem that a large lift could be obtained if the flow velocity V_s, was high at the free surface of the primary flow. For a set value of d/t and α, the velocity of the secondary flow, V_2, can be increased by increasing the exterior top flap angle, β, and thus by decreasing the entrance area, A_2. However, if the secondary flow velocity remains high (and it does) at the surface of the exterior flap, then the gain in lift on the Coanda surface may be eliminated by the increased negative lift on the external flap, since there is a larger projected area in the horizontal plane if β is large.

5. PROCEDURE

5.1 PROCEDURE INDEPENDENT OF THE PRESSURE RATIO OR COANDA SURFACE USED

For any one of the three quadrants considered, the angles, α and β, and the channel width, d, were varied while the diffuser angles, γ and ϕ, remained constant at 6 deg and 0 deg respectively. Since the diffuser angles remained constant, the main change in the diffuser shape was caused by the variation of d, the channel width. One can see that for a given value of β and d, the height of the three exterior flaps (or augmenting surface) with respect to the Coanda surface can be varied by changing the angle α. However, by altering the length of the bottom exterior flap, N (Fig. 3), by extension pieces, the length of the diffuser can be maintained at a constant length equal to the length of the interior flap, M.

Before each run, the three external flaps were fixed at the desired positions corresponding to the required values of α, β, and γ. The zero readings for all the lift and drag strain gauges were then taken on the SR-4 strain indicators. In taking the zero force readings of the thrust augmentation flaps, care was taken to obtain the true values, i.e., to eliminate the friction between the sides of the flaps and the glass side plates which could cause the flaps not to return to the exact equilibrium position. The Palouste gas turbine engine was then started, the required pressure ratio was set, and the test readings were taken.

Next, the nozzle top fairing with its six flush pressure taps was placed on the nozzle, and the readings were observed on a water manometer board. The fairing pressure varied smoothly along this surface. Since physical limitations did not allow pressure taps to be located as far forward as the tip of the fairing, the pressure readings of the six pressure taps were extrapolated for the fairing tip pressure. Thus the lift on the nozzle could be calculated assuming ambient pressure on the lower side of the nozzle.

This lift, L_N, associated with the nozzle, was then added to the lift, L_B, exerted on the entire thrust augmentation rig, to give the total lift, L_T.

5.2 The Three-Inch Coanda Surface

The first Coanda surface (quadrant tested) was of 3-in. radius, and all the combinations of angles between 0 and 90 deg at 30-deg intervals (0°, 30°, 60°, 90°) for both α and β were considered while the channel width, d , was varied (i.e., combinations of $\alpha = 0^\circ, 30^\circ, 60^\circ, 90^\circ$ with $\beta = 0^\circ, 30^\circ, 60^\circ, 90^\circ$) for a pressure ratio of 1.50.

After these data had been collected, it was noted that when the total lift on the rig, L_B, was plotted against d (whether or not a fixed value of α or β was maintained) two general types of curves resulted. One type of curve indicated a monotonic increase in lift with d and an asymtotic approach to a value of lift approximately equal to the isentropic thrust, T_{hi}, of the primary flow. In other words, no thrust augmentation occurred (see, for example, Fig. 15a). However, with the other type of curves, the lift of the rig increased with d as before, but a maximum was reached for $d \simeq 3$ inches, which was greater than the isentropic thrust of the primary flow, T_{hi}. Then, as d was increased further the lift decreased toward a value approximately equal to T_{hi}. The characteristics of the second type of curves showed that there was a maximum vertical lift for d/t equal to about 26 where t , the thickness of the nozzle exit, is 1/8 in. It was also noted that the latter characteristics were strongest for the cases where:

(1) $\alpha = 30^\circ$, $\beta = 0^\circ$, $d/t = 26.0$ (Fig. 15b)

(2) $\alpha = 60^\circ$, $\beta = 30^\circ$, $d/t = 26.0$ (Fig. 13b)

(3) $\alpha = 90^\circ$, $\beta = 60^\circ$, $g/t = 60.0+$ (Fig. 23a)

where g (see Figs. 3 and 6) is the distance from the top of the quadrant next to the nozzle to the lip of the top exterior flap. In the last case where $\alpha = 90^\circ$, d is entirely dependent on the angle β ; thus the variable g/t is used since d/t remains constant if β is constant. Thus, case (3) is not as truly indicative as cases (1) and (2), since the vertical lift is highly dependent on the value of d/t.

However, the result did infer a possibility that a linear relationship may exist between α and β (i.e., $\alpha - \beta = 30^\circ$) for the cases where a maximum in thrust augmentation might occur.

To test whether a linear relationship did exist, the intervals at which the angles of α and β were changed were reduced to 10 deg from 30 deg. The effect of keeping β constant at certain values while α and d were varied was examined. Also, α was kept constant at specific angles while β and d were varied appropriately in consideration of the possible linear relationship. As observed from the results indicated in Figs. 23b, 24a and b, and 25a and b, the relationship $\alpha - \beta = 30^{\circ} \pm 2^{\circ}$ seemed to hold true for the lift on the thrust augmentation rig, using the 3-in. Coanda surface at a pressure ratio of $p_t/P_a = 1.50$.

5.3 The Two-Inch Quadrant

Next, the two-in. Coanda surface (as shown in Fig. 2a) was used in place of the three-in. quadrant, with the interior flap still vertical and the bottom external flap again at six degrees to the vertical. A test similar to that conducted for the three-in. quadrant was performed to see if there was still a linear relationship between α and β. As can be observed from Figs. 12 and 13, the relationship $\alpha - \beta = 40^{\circ} \pm 2^{\circ}$ seems to yield the maximum value of total lift, L_T, if d/t has a value of about 26. It should also be noted in Fig. 13a that for $\alpha = 90^{\circ}$, the maximum L_T is at β equal to about 54 deg since d, which increases with β, tends towards the optimum width of $d/t = 26$.

5.4 The Four-Inch Quadrant

Again using the same diffuser angles and a pressure ratio of 1.50, the four-in. quadrant was tested in a procedure similar to that outlined for the two preceding Coanda surfaces. It was observed that $\alpha - \beta = 20^{\circ} \pm 2$ for d/t equal to about 26 yielded the maximum set of total lifts, L_T. (See Figs. 32 and 33.)

5.5 Effect of Pressure Ratio

Keeping the four-in. quadrant in place, the pressure ratio, p_t/P_a, was increased from 1.50 to 1.89 and then to 2.00 for the same positions of α, β, and d. Consequently, the primary jet flow was sonic for the pressure ratio of 1.89 and underexpanded for the pressure ratio of 2.00, since the nozzle was subsonic in design.

The same angle relationship, $\alpha - \beta = 20^{\circ} + 2^{\circ}$, was observed again at the pressure ratios of 1.89 (Figs. 39 and 40) and 2.00 (Figs. 46 and 47). But the non-dimensional channel width, d/t, corresponding to the maximum lift was increased (from 26 at $p_t/P_a = 1.50$) to about 28 for the primary flow at sonic velocity. For the underexpanded flow, d/t was found to be between 28 and 30.

5.6 The Non-Dimensionalized Measured Forces

Each "non-dimensional" force was obtained by taking the actual measured force, F (reduced to pounds), and dividing it by the corresponding product of the mass flow, m, and $\sqrt{T}$, the square root of the total primary flow temperature in degrees Rankine. The values of $m \cdot \sqrt{T}$ are 0.342, 0.459 and 0.488 (slugs/sec. $\sqrt{^{\circ}R}$) for the pressure ratios of 1.50, 1.89 and 2.00 respectively and at the atmospheric pressure of 29.44 in. of mercury.

5.7 Definition of Thrust Augmentation

The definition of thrust augmentation used was the ratio of the measured "non-dimensional" total lift, $L_T/m\sqrt{T}$, to the ideal or isentropic "non-dimensional" jet thrust given by

$$\frac{V}{\sqrt{T_T}} = 2 \cdot R \cdot T \cdot \frac{\gamma}{\gamma-1} \frac{(p_t/P_a)^{\frac{\gamma-1}{\gamma}} - 1}{(p_t/P_a)^{\frac{\gamma-1}{\gamma}}} \quad . \qquad (5\text{-}1)$$

Thus

$$\Phi = \frac{L_T}{m\sqrt{T} \cdot V/\sqrt{T}} \quad . \qquad (5\text{-}2)$$

Assuming a nozzle exit area of exactly 1.00 sq. in. with a 1.50 pressure ratio, the isentropic thrust at an ambient pressure of 29.44 in. of mercury would be 12.45 lb. The measured value of $m \cdot \sqrt{T}$ was 0.342 slug/sec $\sqrt{^{\circ}R}$, while the ideal value for $V/\sqrt{T}$ for a pressure ratio of 1.50 is 36.2 ft/sec - $\sqrt{^{\circ}R}$. Thus the measured thrust, L_T, is 12.40 lb. The difference between the isentropic thrust

and the measured thrust is less than one percent (see Sec. 6.3.4 for an explanation). Also, the exit area of the 1/8-in. nozzle might be slightly larger than 1.00 sq. in.

5.8 Effect of Diffuser Angles

The variation of the total lift and drag was investigated at $\alpha = 60^\circ$, $\beta = 40^\circ$ and $d/t = 26$ for the four-in. quadrant. The interior flap angle, ϕ, was set at 0°, -1° and -2°; and γ, which was 6 deg throughout the previous experiments, was varied. The results are shown in Figs. 49 and 50. Figure 50b indicates a slight gain in the "non-dimensional" total lift for $\phi = -1^\circ$; but when ϕ is increased to -2°, the lift drops substantially. Note also that the diffuser yields the optimum L_T at an included angle of $\gamma - \phi = 6^\circ$ for all three values of ϕ.

Separation of flow seems to occur at $\gamma \geq 7^\circ$, as indicated, especially in Fig. 49b, by the sudden decrease in lift in the region of larger γ values. This was also observed by the DeHavilland Aircraft of Canada, Limited.

By the use of wool tufts, it was found that at $\phi = 0^\circ$ and $\gamma = 6^\circ$, the outlet flow was vertical, except very near the exterior flap, where the flow velocity was comparatively low. Even when ϕ was made negative, the exit flow remained mainly vertical.

Since the exit flow velocity profile (see Fig. 52b) was parabolic in shape with the maximum velocity at the center of the diffuser and the flow direction mainly vertical, little could be hoped to be gained by increasing the magnitude of ϕ and decreasing γ. However, it seemed odd that for $\phi = -2^\circ$ there is a definite decrease in lift. It is believed that this is due to the large suction pressure on the interior flap, especially near the Coanda surface, where the flow velocity is large. This suction pressure is just a result of the extension of the Coanda effect into the diffuser. (The magnitude of ϕ could be increased to, at least, minus 15 deg without separation of the flow at the bottom of the interior flap.) The pressure on the upper portion of the interior flap, where there is probably separation and reattachment, becomes more and more negative, causing a further decrease in lift as ϕ is increased in magnitude.

6. DISCUSSION OF RESULTS

6.1 THE LINEAR RELATIONSHIP OF α AND β

The linear relationship of $\alpha - \beta = 40^{\circ}$, 30° and $20^{\circ} \pm 2^{\circ}$ for the two-, three- and four-in. quadrant, respectively (where d/t has certain values depending on the pressure ratio), determines whether a maximum value of lift has been reached for a particular value of α or β). However, as noted in Figs. 13b, 33b, 39b, 46a, and 47b, the curves are relatively flat around the maximum. This indicates that the configuration defined by the relationship of $(\alpha - \beta)$ is not necessarily the only possible one whereby a maximum value of lift can be obtained for a particular value of α or β.

From the results obtained for the two- and three-in. quadrants, it can be seen that if the angle difference $(\alpha - \beta)$ is more than 20 deg from the observed constant optimum (40° for R = 2.0 in. and 30° for R = 3.0 in.), then the lift drops appreciably. This fact was made use of when the four-in. quadrant was tested. The range of varying α and β about the optimum value of $\alpha - \beta = 20^{\circ} \pm 2^{\circ}$ was therefore reduced.

Figures 14, 26, 34, 41, and 48, which indicate the variation of the non-dimensional lift and drag forces with α in accordance with the optimum linear relationship of α and β, show that the non-dimensional total lift is an almost constant maximum when β is larger than 20 deg and until α approaches 80 deg. These maximum total lift values are as listed below:

PRESSURE RATIO	MAXIMUM TOTAL LIFT, $L_T/m\sqrt{T}$ $(ft/sec\sqrt{^{\circ}R})$
1.50	43.0 to 43.5
1.89	52.0
2.00	53.25

However, if β is increased beyond 20 or 30 deg, it is evident that the non-dimensional lift, L_B, and drag, D_B, measured by the strain gauge balance, decrease slightly as α and β are continuously increased according to the linear relationship of $\alpha - \beta$ = constant.

Since L_B and D_B are highly dependent on the secondary flow inlet momentum, and since they both decrease simultaneously, it must be inferred that the secondary flow inlet momentum must decrease slightly with increasing α, or that the momentum flow must enter in a more vertical direction as α and β are increased. A combination of these two possibilities is highly likely as well as an increase in the negative pressure momentum term, $\lambda_2/2(\bar{V}_2)^2(1-\cos\alpha)(A_2)$, associated with an increas in α.

.2 The Secondary Flow Entrance

Even though the streamline angle of the secondary flow, ϵ', increases in general with α, there is no noticeable increase in the total lift when β is increased beyond 0 or 30 deg.

Take the momentum box defined in Fig. 4 with the secondary flow entrance defined by α''' (α''' is not necessarily equal to ϵ'''). It would be reasonable to assume that, in general, as α''' is increased, α''' increases faster than ϵ''', especially in the important region near the lip of the top exterior flap, where the momentum per unit area is the highest. This more rapid increase of α''' near the top flap's lip has the tendency to decrease the rig's lift (see Eq. 4-9).

In addition to the above detrimental effect while increasing α, the entrance area, A_2, of the secondary flow as illustrated in Fig. 6) does not decrease with α if α is increased beyond about 40 deg. The following three reasons may be responsible for the inability to decrease the area A_2 and consequently potentially to increase the lift:

(1) the acquiring of a favorable pressure gradient on the metal sheet joining the top and center exterior flaps.

(2) the blockage of the entrained flow.

(3) the velocity profile at the entrance, A_2.

6.2.1 Favorable Pressure Gradient

To achieve a favorable pressure gradient along the metal sheet (see Fig. 3) attached to the exterior flaps, the velocity of the flow along it should continually increase. This requires a continually converging cross-section. Figure 7 illustrates an optimum configuration for the four-in. quadrant where $\alpha = 60^{\circ}$ and $\beta = 40^{\circ}$. Also shown for $\alpha = 60^{\circ}$ are the configurations where β is 30° and 50°. Note that where β is less than 40 deg, the secondary flow channel is converging. For $\beta > 40^{\circ}$, the channel, initially convergent, begins to diverge. Consequently, future experimentation should include some variation of the distance at which the metal sheet begins to separate from the top exterior flap (as indicated as a dashed line for $\beta = 50^{\circ}$ in Fig. 7).

6.2.2 Blockage of the Secondary Flow

As stated in Ref. 3, obstruction of the secondary flow is a major reason for low values of thrust augmentation. Figures 1 and 2b show that blockage of the secondary flow can be caused not only by the nozzle in combination with the top exterior flap, but also by the settling tank, especially as α and β are increased.

6.2.3 Secondary Flow Velocity Profile

The obstruction to the secondary flow is reflected in the velocity profile across the entrance, A_2, as indicated in Fig. 51. For the optimum values of d/t, the velocity, and thus the inlet momentum per unit area, is highest near the lip of the top flap. This seems to be caused by the obstruction of the flow due to the settling tank and by the flow's enforced departure from its natural path of entrainment. For smaller values of α, this portion of the total inlet momentum is tending to flow in a less vertical direction than for higher values of α, where the flow along the lip of the top flap becomes more vertical. However, for the portion of the secondary flow nearer the nozzle, where the momentum per unit area is lower, increasing the values of α and β does cause that portion of the flow to enter at an angle more parallel to the axis of the nozzle (i.e., ϵ or ϵ' approach 90°).

Through flow visualization experiments, a closer inspection of the increase in momentum per unit area near the lip of the top flap as well as the magnitude of turning of the remainder of the secondary flow as a function of β and for certain values of α and d/t might be useful for improvements in the design of the secondary air inlet.

If the positions of maximum and minimum velocities could be interchanged, the lift on the Coanda surface could definitely be increased (high values of ϵ), while the negative lift on the top exterior flap would be decreased in magnitude (low ϵ). Thus the amount of thrust augmentation should be noticeably higher.

6.3 Thrust Augmentation

6.3.1 The Deflection of the Secondary Flow

As stated before, the important function of the top external flap was to lessen the vertical component of the inlet momentum without decreasing the actual magnitude of the inlet momentum. By increasing β from zero to 20 deg to 30 deg, this can be achieved to a certain extent. The possible gain in lift increases in proportion to the radius of the Coanda surface (although the maximum possible total lift is independent of the radius used). For a pressure ratio of 1.50, the optimum measured augmentation is four per cent for the two-in. quadrant, but almost seven per cent for the four-in. quadrant. The reason is that for the smaller quadrant, the velocity over the nozzle and secondary flow over the free surface of the primary flow over the Coanda surface is noticeably higher for the condition of $\beta = 0^{\circ}$ and $\alpha = 40^{\circ}$ for the two-in. quadrant than for the four-in. quadrant with $\beta = 0^{\circ}$ and $\alpha = 20^{\circ}$. This is illustrated in Figs. 8a, 15b, and 27a, where the static pressure over the

nozzle is inversely proportional to the radius and quite constant with the varying channel width. Thus a greater portion of the secondary flow (assuming approximately equal secondary mass flows) has a higher value of ϵ for the quadrants of lower radii, R. This leads to a higher initial lift, L_B, for $\beta = 0^\circ$ for small radii.

6.3.2 Lift on the Coanda Surface

Since the lift on the Coanda surface, excluding the thrust augmenting effects of additional surfaces, is, according to theory,

$$R(P_a - p_c) = R(P_a - p_s) + \rho_1 \cdot t \cdot \overline{V_1^2} , \qquad (4\text{-}21)$$

it follows that for a certain pressure ratio, nozzle, and $\beta = 0^\circ$, the lift should be a constant and independent of the quadrant's radius since $(P_a - P_s)$ could be considered to be approximately proportional to $(1/R)$ if the lift over the nozzle can be considered to be a reasonable representation of the magnitude of the secondary flow velocity, V_s, at the free surface of the primary flow.

A possible reason for the above-mentioned higher velocity of the non-entrained secondary flow over the Coanda surface for smaller radii is that in order for that portion of the secondary flow, which has not received direct energy transfer from the primary flow, to avoid undue total pressure losses, the secondary flow must be ideally irrotational. Thus, the velocity would tend to be inversely proportional to the magnitude of the radius of curvature of its streamlines. For a smaller radius quadrant, the radius of curvature of the secondary flow of the assumed interface between the primary and secondary flows over the Coanda surface would naturally be lower; thus the velocity would be higher. Of course, the frictional effects in the flow prevent a purely irrotational flow.

However, the total lift depends not only on the lift on the Coanda surface, but also on the magnitudes of the lift on the nozzle fairing and on that (usually negative) acting on the external flaps.

The lift on the exterior flaps is highly dependent on the static pressure on the underside of the top external

flap. Also, the velocity profile of the secondary flow at the entrance, A_2, (Fig. 51), indicates a low pressure and high velocity near the flap. For the same reason that the secondary velocity is approximately inversely proportional to the radius of curvature of its streamline over the Coanda surfaces, the velocity at the top flap and its lip can probably be decreased by increasing the radius of curvature of the lip at its bottom, thereby reducing the radius of curvature of the streamlines near the lip. If this velocity is reduced, then the negative lift on the top flap will be reduced. For this reason, as well as for obtaining a converging entrance channel, an optimum entrance as shown in Fig. 5 is suggested. This configuration is simply a curve that is the envelope of top and center flap surfaces shown in Fig. 6 for the four-in. quadrant.

6.3.3 Thrust Augmentation at Low Pressure Ratios

Using the four-in. quadrant with the flaps having the configuration corresponding to $\alpha = 60^\circ$, $\beta = 40^\circ$, $\gamma = 6^\circ$ and $\phi = 0^\circ$, the channel width, d, was varied for pressure ratios of 1.30 and 1.10.

For the pressure ratio of 1.30, a maximum value of thrust augmentation of 1.21 was obtained when d/t equaled 25.0.

Approximately the same thrust augmentation was measured for a pressure ratio of 1.10, with d/t being between 24 and 25. These values of Φ were identical with the maximum thrust augmentation for a pressure ratio of 1.50.

6.3.4 Change in Pressure Ratio with Constant Throttle Setting

An increase in the momentum of the primary flow should result if α and β are increased at a fixed primary total pressure, since the static pressure at the nozzle exit is decreased. However, for a total pressure, p_t, equal to 1.5 times the atmospheric pressure, P_a, the change in the actual pressure is less than 0.5 per cent. For example, for $p_t = 2.00$, the per cent change of p_t/P_a is still less than 0.75 per cent for the configurations investigated.

6.3.5 Lift on the External Flaps

As noted in Figs. 8 through 11, 15 through 23, etc., where the non-dimensional lift is plotted against, d/t, the lift on the external flaps increases rapidly as the channel width initially increases. Then, as the channel width is increased further, the flaps' lift approaches a value close to zero. The lift on the flaps (positive or negative) depends on the pressure difference acting across them and on the magnitude of projected horizontal area. If α and d are held constant, then the larger the value of β, the larger are both the pressure difference across the external flaps and their projected horizontal area. The lift on the exterior flaps can only be positive for a small angle of β, since only then is the projected horizontal flap area small, allowing the flow over the lip of the top flap to cause a positive contribution to the lift. The velocity of the flow over the lip is increased the closer the lip is to the primary flow, or the smaller the entrance areas. (Compare the values of $L_F/m\sqrt{T}$ in Figs. 27b, 28a, and 28b, where the maximum value of L_F is for $\beta = 20^\circ$.)

However, when the pressure ratio is increased, any positive contribution of the external flaps decreases (see Figs. 41 and 48) and even becomes negative for the respective values of optimum channel width and low values of β. It seems that the pressure and frictional forces on the bottom exterior flap (at $\gamma = 6^\circ$) offset the gain attributed to the lip of the top flap with increasing pressure ratio.

For the tests where the internal flap was vertical ($\phi = 0^\circ$), the magnitude of the distance between the curves, $L_B/m\sqrt{T}$ and $L_F/m\sqrt{T}$, for any value of d/t represents the quantity of non-dimensional lift on the Coanda surface alone (see Figs. 8 through 11, 15 though 23, 27 through 31, etc.).

6.3.6 Drag on the External Flaps, D_F

The drag is, of course, due to the same pressures as the lift, except that now the projected vertical areas, instead of the projected horizontal flap areas determine its magnitude. Since the projected vertical area of the lip of the top flap is negligible, the drag force on the thrust augmenting surface acts inward or in the negative direction. Only when d/t is large enough so that the velocity of the secondary flow near the exterior flap is small does the flaps' drag approach zero.

6.3.7 Lift on the Nozzle Fairing, L_N

Since there is a decrease in pressure over the nozzle toward its exit, caused by the secondary flow velocity increase, there will be a resultant lift due to the pressure difference across the nozzle. As noted in Figs. 8 through 11, 18 and 22, and 27 through 31, a maximum lift on the nozzle is approached as d/t is increased from zero. The value of d/t where the maximum nozzle lift occurs is usually less than that value of d/t corresponding to the maximum value of total lift. As d/t is increased further, the nozzle lift, L_N, decreases to a value corresponding to an unshrouded Coanda surface and nozzle (but this value is not zero).

The maximum nozzle lift is the result of (a) an increase in the secondary flow velocity due to a decrease in its entrance area, A_2, and (b) the effect of blockage to the secondary flow entrainment, created by the boundary of the exterior flaps. Assuming that α and β as well as the entrained secondary mass flow remain constant, the smaller the entrance area, the larger is the velocity of the secondary flow over the nozzle fairing. However, the entrained mass flow is not constant with respect to d/t, for there are blockage or interference effects on the secondary flow mixing by the external flaps. As the exterior flaps are moved farther out, this blockage or obstruction to entrainment will be decreased and the secondary mass flow will consequently increase.

6.3.8 Lengthening of the Diffuser

In order to maximize the kinetic energy of the exit flow, an optimum amount of mixing should be achieved. Upon lengthening the diffuser in increments of three in. up to one foot, above that length of M used during most of the experiments (see Figs. 1 and 2b), no significant increase in total lift was observed. Thus, it could be concludeded that the initial length of the diffuser was sufficient.

6.4 Suggestions for the Increase of Thrust Augmentation

1. At present, the flexible metal sheet joining the two top exterior flaps does not provide a continuously converging channel for large values of β and, consequently, smaller secondary flow entrance areas, A_2. In order that a favorable pressure gradient may exist throughout the entrance

channel, the metal sheet should be fastened to the top external flap so that it would be able to diverge from the top flap to a larger extent. Thus, for a given value of α and d/t, β may be increased to a further extent than before, and yet a converging channel may still be maintained. Also, the middle exterior flap angle, δ (Fig. 3), could be varied so as to form an optimum shaped channel (especially for $\alpha = 90^{c}$).

2. For any flow to be isentropic, the velocity of that flow must be inversely proportional to the radius of curvature of its streamlines. Consequently, it might be advisable to increase the radius of curvature as the lower portion of the lip attached to the top external flap. If the entrance area, A_2, of the secondary flow (proportional to the proximity of the top flap to the primary flow) is not altered, then the velocity along the top external flap should decrease, leading to a decrease in magnitude of the negative lift on the exterior flaps for large values of β.

Figure 5 illustrates both a continuously converging channel and a large radius of curvature on the lower portion of the lip.

3. If it is desirable to change the constant angle difference $(\alpha - \beta)$ in the linear relationship of α and β while keeping the radius of the quadrant constant, then the length of the top flap could be altered. However, it is believed that small changes in length will affect the total lift no more than a change in the radius of the quadrant.

4. According to Ref. 4, related increases in the horizontal and vertical distances of the quadrant from the nozzle exit will cause a lift increase on the Coanda surface. This is due to the decrease in primary flow velocity over the surface caused by the air entrained into the jet sheet underside, whereby the frictional losses along the Coanda surface are decreased.

The maximum possible angle ϵ of the secondary flow at the secondary entrance was 90 deg (due to the boundary created by the nozzle). However, in the case of horizontal and vertical gaps (on the upper side of the jet sheet), the angles of entrainment could range between 90 deg and 180 deg on the lower side (corresponding to high angles of ϵ' for the secondary flow).

5. According to verbal information obtained from experiments performed at the DeHavilland Aircraft Company of Canada, Ltd., and at the National Research Council of Canada, Ottawa, thrust augmentation devices using the Coanda effect were greatly improved by the introduction of a tertiary flow entrance below the Coanda surface. The interior flap, then separate from the quadrant and having a suitable lip, should be adjusted vertically, horizontally, and angularly with respect to the quadrant.

6. In Ref. 5, a four-in. quadrant was used with 1/8-in. nozzle ($l = a = 0$). It was found that if the quadrant was rotated through 20° (such that the top of the quadrant was rotated away from the nozzle), the lift on the quadrant was increased.

This increase came about because the flow was rotated in such a way that the outlet momentum became a maximum in the vertical direction.

For a fixed channel width, d, the practical diffuser angle or the boundaries of the flow in the thrust augmentation rig diffuser are restricted by (a) separation along the exterior flap ($\gamma > 7^{\circ}$) and (b) the increase of negative pressure along the upper portion of the interior flap (due to the Coanda effect) with the increase in magnitude of ϕ. Since two requirements for high thrust augmentation are a high value of A_{32} (maximum of two theoretically) and efficient mixing, it might be advisable to turn the Coanda surface and possibly obtain a high area ratio, A_{32}, along with more efficient mixing. Also with the increase of A_{32}, the negative pressures along the flaps may be reduced. Furthermore, a tertiary entrance may become more effective.

7. From the results obtained from theory as well as from the velocity and pressure profiles of the secondary flow (Fig. 51), another inlet (see point "A" in Fig. 5) just above the diffuser on the exterior flap side would be desirable. Thus the secondary flow would be allowed to enter at angles of up to -180° even for high values of α. (In the present configuration, the flow angle would be limited to $+90^{\circ}$ by the nozzle.) Furthermore, this air inlet in the exterior flaps would allow the entrained flow to enter in a more natural direction and may consequently increase the efficiency of the mixing. Also, by lessening the enforced departure of the entrained flow from its natural path of entrainment (that path of the entrained flow if no exterior

flap was present), the negative pressure causing a negative lift for higher values of α on the top exterior flap would be greatly diminished.

With the problem of obstruction to the secondary flow decreased by a suitably shaped exterior flap entrance, the flap angle, α, could be made more effective by increasing the entrance angles, ϵ or ϵ', while a high velocity may still be maintained for the primary air flowing over the Coanda surface, V_s (see Sec. 4.4), by decreasing the entrance area, A_2, appropriately.

7. CONCLUSIONS

The following conclusions can be drawn from the presented experimental results:

1. The Maximum Total Lift Is Independent of the Radius of the Coanda Surface

When a pressure ratio of 1.50 or less (1.30 and 1.10) was used, the thrust augmentation for the three Coanda surfaces used was at a maximum between 1.20 and 1.21. However, when the primary flow was approximately sonic, the thrust augmentation ratio was only a little greater than 1.16. When the pressure ratio was increased to 2.00, the thrust augmentation ratio, Φ, decreased slightly to a little less than 1.16 for the subsonic nozzle.

Consequently, it would seem that as the pressure ratio is increased above 1.50, the thrust augmentation ratio decreases. This is in accordance with the theory which indicates that the highest thrust augmentation is obtained when the flows are incompressible. Also, frictional effects are less for smaller velocities.

2. The Most Effective Increase Is in Total Lift Due to the Variable Top External Flap

Under the present experimental conditions, little gain in the total lift, L_T, if any, is obtained by increasing the angle β of the top exterior flap beyond 20 or 30 deg. The gain in total lift that can be obtained by increasing β from 0° (which corresponds closely to the use of one single inflexible exterior flap) increases as the radius of the Coanda surface is increased, even though the maximum total lift remains constant for a constant pressure ratio. For a pressure ratio of 1.50, the possible gain in total lift obtained by altering β from zero degrees is approximately four per cent for the two-in. quadrant and is almost seven per cent for the four-in. quadrant.

When the pressure ratio is increased to 1.89 and 2.00, the ratio of the maximum lift (at $\beta \geq 20^\circ$ and $\alpha < 80^\circ$) to that lift obtained for $\beta = 0^\circ$ is about 1.05.

3. **The Maximum Thrust Augmentation Decreases as Pressure Ratio Increases**

As the pressure ratio was increased beyond 1.50, there was an appreciable decrease in maximum thrust augmentation. A large portion of this decrease is caused by the low aspect ratio of the thrust augmentation rig resulting in large frictional losses for high-velocity flows.

BIBLIOGRAPHY

1. Von Karman, T., "Theoretical Remarks on Thrust Augmentation," Reissner Anniversary Volume - Contributions to Applied Mechanics, 1949.

2. Chisholm, R. G. A., "Design and Calibration of an Air Ejector to Operate Against Various Back Pressures," UTIA, Technical Note No. 39, September 1960.

3. Simonson, A. J., and Schmeer, James W., "Static Thrust Augmentation of a Rocket-Ejector System with a Heated Supersonic Primary Jet," NASA, Technical Note D-1261, 1962.

4. Korbacher, G. K., "The Coanda Effect at Deflection Surfaces Detached from the Jet Nozzle," Can. Aero. and Space Journal, Vol. 8, No. 1, January 1962.

5. Bailey, A. B., "Use of the Coanda Effect for the Deflection of Jet Sheets Over Smoothly Curved Surfaces," UTIA, Technical Note No. 49, August 1961.

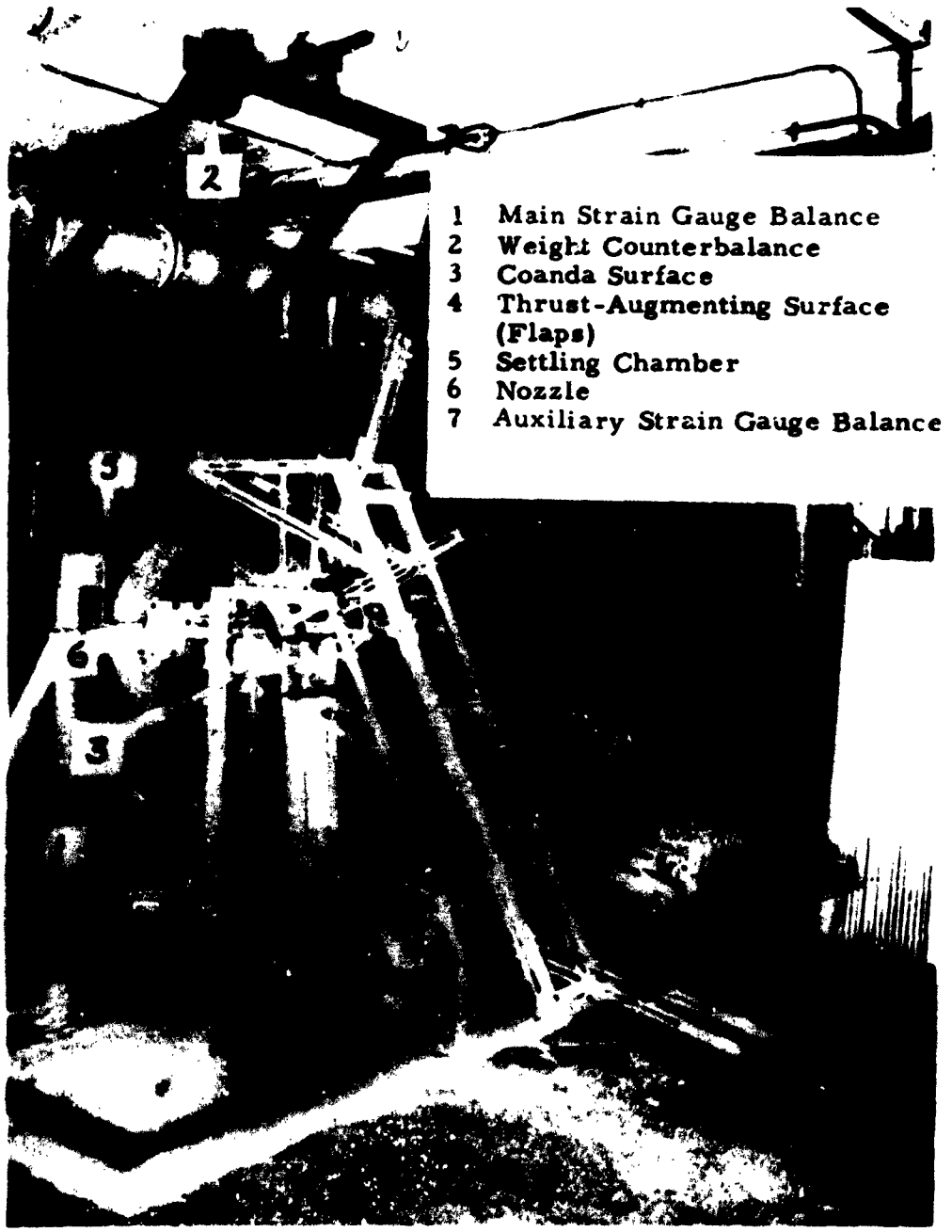

FIG. 1 THE THRUST AUGMENTATION TEST RIG AND SETUP

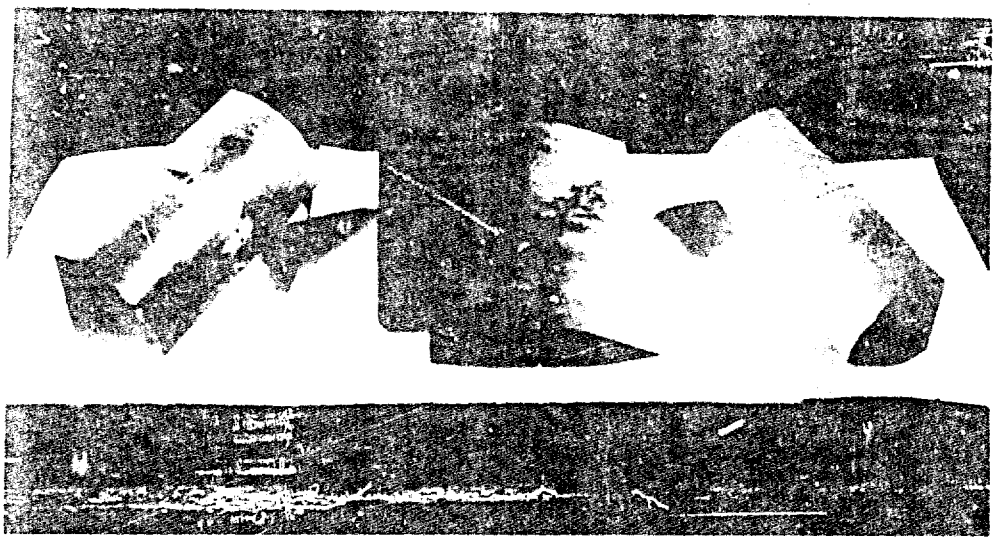

FIG. 2(a) COANDA SURFACES (2- and 3-Inch Radii) AND THE NOZZLE FAIRING

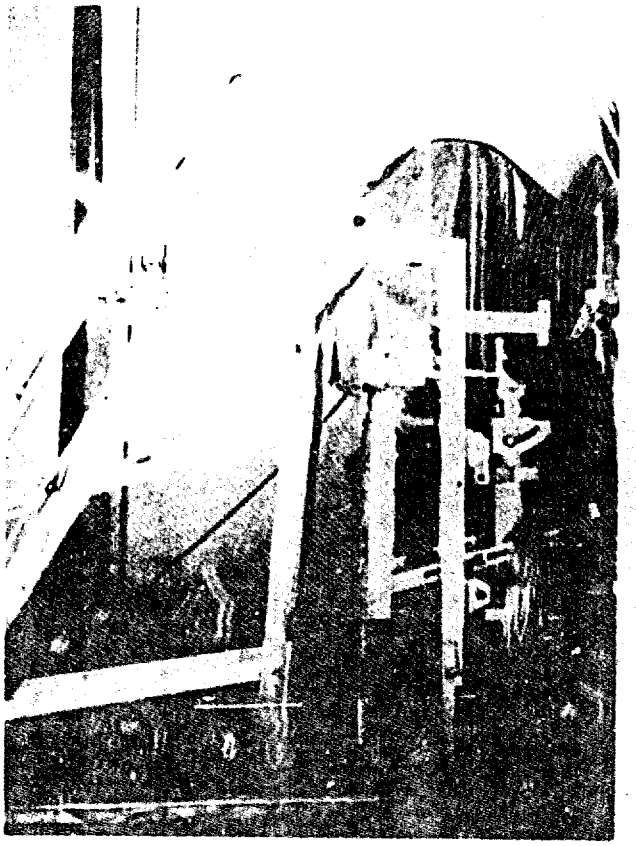

FIG. 2(b) THE THRUST-AUGMENTING SURFACES, QUADRANTS, AND NOZZLE

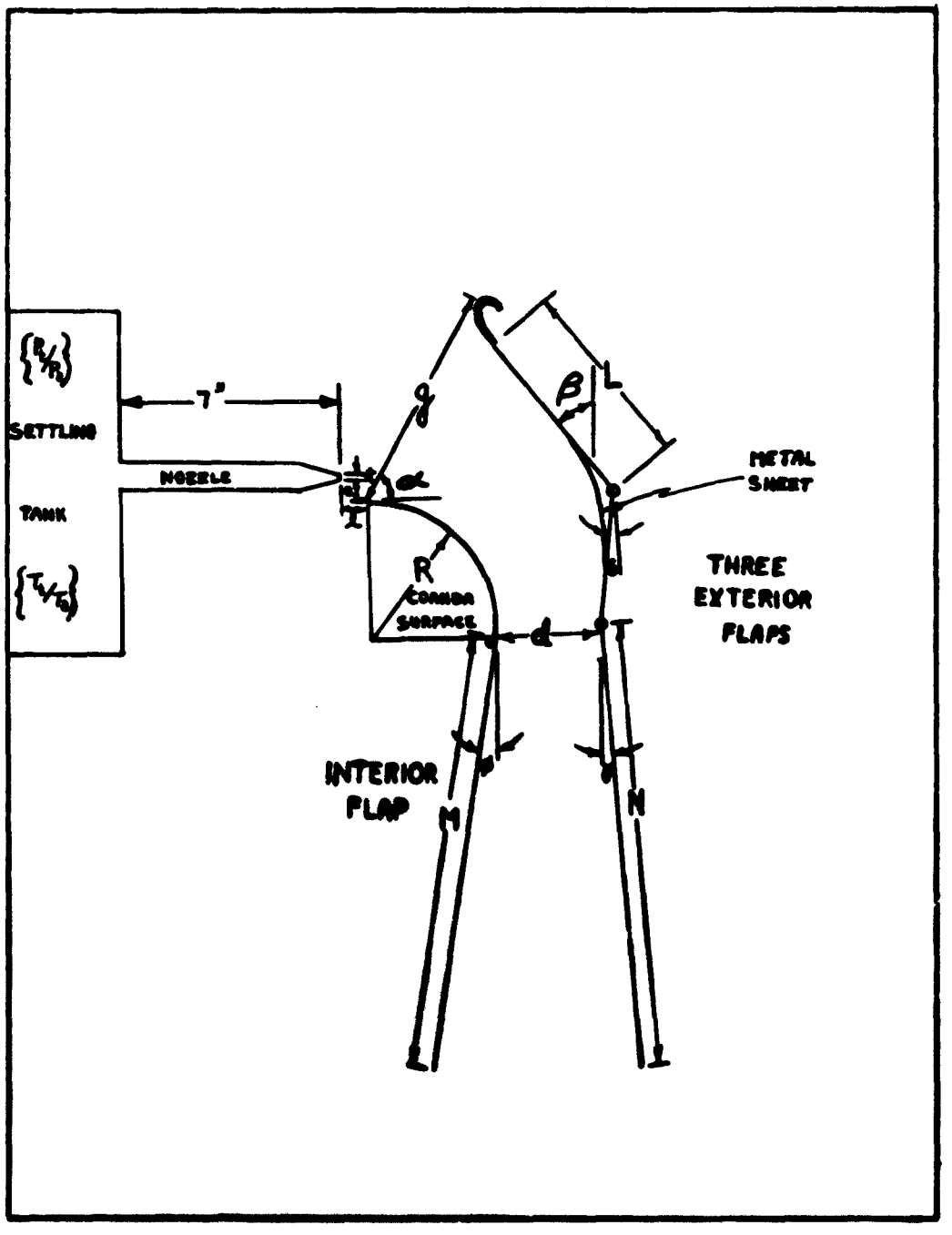

FIG. 3 SCHEMATIC DIAGRAM ILLUSTRATING THE FIFTEEN INDEPENDENT VARIABLES

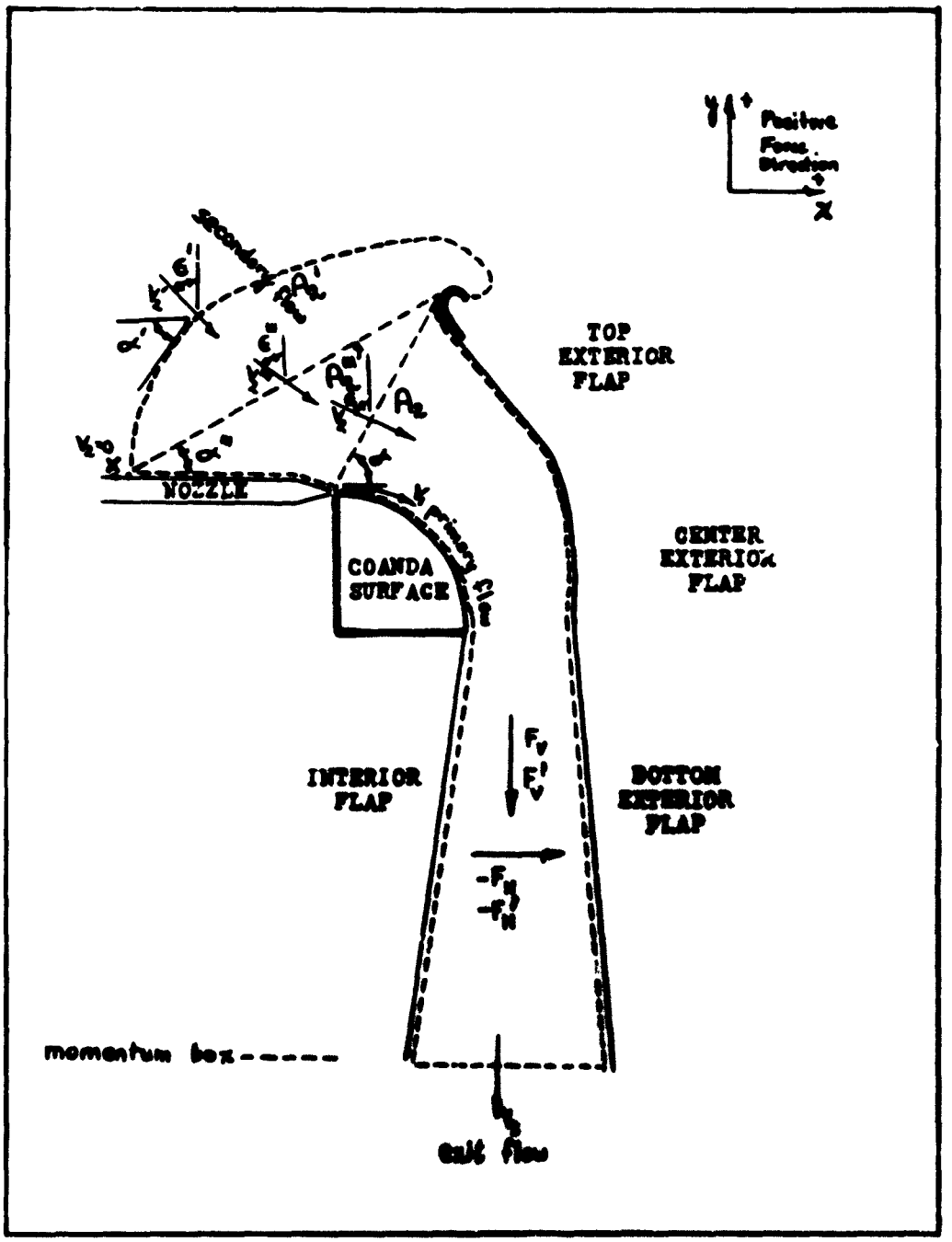

FIG. 4 DIAGRAM INDICATING THE VARIABLES OF THE MOMENTUM BOXES

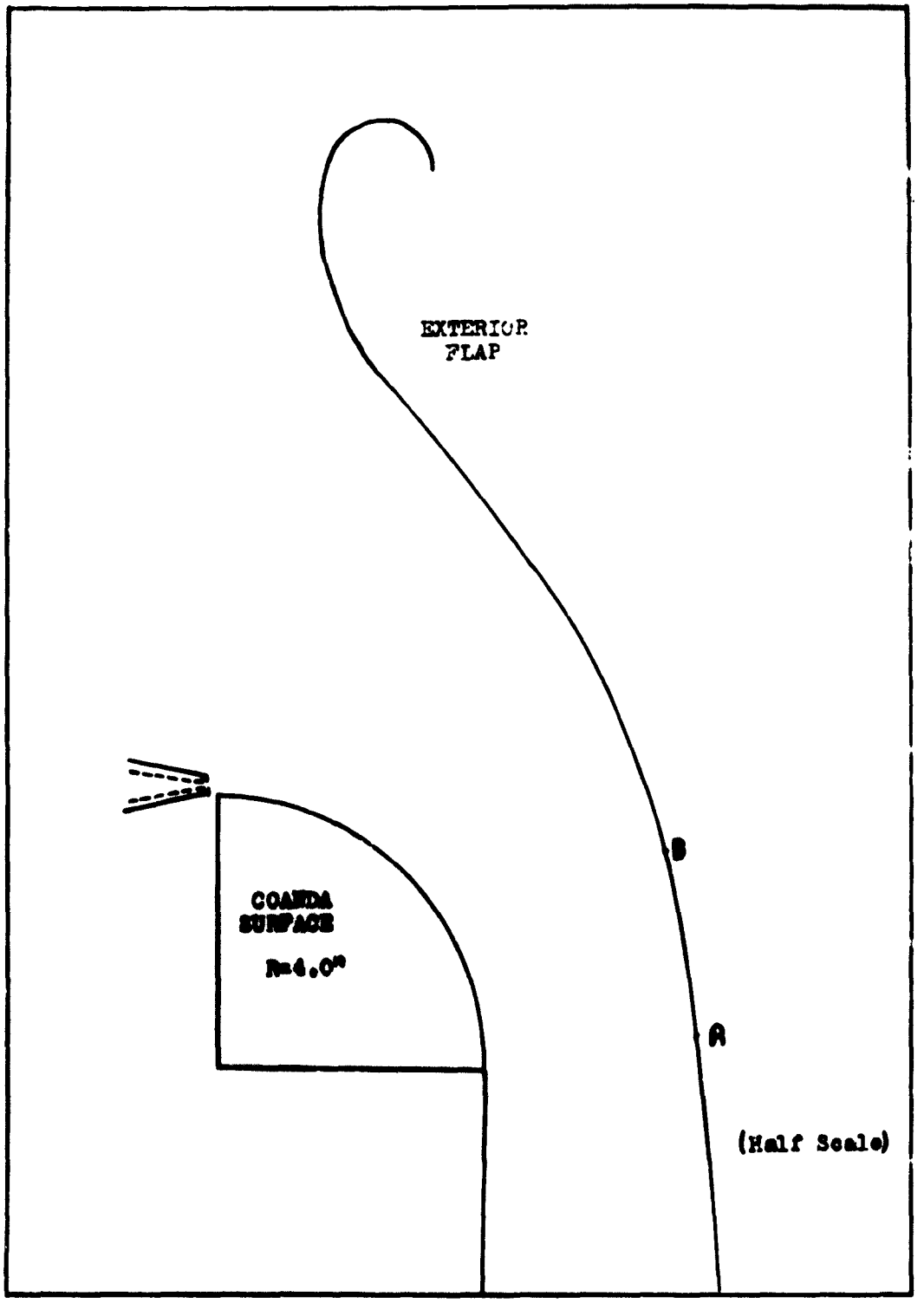

FIG. 5 PROPOSED DESIGN OF THE SECONDARY FLOW CHANNE

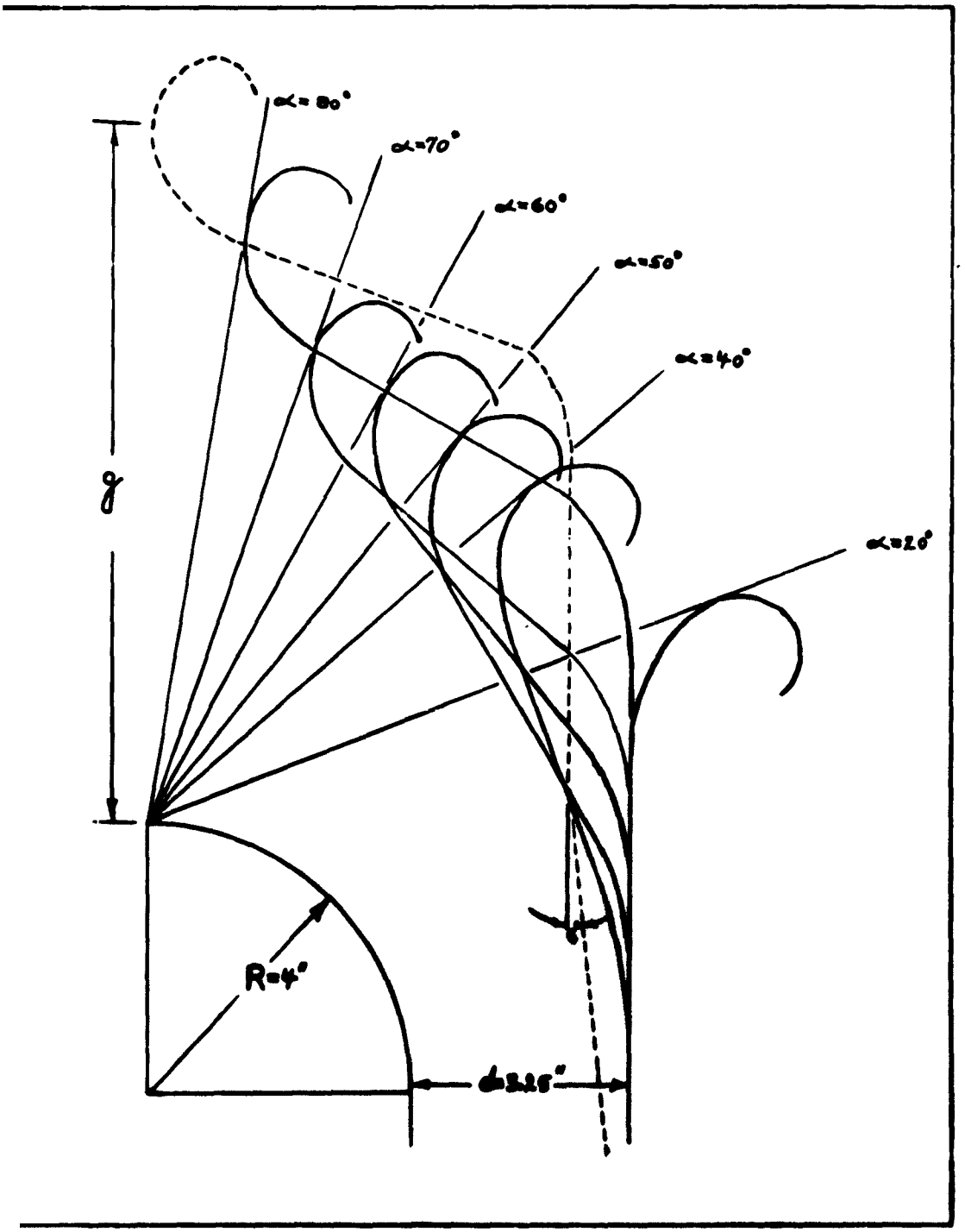

6 CONFIGURATION OF THE EXTERNAL FLAPS IN RESPECT TO THE FOUR-INCH COANDA SURFACE WHERE $\alpha - \beta = 20^{\circ}$ AND d = 3.25 Inches

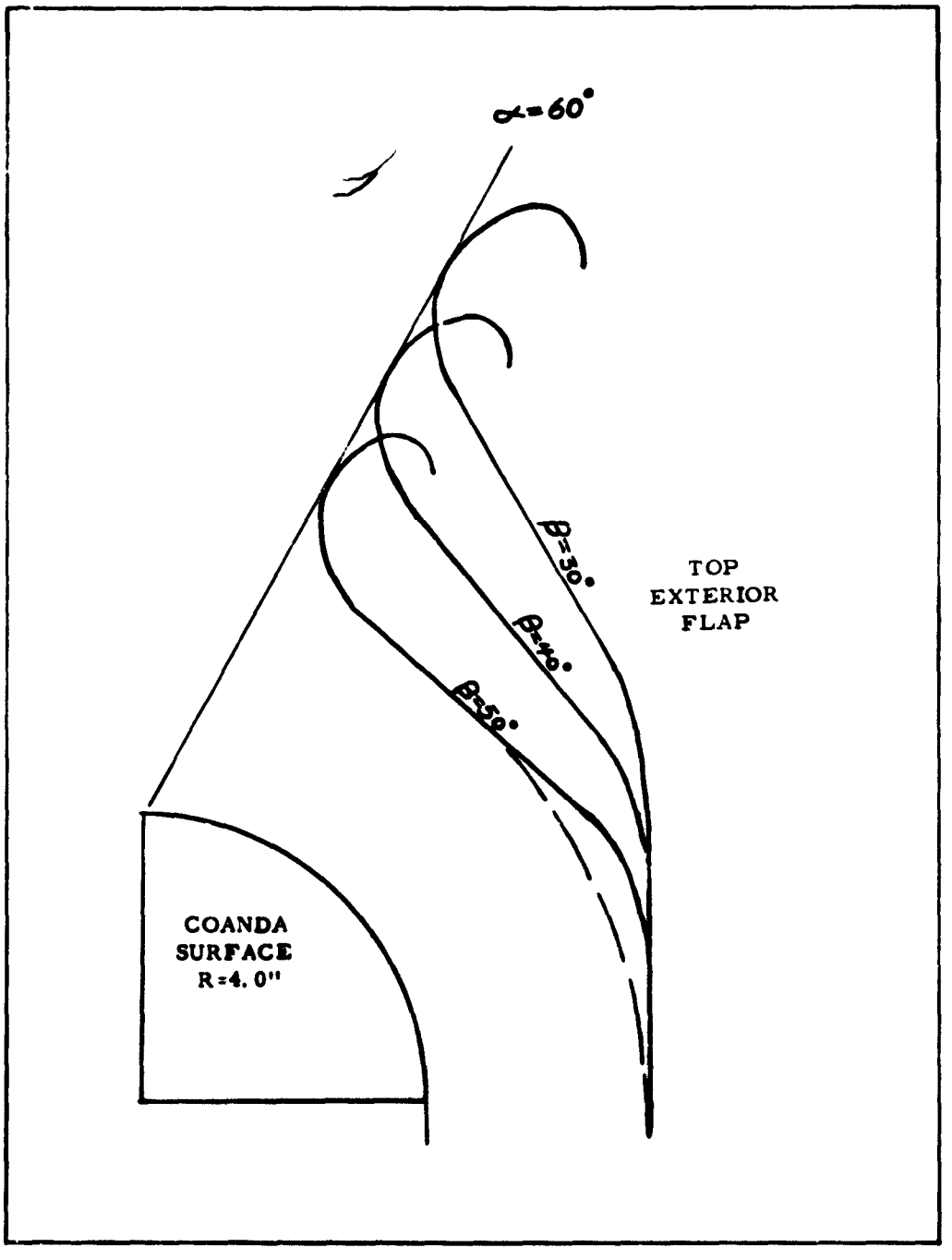

FIG. 7 CONFIGURATIONS OF THE TOP EXTERNAL FLAP FOR $\alpha = 60^{o}$ WITH THE FOUR INCH QUADRANT.

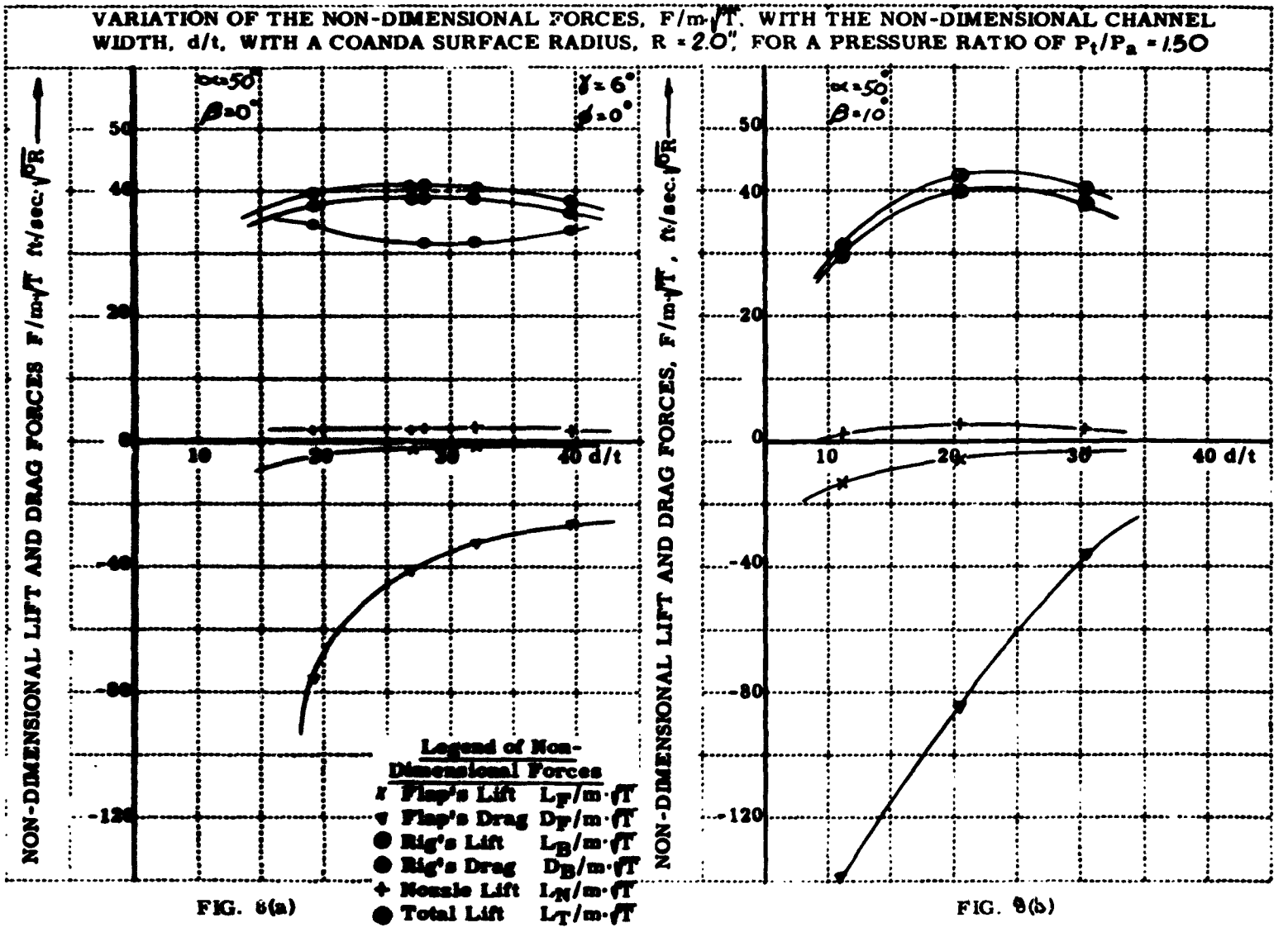
VARIATION OF THE NON-DIMENSIONAL FORCES, F/m·√T, WITH THE NON-DIMENSIONAL CHANNEL WIDTH, d/t, WITH A COANDA SURFACE RADIUS, R = 2.0", FOR A PRESSURE RATIO OF Pt/Pa = 1.50
NON-DIMENSIONAL LIFT AND DRAG FORCES F/m·√T ft/sec.·√R
α=50
β=0°
γ=6°
φ=0°
50
40
20
0
-40
-80
-120
10
20
30
40 d/t
Legend of Non-Dimensional Forces
Flap's Lift LF/m·√T
Flap's Drag DF/m·√T
Rig's Lift LR/m·√T
Rig's Drag DR/m·√T
Nozzle Lift LN/m·√T
Total Lift LT/m·√T
NON-DIMENSIONAL LIFT AND DRAG FORCES, F/m·√T, ft/sec.·√R
α=50°
β=10°

FIG. 8(a)

FIG. 8(b)

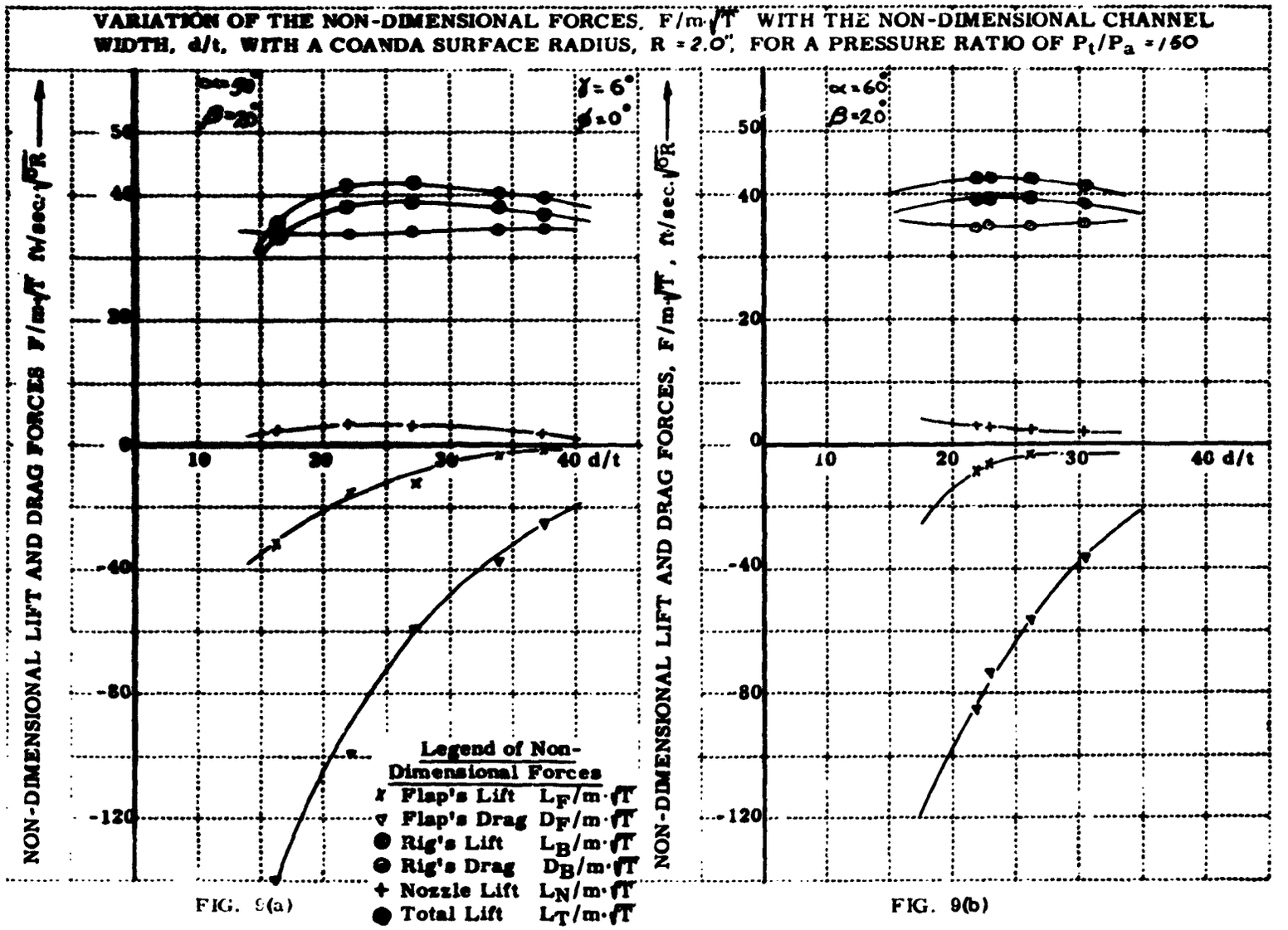
VARIATION OF THE NON-DIMENSIONAL FORCES, F/m·√T WITH THE NON-DIMENSIONAL CHANNEL WIDTH, d/t, WITH A COANDA SURFACE RADIUS, R = 2.0", FOR A PRESSURE RATIO OF Pt/Pa = 1.60
NON-DIMENSIONAL LIFT AND DRAG FORCES F/m·√T ft/sec.·√R
γ = 6°
φ = 0°
α = 60°
β = 20°
50
40
20
0
-40
-80
-120
10
20
30
40 d/t
Legend of Non-Dimensional Forces
Flap's Lift LF/m·√T
Flap's Drag DF/m·√T
Rig's Lift LB/m·√T
Rig's Drag DB/m·√T
Nozzle Lift LN/m·√T
Total Lift LT/m·√T

FIG. 9(a)

FIG. 9(b)

VARIATION OF THE NON-DIMENSIONAL FORCES, $F/m\cdot\sqrt{T}$, WITH THE NON-DIMENSIONAL CHANNEL WIDTH, d/t, WITH A COANDA SURFACE RADIUS, R = 2.0", FOR A PRESSURE RATIO OF P_t/P_a = 1.50

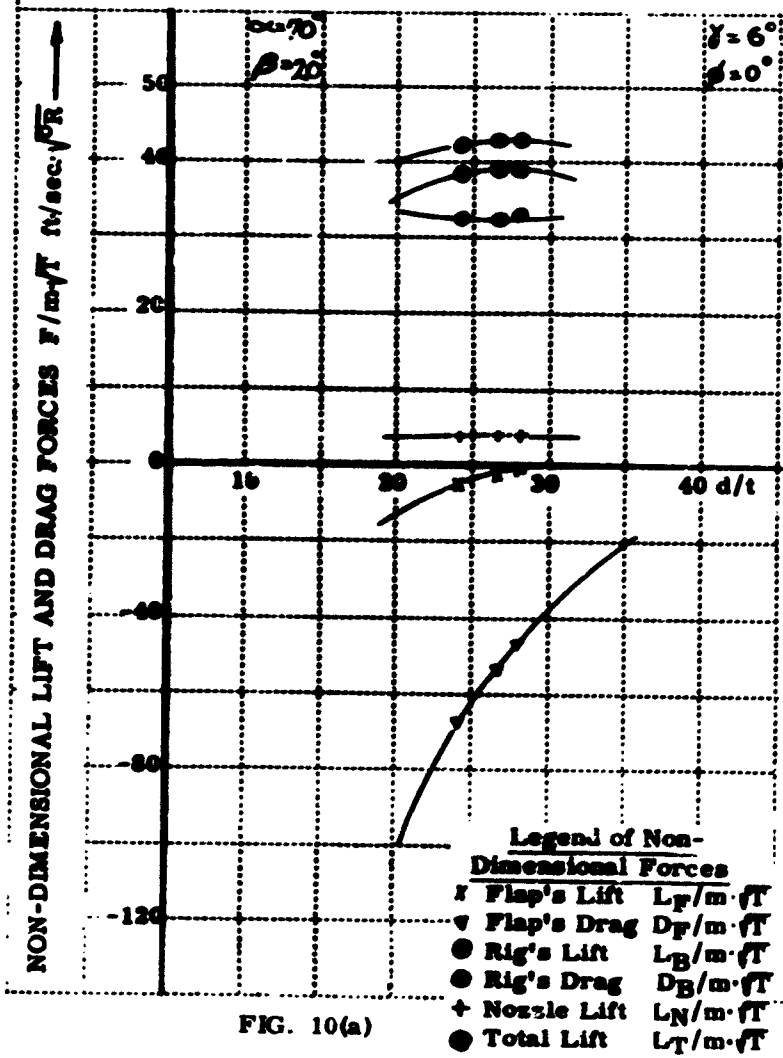

FIG. 10(a)

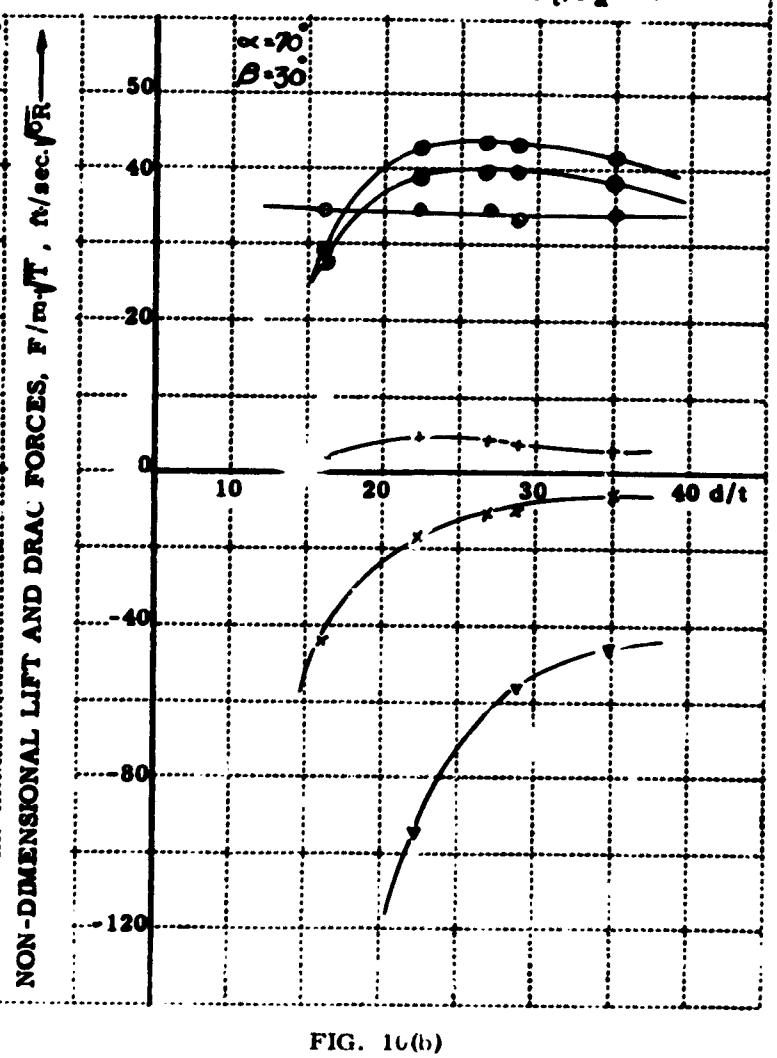

FIG. 10(b)

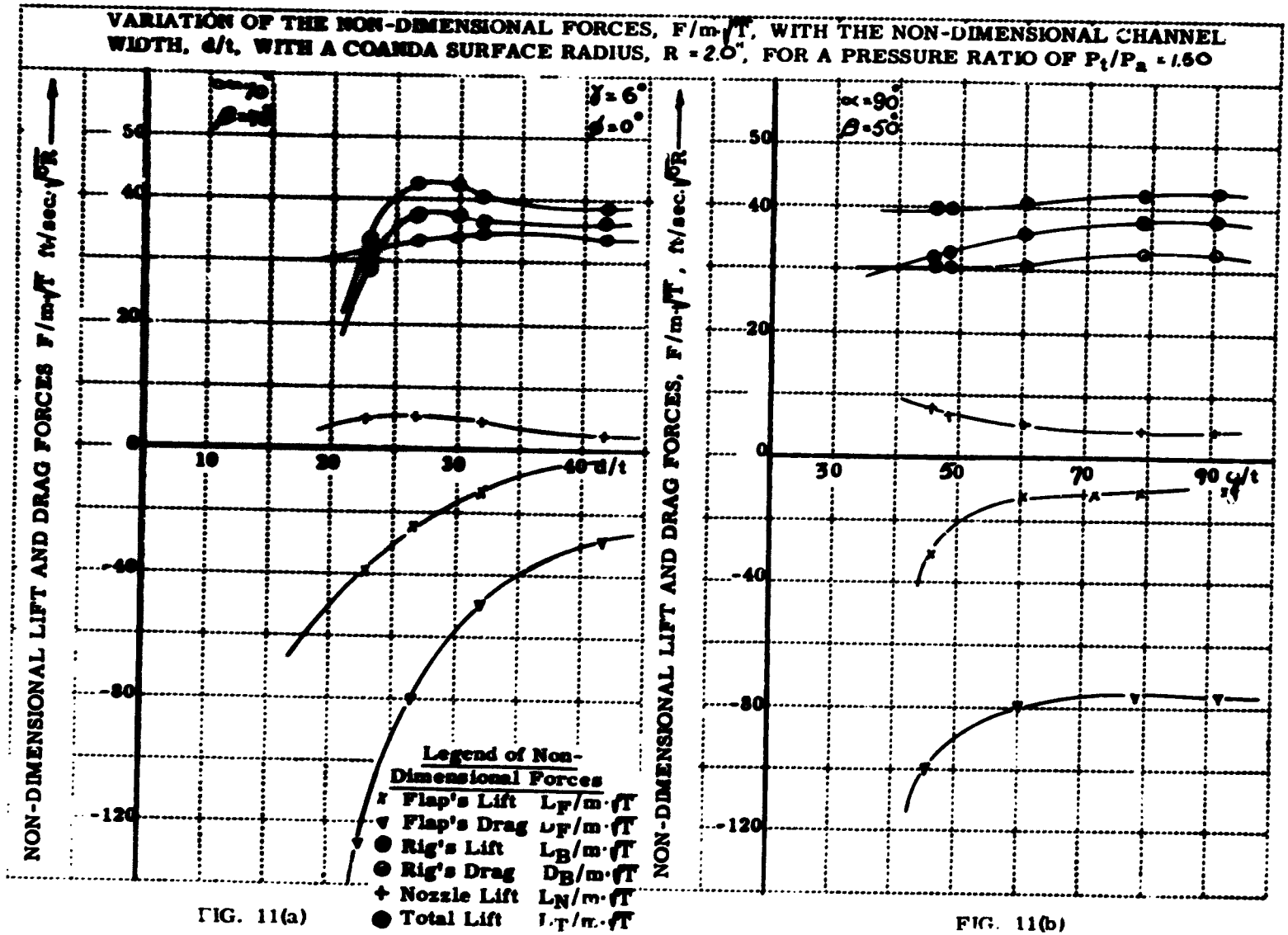

FIG. 11(a)

FIG. 11(b)

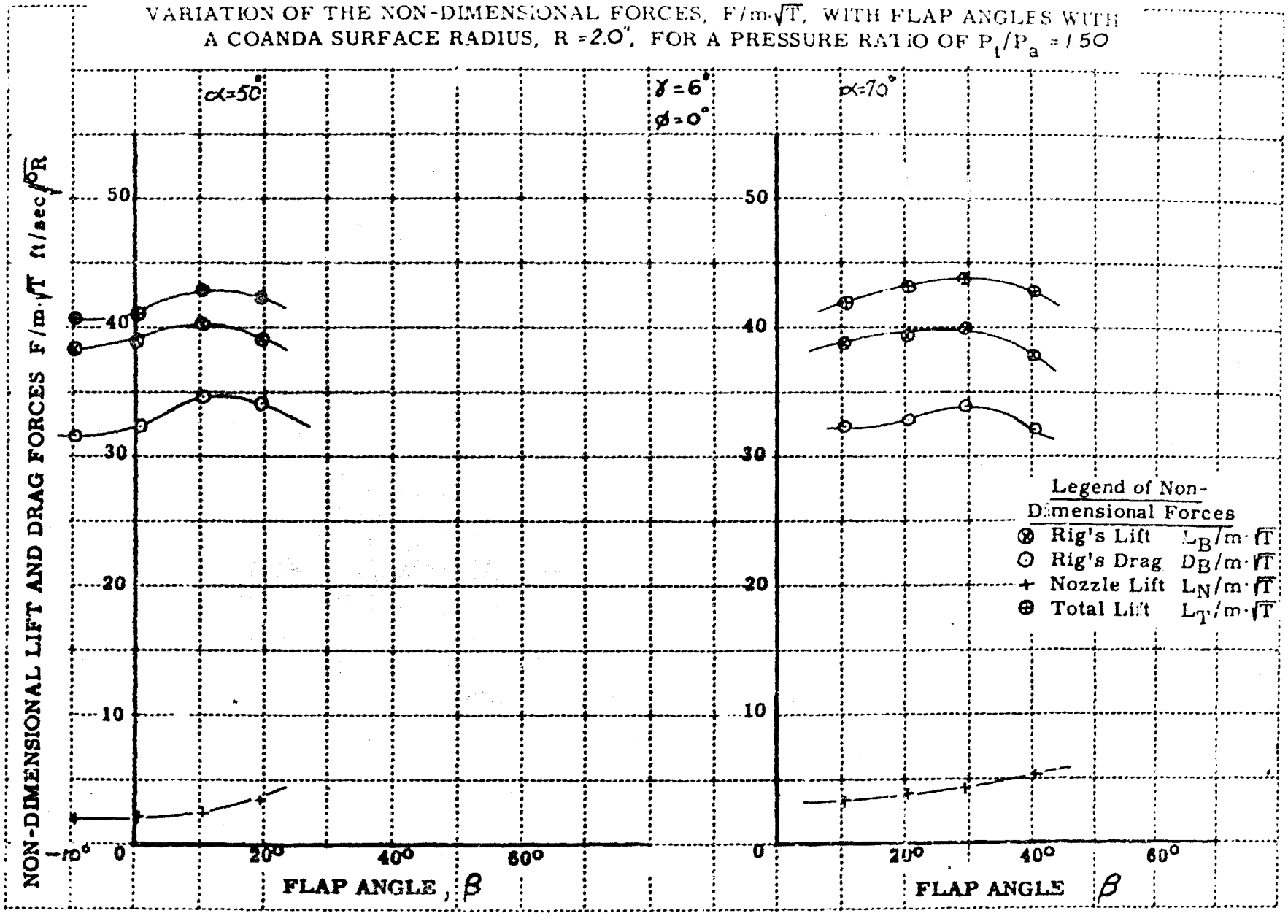

FIG. 12(a)

FIG. 12(b)

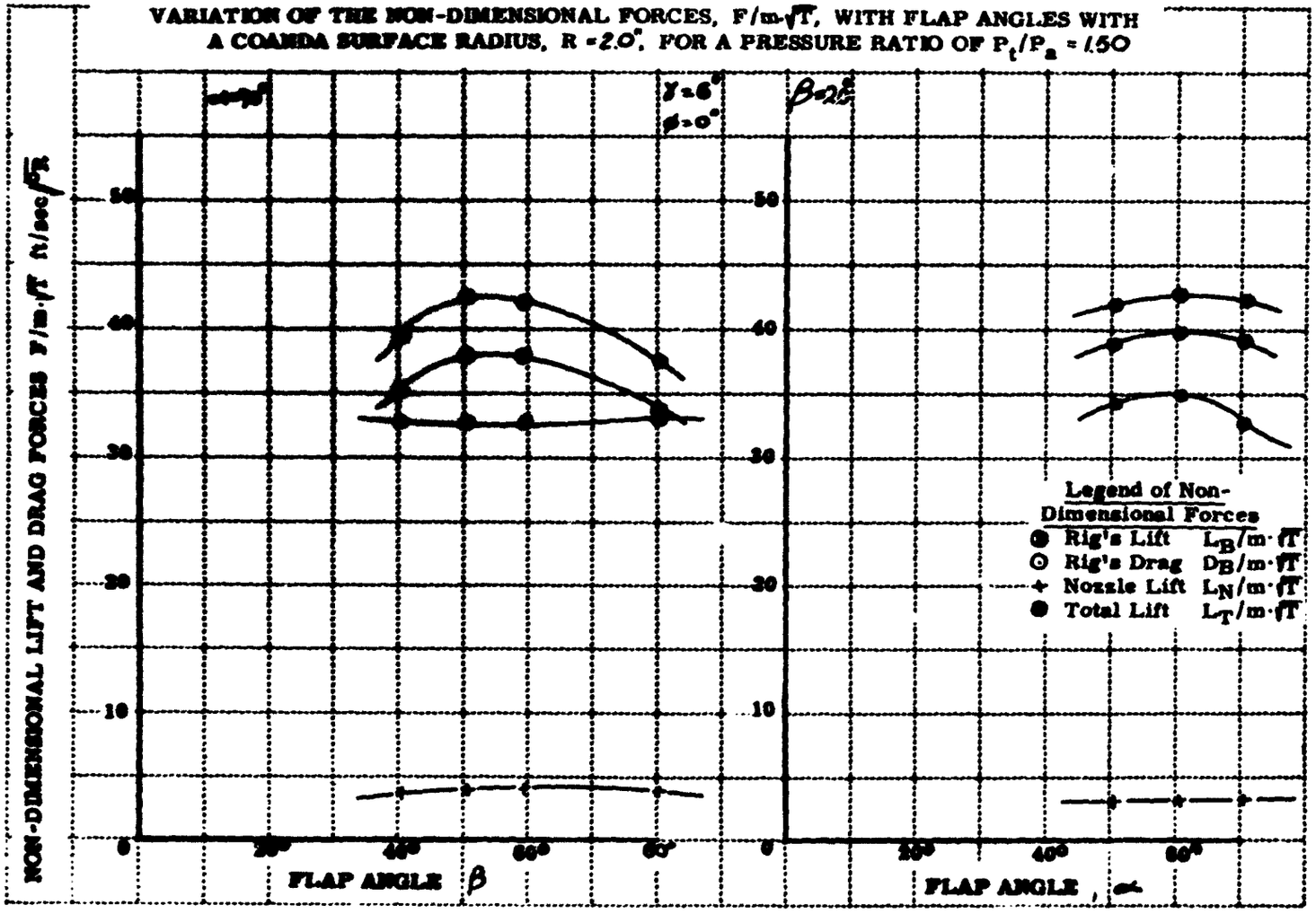

FIG. 13(a)

FIG. 13(b)

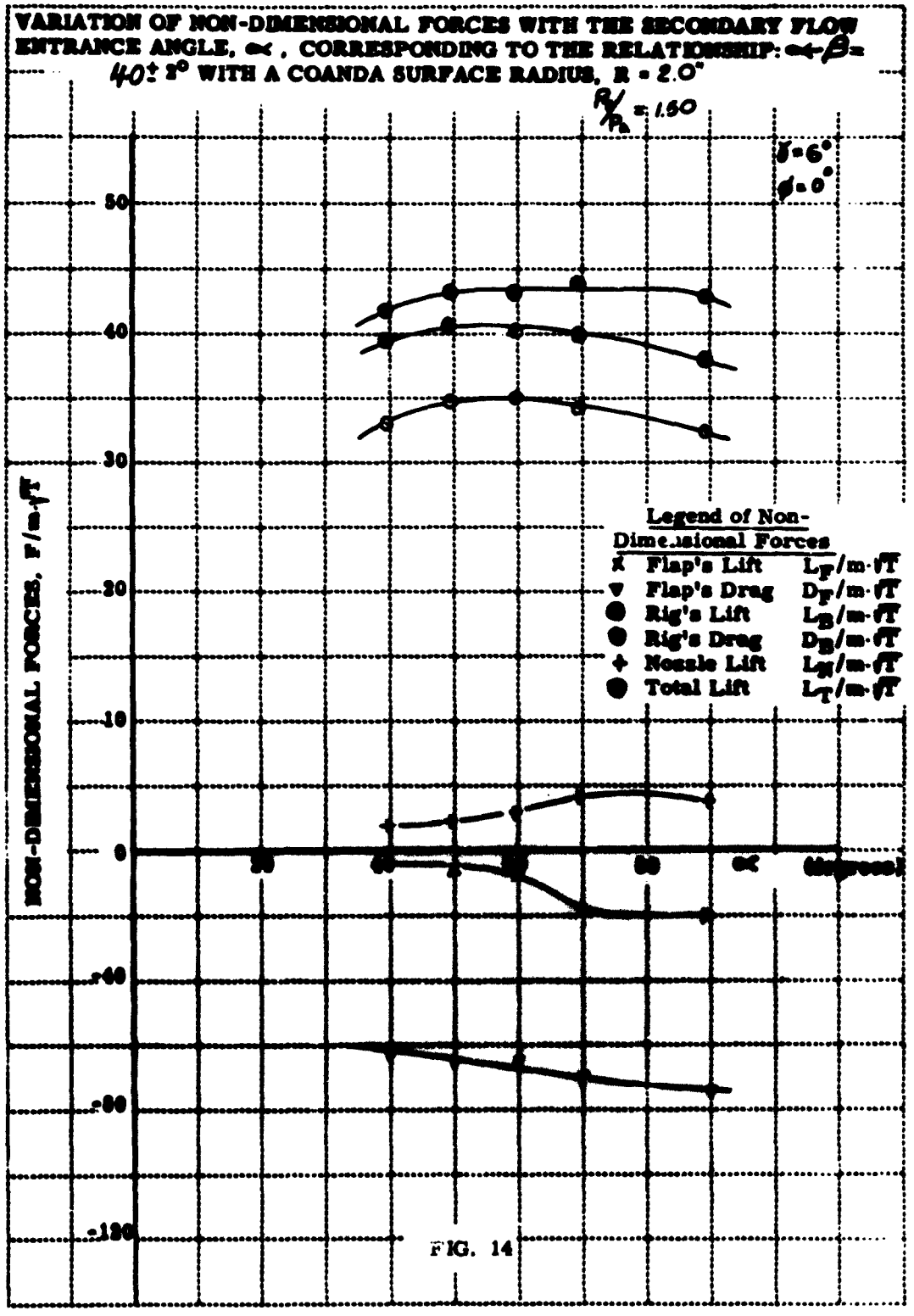
VARIATION OF NON-DIMENSIONAL FORCES WITH THE SECONDARY FLOW ENTRANCE ANGLE, ∝, CORRESPONDING TO THE RELATIONSHIP: ∝+β= 40± 2° WITH A COANDA SURFACE RADIUS, R = 2.0"
P/Pa = 1.50
δ=6°
φ=0°
NON-DIMENSIONAL FORCES, F/m·√T
50
40
30
20
10
0
-40
-80
-120
Legend of Non-Dimensional Forces
Flap's Lift LF/m·√T
Flap's Drag DF/m·√T
Rig's Lift LR/m·√T
Rig's Drag DR/m·√T
Nozzle Lift LN/m·√T
Total Lift LT/m·√T

FIG. 14

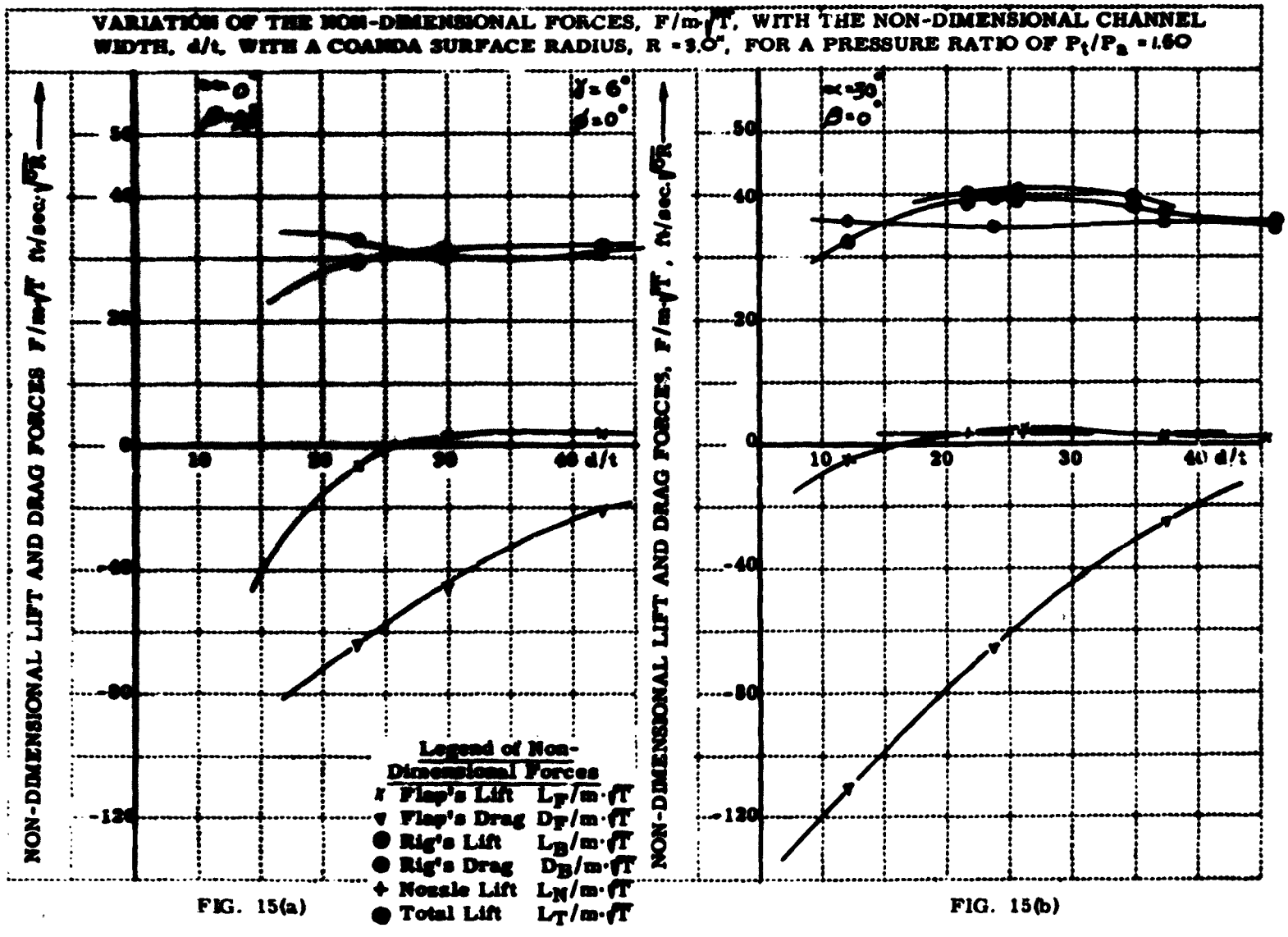

FIG. 15(a)

FIG. 15(b)

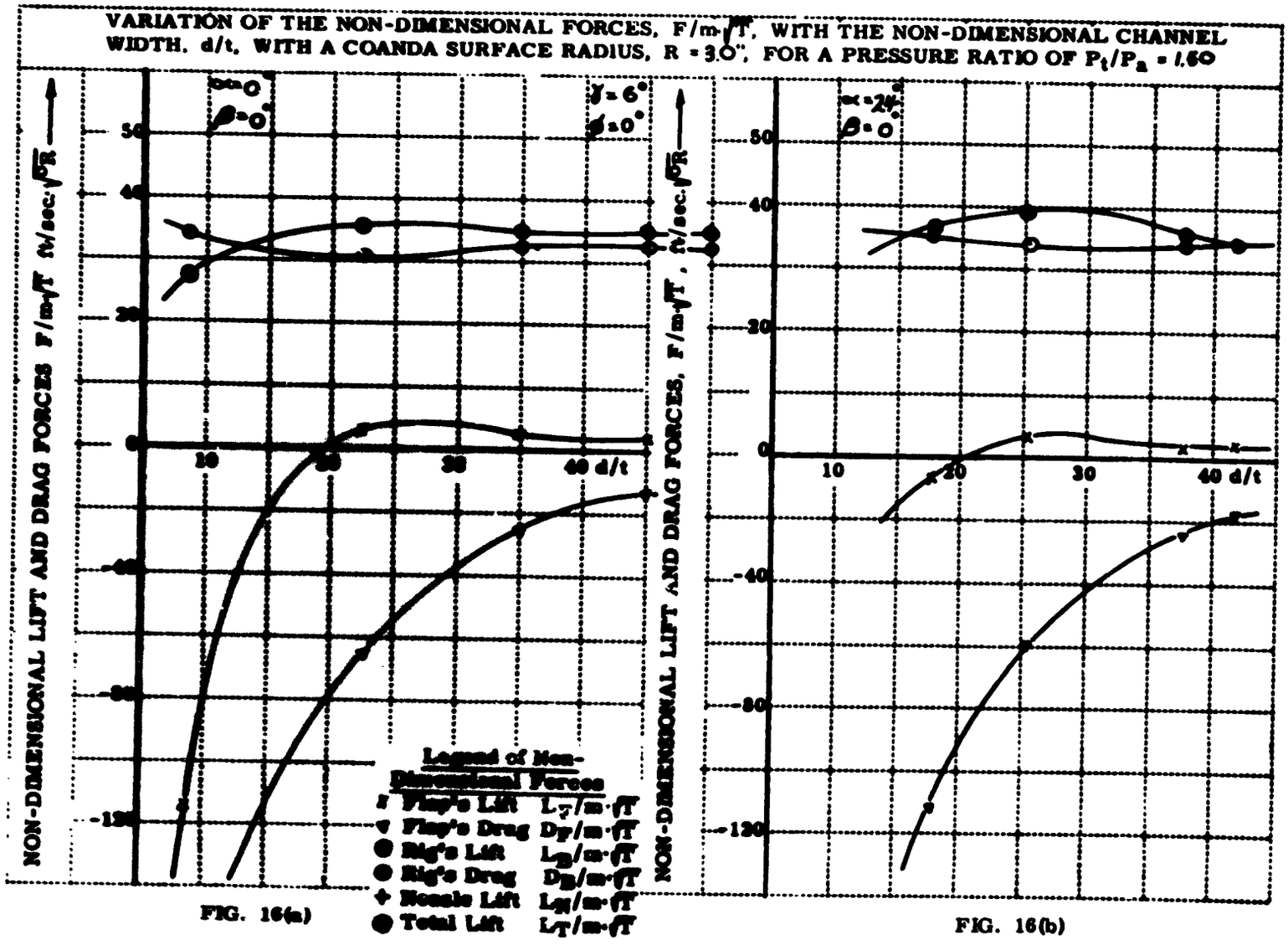

FIG. 16(a)

FIG. 16(b)

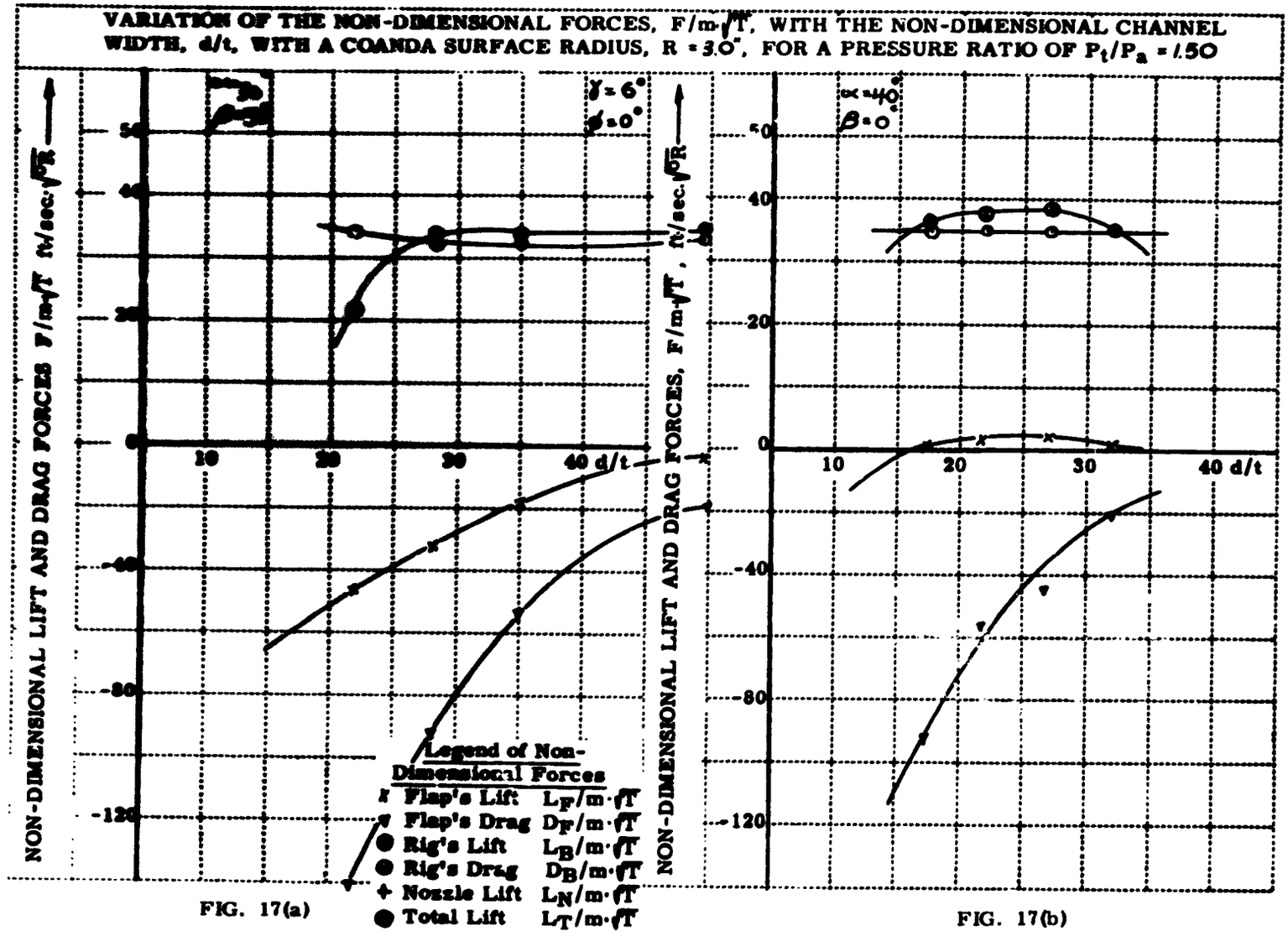

FIG. 17(a)

FIG. 17(b)

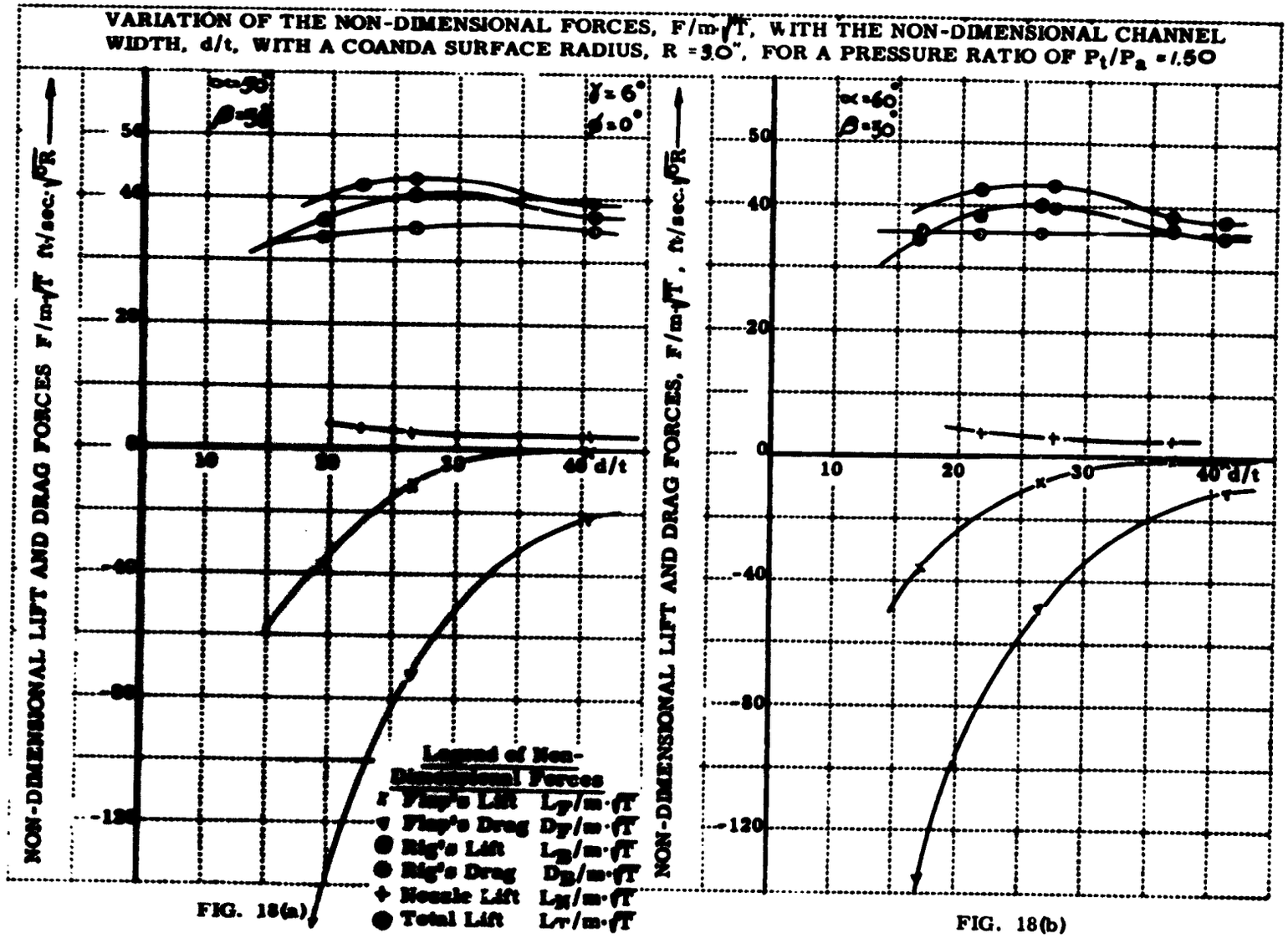
VARIATION OF THE NON-DIMENSIONAL FORCES, F/m·√T, WITH THE NON-DIMENSIONAL CHANNEL WIDTH, d/t, WITH A COANDA SURFACE RADIUS, R = 3.0", FOR A PRESSURE RATIO OF Pt/Pa = 1.50
NON-DIMENSIONAL LIFT AND DRAG FORCES F/m·√T ft/sec·√R
d/t
Legend of Non-Dimensional Forces
Flap's Lift Lf/m·√T
Flap's Drag Df/m·√T
Big's Lift Lb/m·√T
Big's Drag Db/m·√T
Nozzle Lift Ln/m·√T
Total Lift Lt/m·√T
FIG. 18(a)
FIG. 18(b)

VARIATION OF THE NON-DIMENSIONAL FORCES, $F/m\cdot\sqrt{T}$, WITH THE NON-DIMENSIONAL CHANNEL WIDTH, d/t, WITH A COANDA SURFACE RADIUS, R = 3.0", FOR A PRESSURE RATIO OF P_t/P_a = 1.50

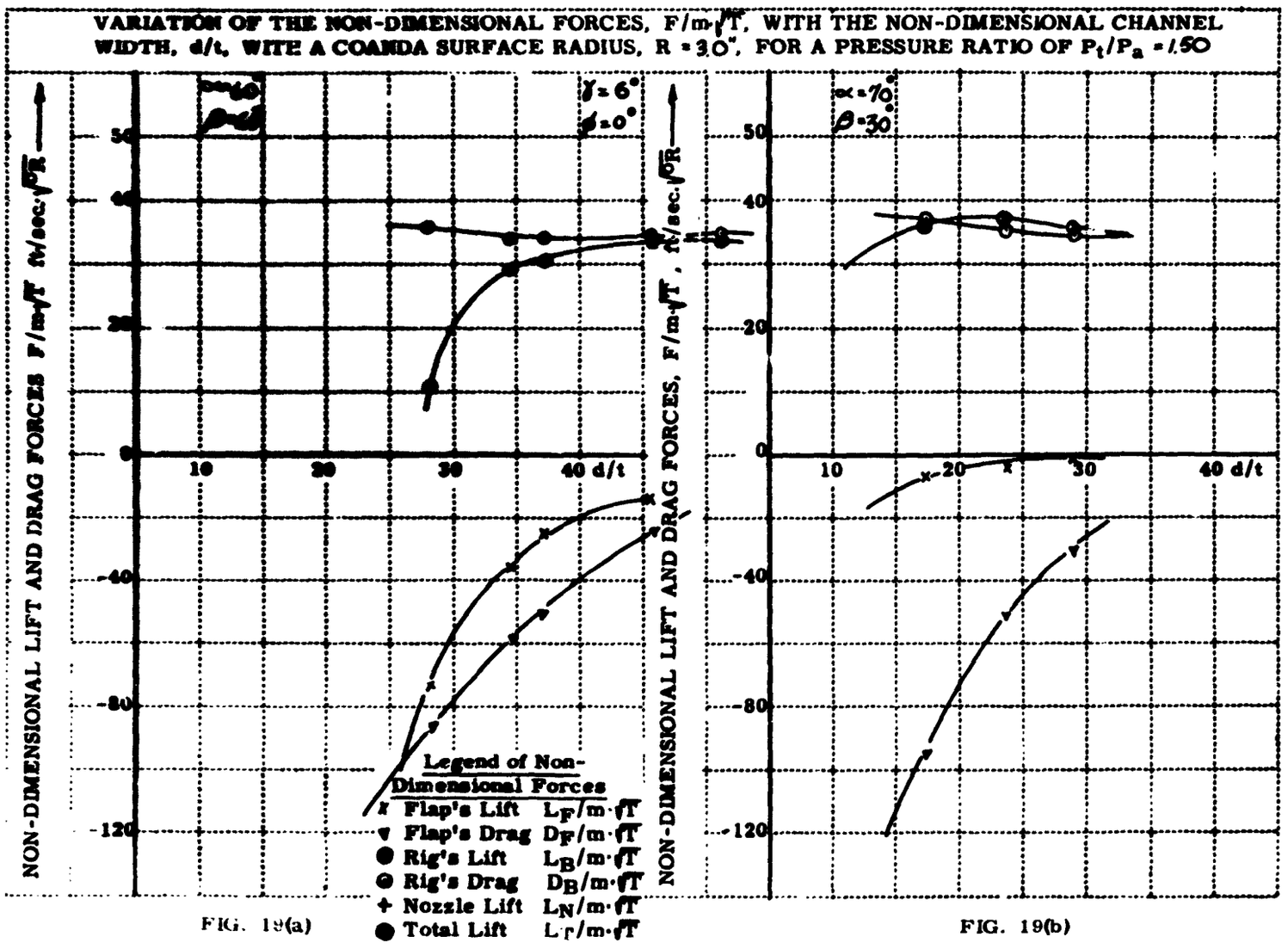

FIG. 19(a)

FIG. 19(b)

VARIATION OF THE NON-DIMENSIONAL FORCES, $F/m\cdot\sqrt{T}$, WITH THE NON-DIMENSIONAL CHANNEL WIDTH, d/t, WITH A COANDA SURFACE RADIUS, R = 3.0", FOR A PRESSURE RATIO OF P_t/P_a = 1.50

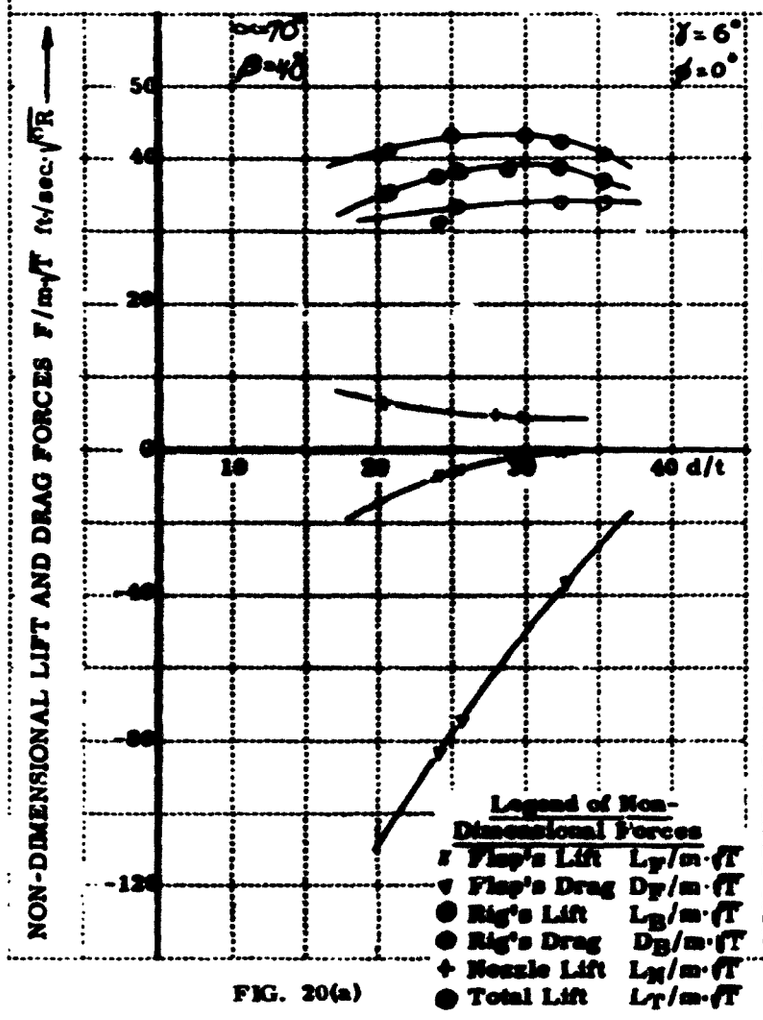

FIG. 20(a)

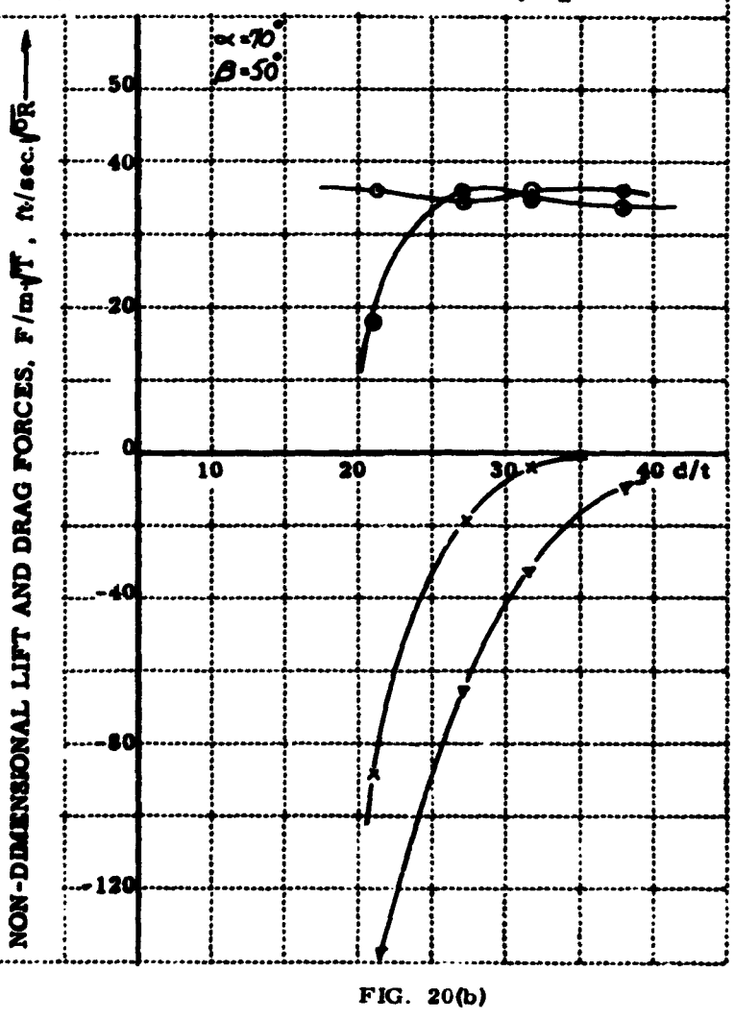

FIG. 20(b)

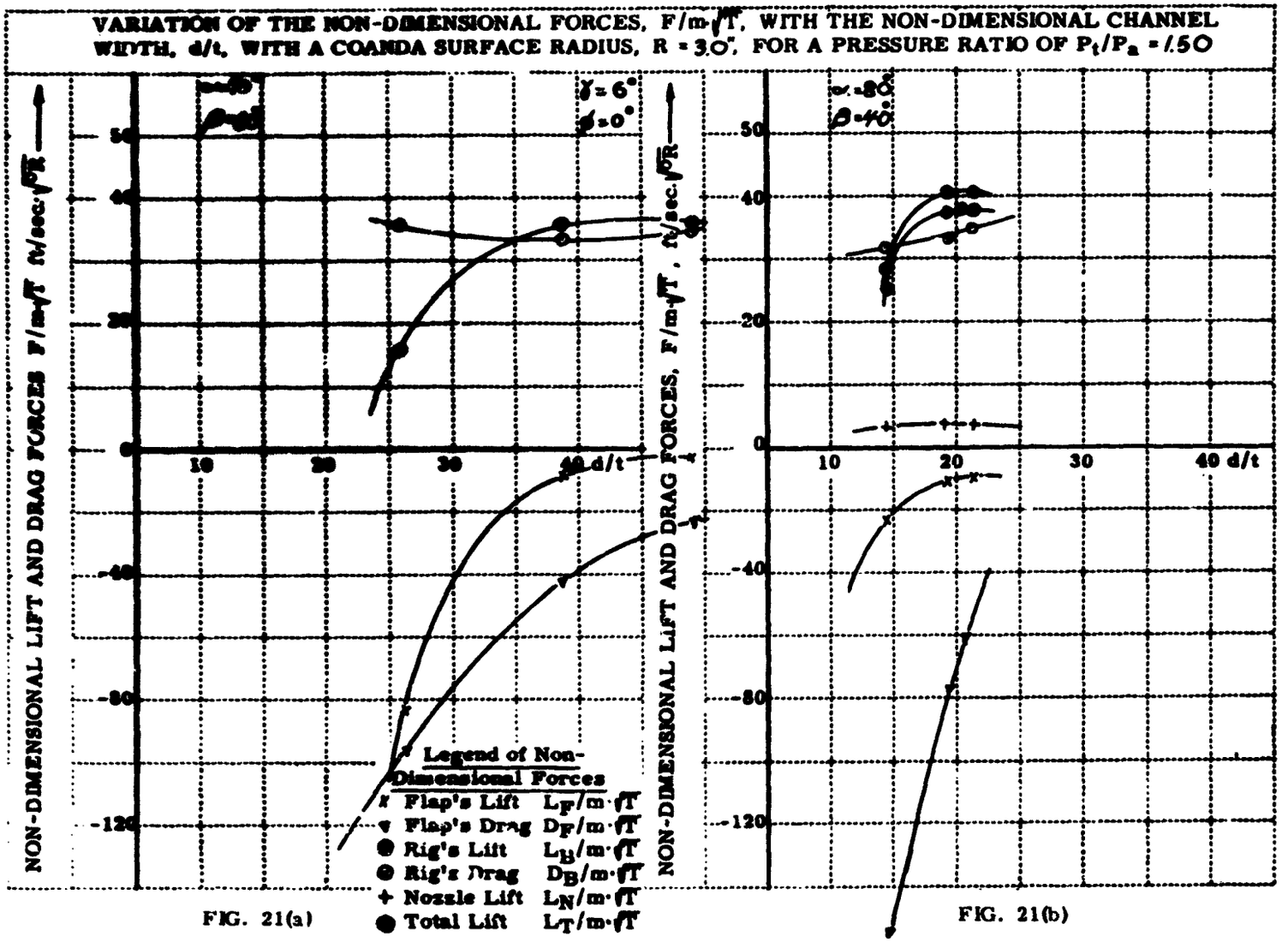

FIG. 21(a)

FIG. 21(b)

VARIATION OF THE NON-DIMENSIONAL FORCES, F/m·√T, WITH THE NON-DIMENSIONAL CHANNEL WIDTH, d/t, WITH A COANDA SURFACE RADIUS, R = 3.0", FOR A PRESSURE RATIO OF P_t/P_a = 1.50

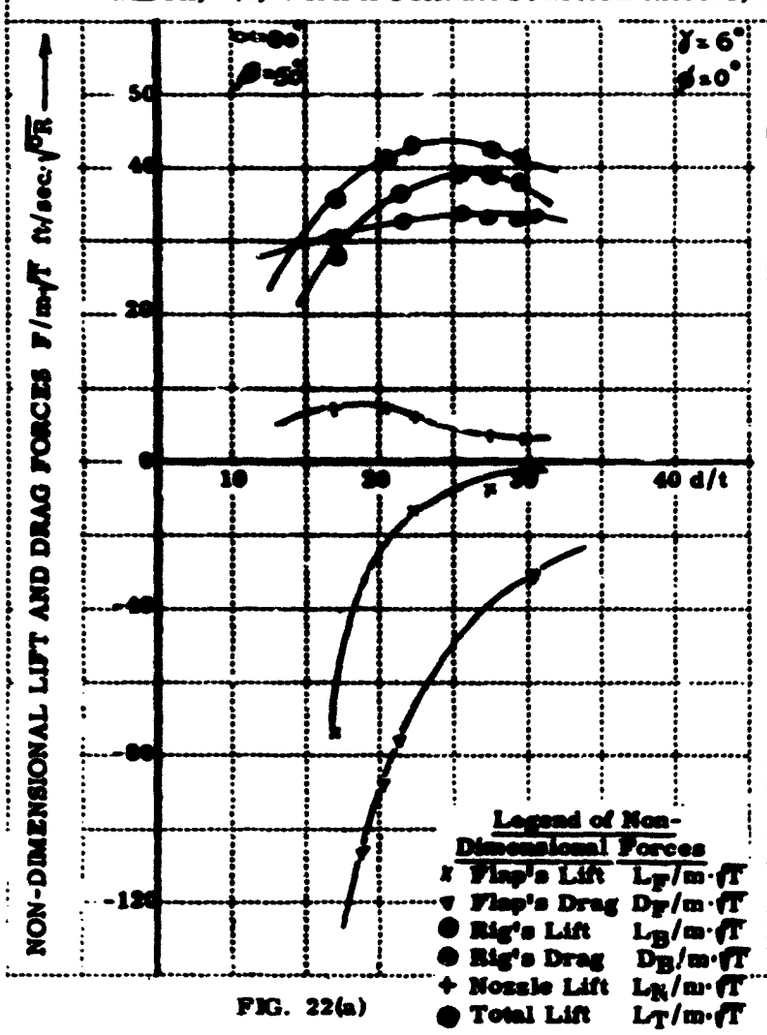

FIG. 22(a)

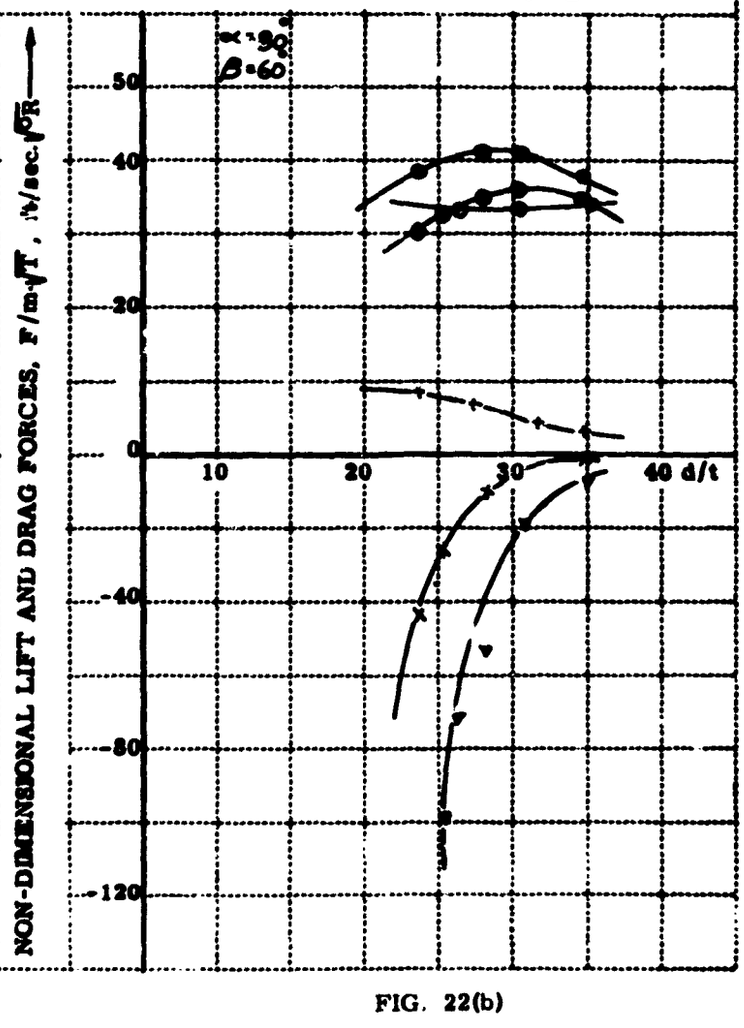

FIG. 22(b)

VARIATION OF THE NON-DIMENSIONAL FORCES, F/m·√T, WITH THE NON-DIMENSIONAL CHANNEL WIDTH c/t, WITH A COANDA SURFACE RADIUS, R = 3.0", FOR A PRESSURE RATIO OF P_t/P_a = 1.50

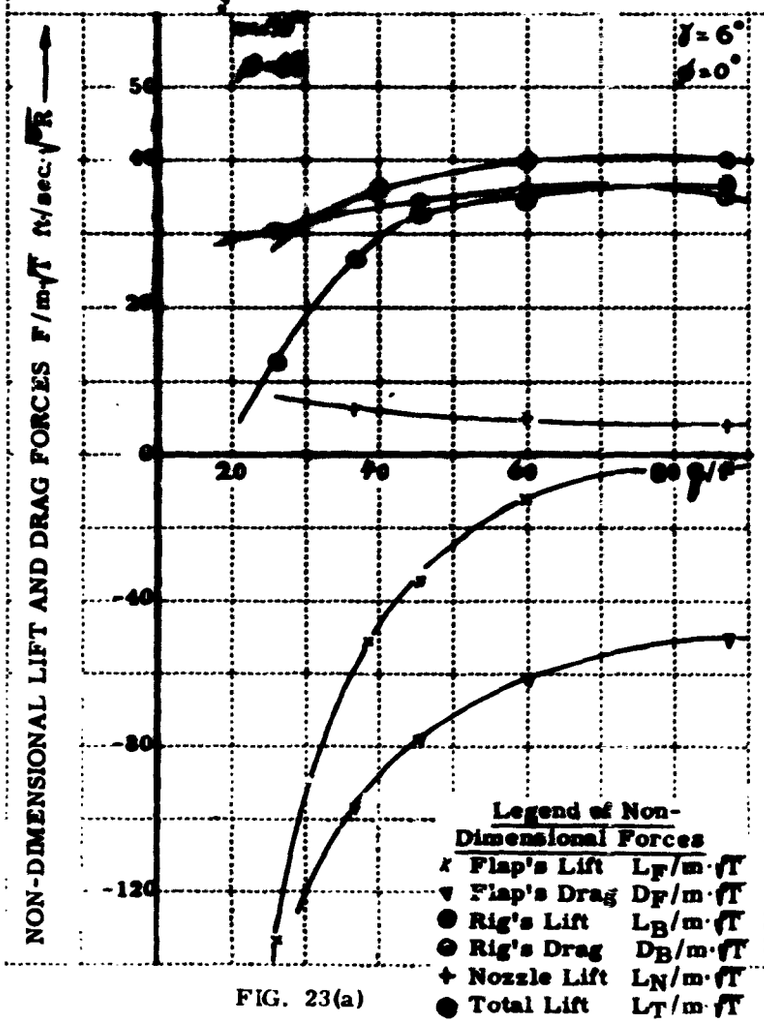

FIG. 23(a)

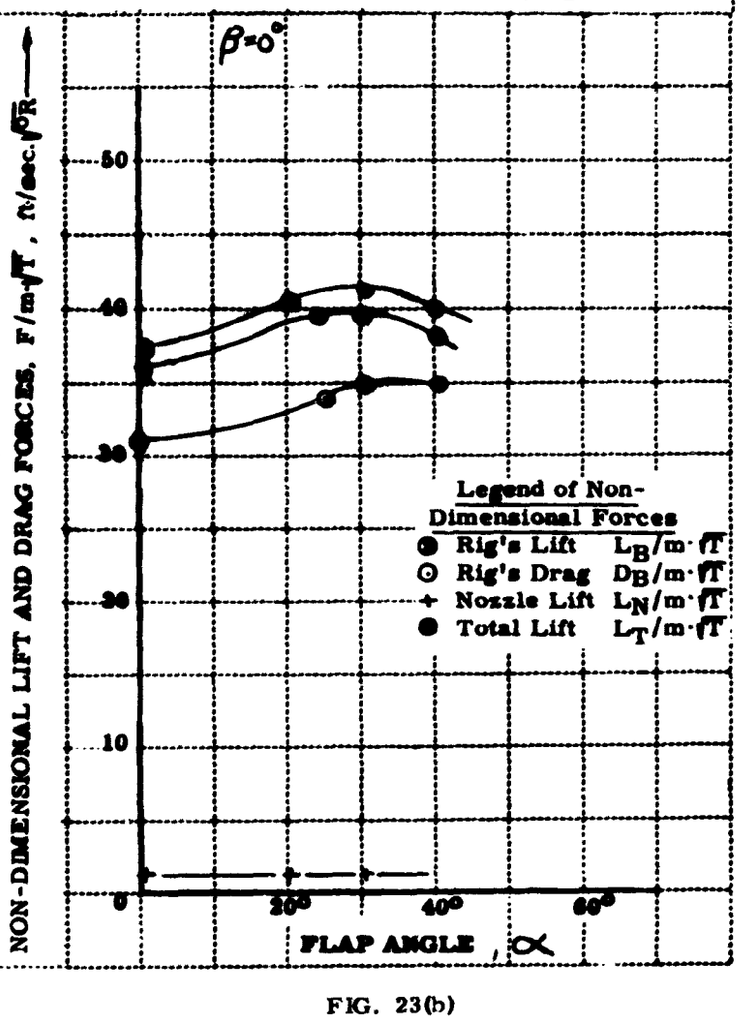

FIG. 23(b)

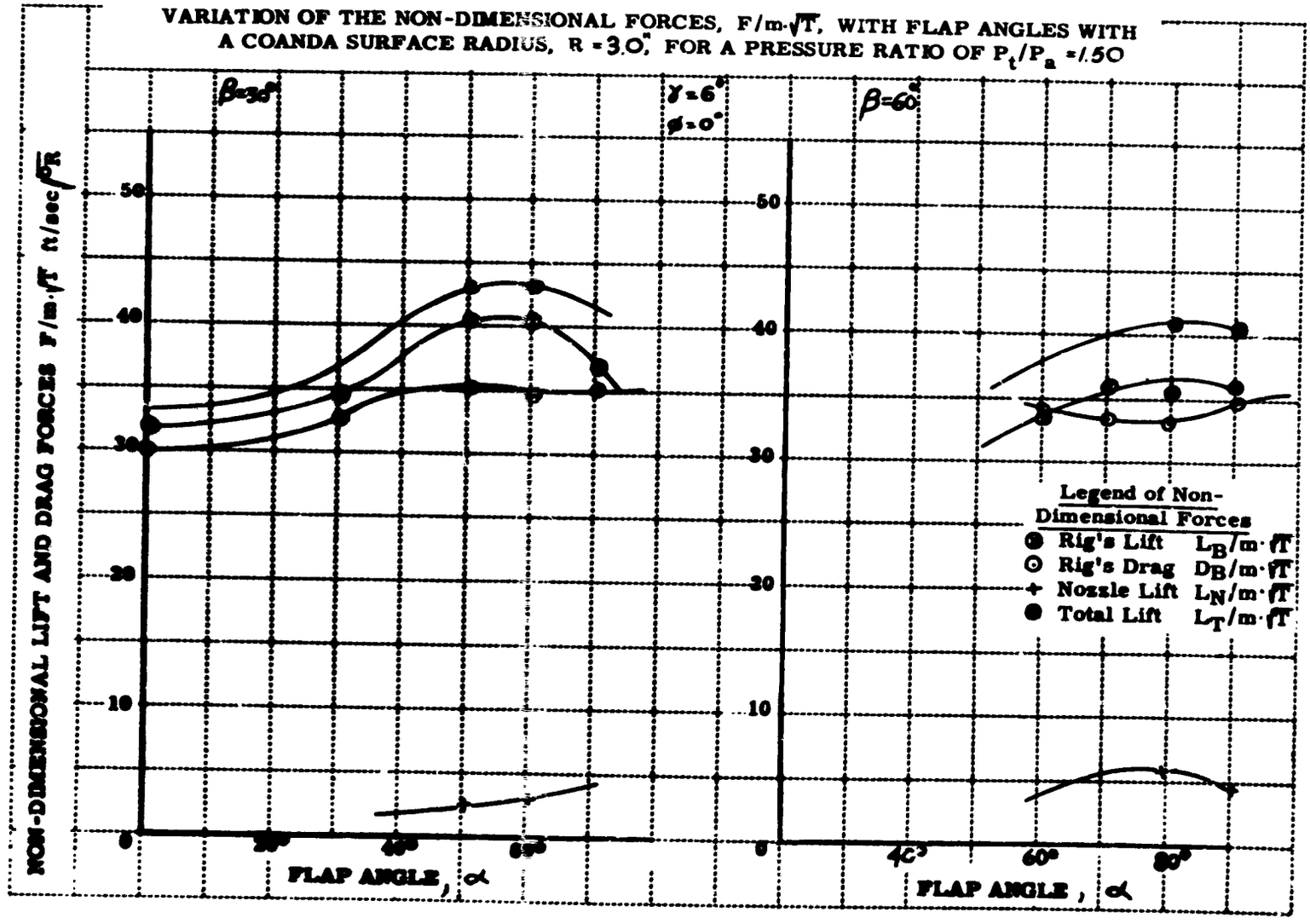

FIG. 24(a)

FIG. 24(b)

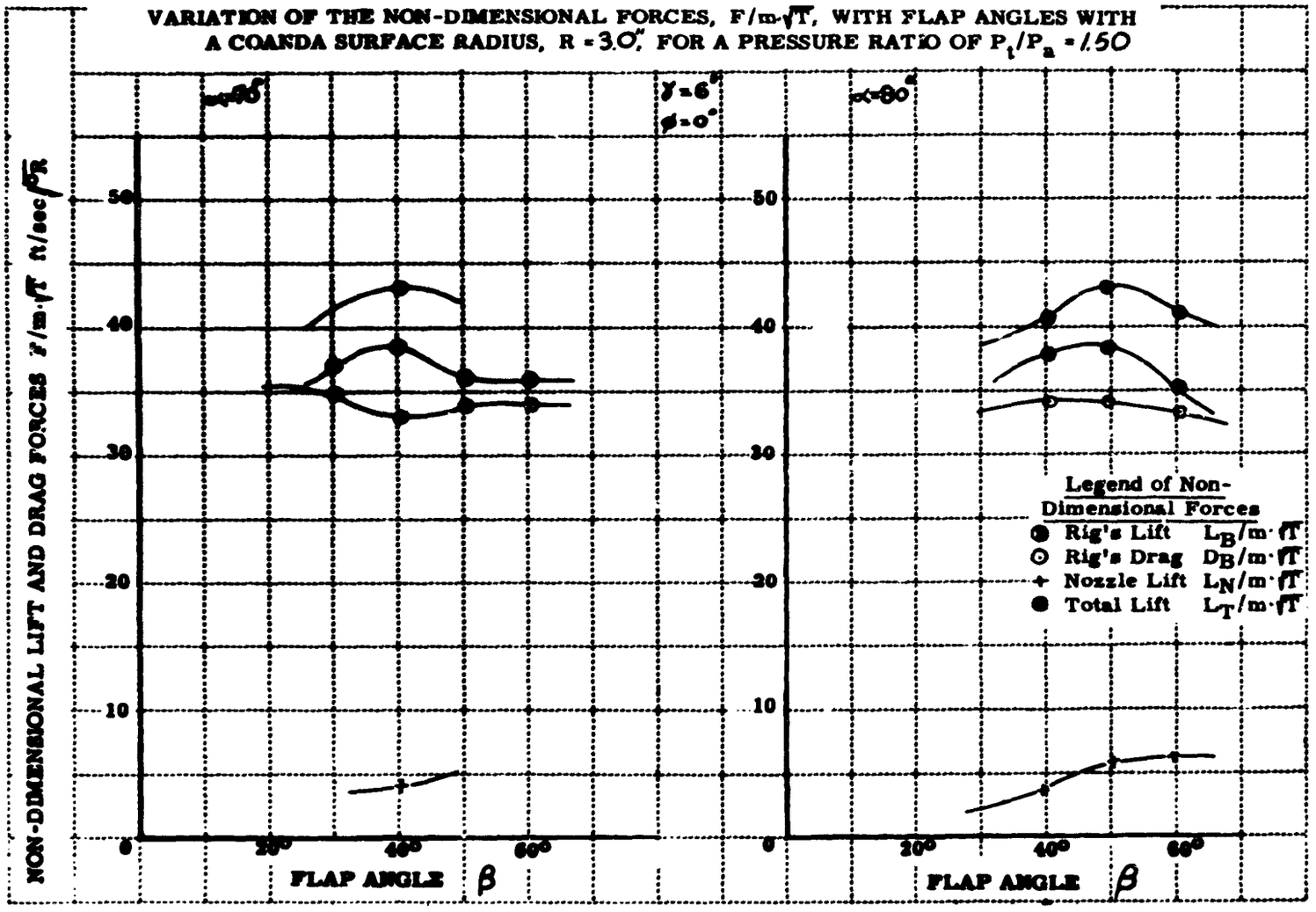

FIG. 25(a)

FIG. 25(b)

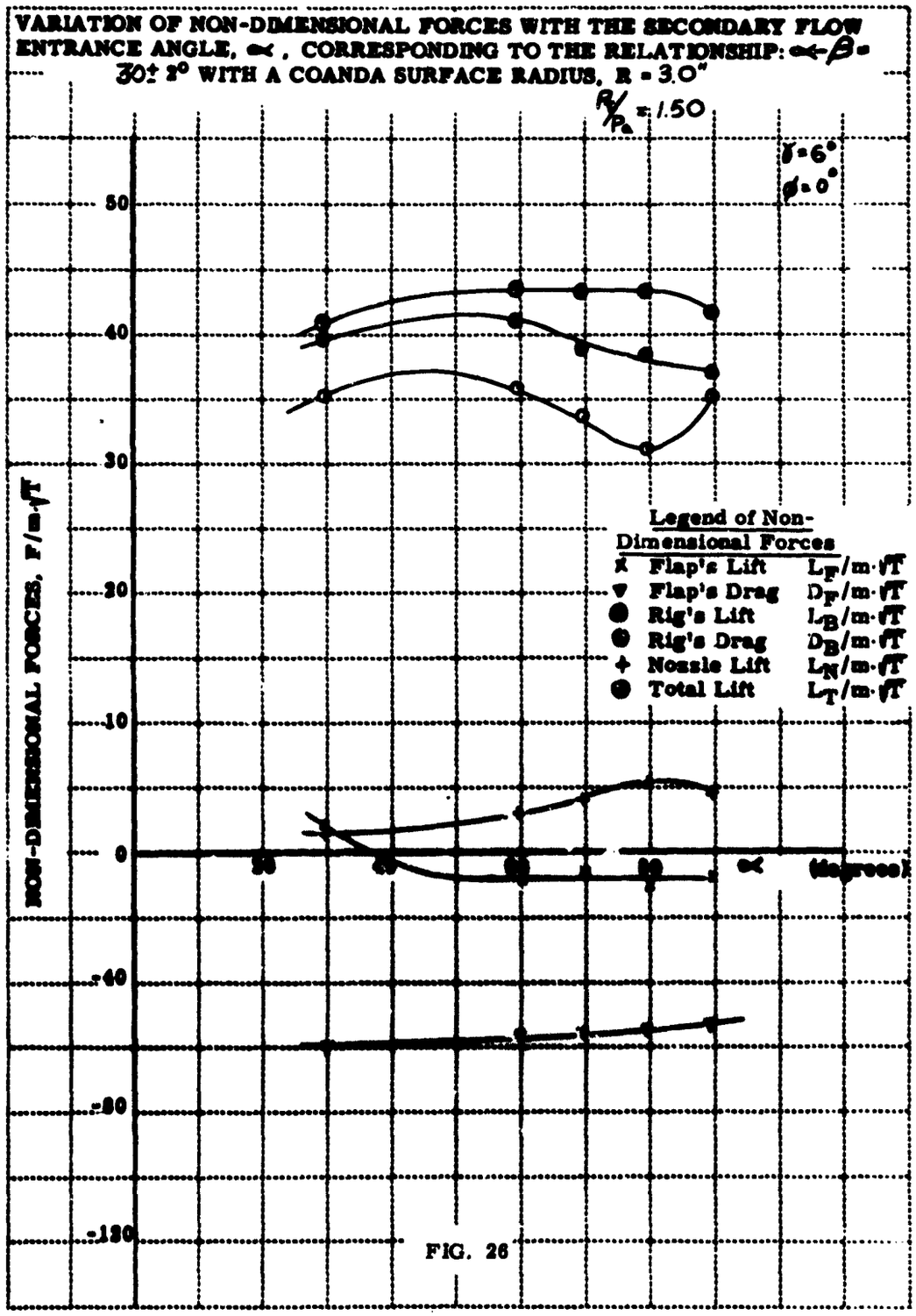
VARIATION OF NON-DIMENSIONAL FORCES WITH THE SECONDARY FLOW ENTRANCE ANGLE, ∝, CORRESPONDING TO THE RELATIONSHIP: ∝ = β = 30± 2° WITH A COANDA SURFACE RADIUS, R = 3.0"
P/P∞ = 1.50
β = 6°
φ = 0°
50
40
30
20
10
0
-40
-80
-120
NON-DIMENSIONAL FORCES, F/m·√T
∝ (degrees)
Legend of Non-Dimensional Forces
Flap's Lift L_F/m·√T
Flap's Drag D_F/m·√T
Rig's Lift L_B/m·√T
Rig's Drag D_B/m·√T
Nozzle Lift L_N/m·√T
Total Lift L_T/m·√T

FIG. 26

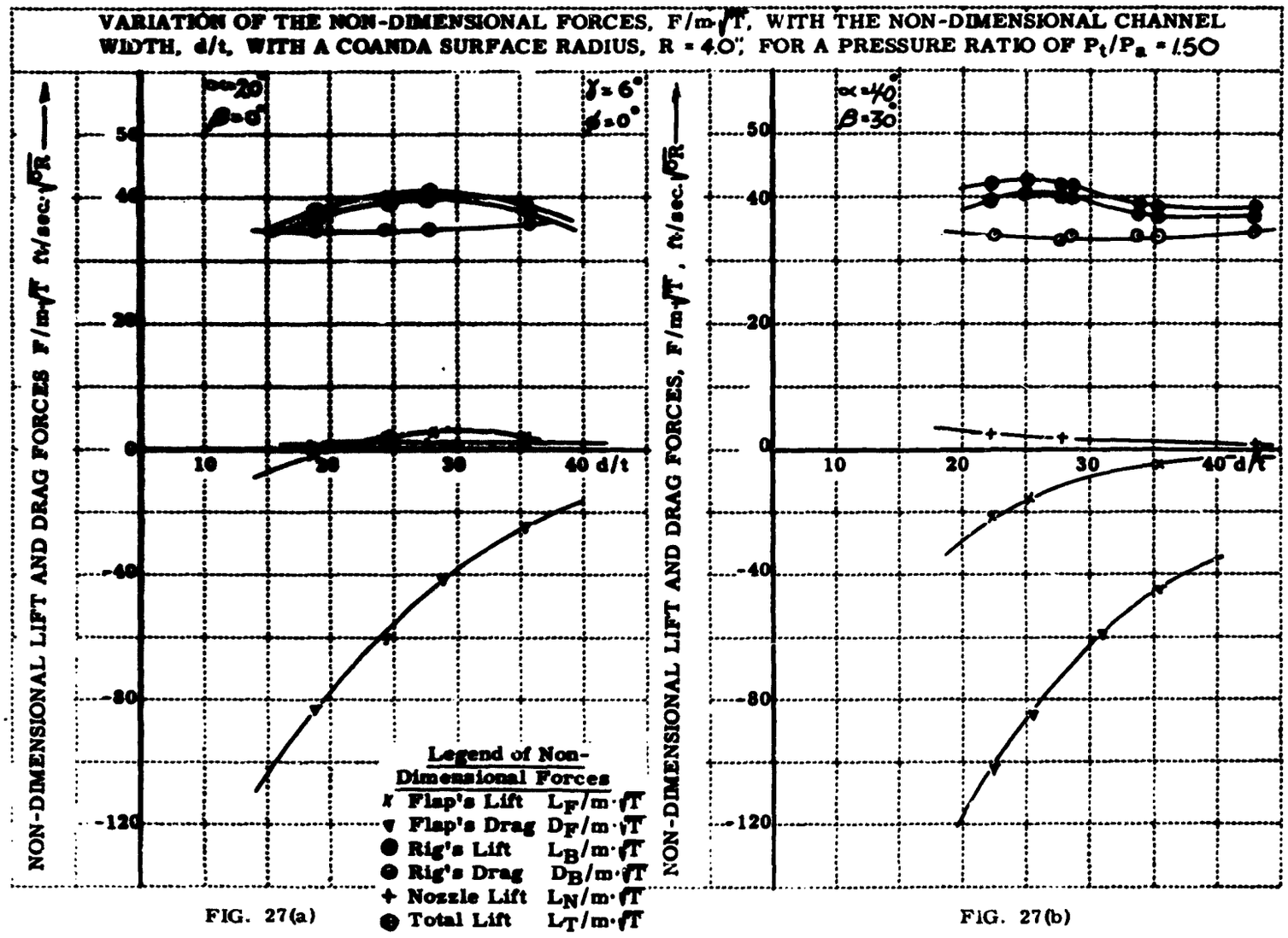

FIG. 27(a)

FIG. 27(b)

VARIATION OF THE NON-DIMENSIONAL FORCES, F/m·√T, WITH THE NON-DIMENSIONAL CHANNEL WIDTH, d/t, WITH A COANDA SURFACE RADIUS, R = 4.0", FOR A PRESSURE RATIO OF P_t/P_a = 1.50

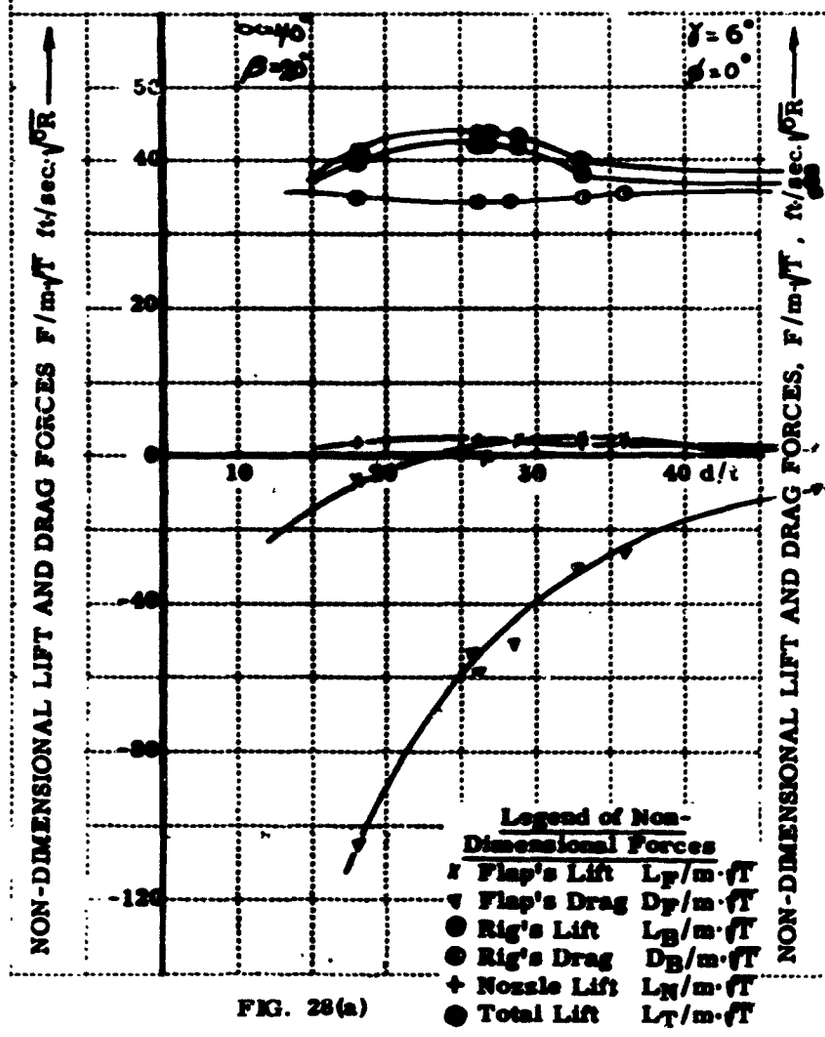

FIG. 28(a)

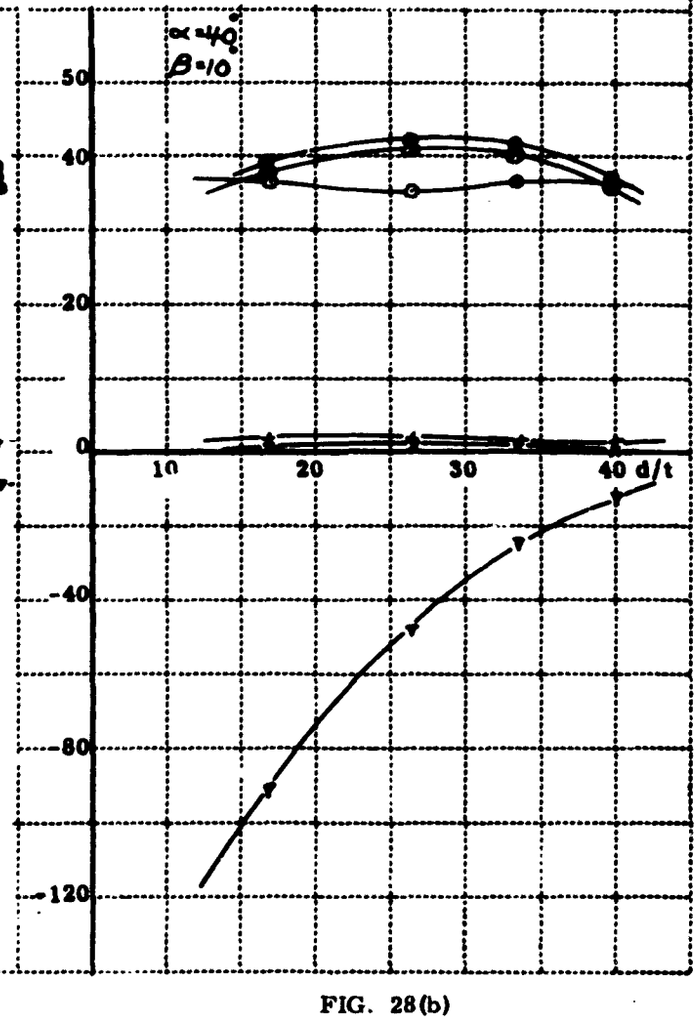

FIG. 28(b)

VARIATION OF THE NON-DIMENSIONAL FORCES, $F/m\cdot\sqrt{T}$, WITH THE NON-DIMENSIONAL CHANNEL WIDTH, d/t, WITH A COANDA SURFACE RADIUS, R = 4.0", FOR A PRESSURE RATIO OF P_t/P_a = 1.50

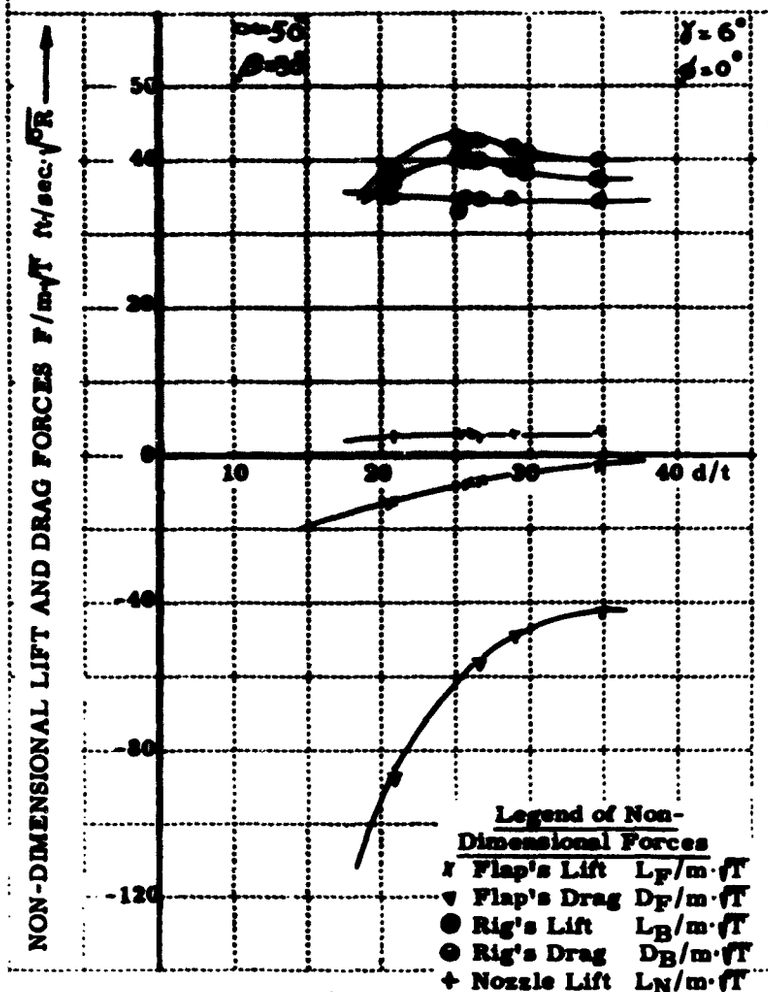

FIG. 29(a)

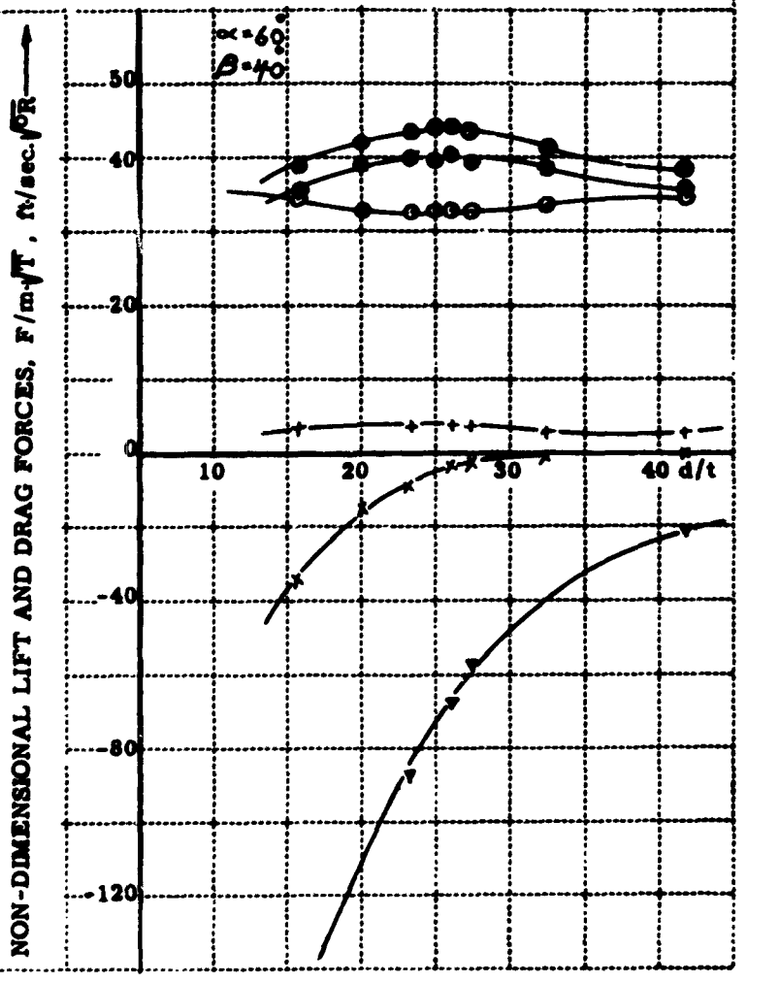

FIG. 29(b)

VARIATION OF THE NON-DIMENSIONAL FORCES, $F/m\cdot\sqrt{T}$, WITH THE NON-DIMENSIONAL CHANNEL WIDTH, d/t, WITH A COANDA SURFACE RADIUS, R = 4.0", FOR A PRESSURE RATIO OF P_t/P_a = 1.50

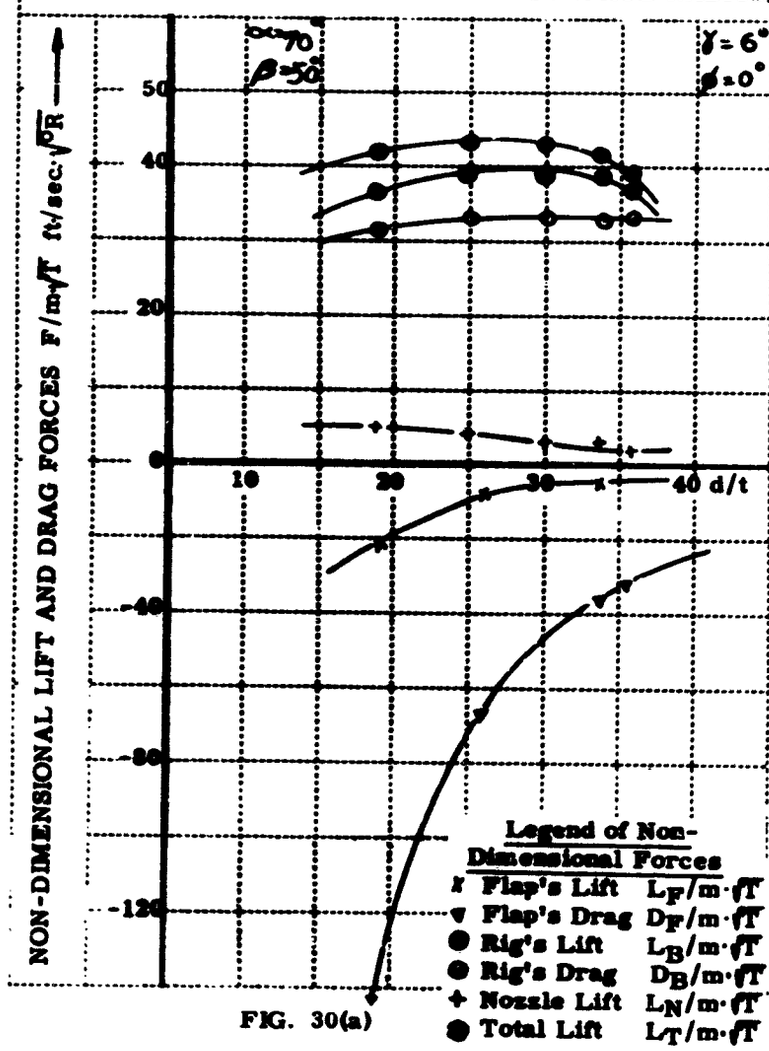

FIG. 30(a)

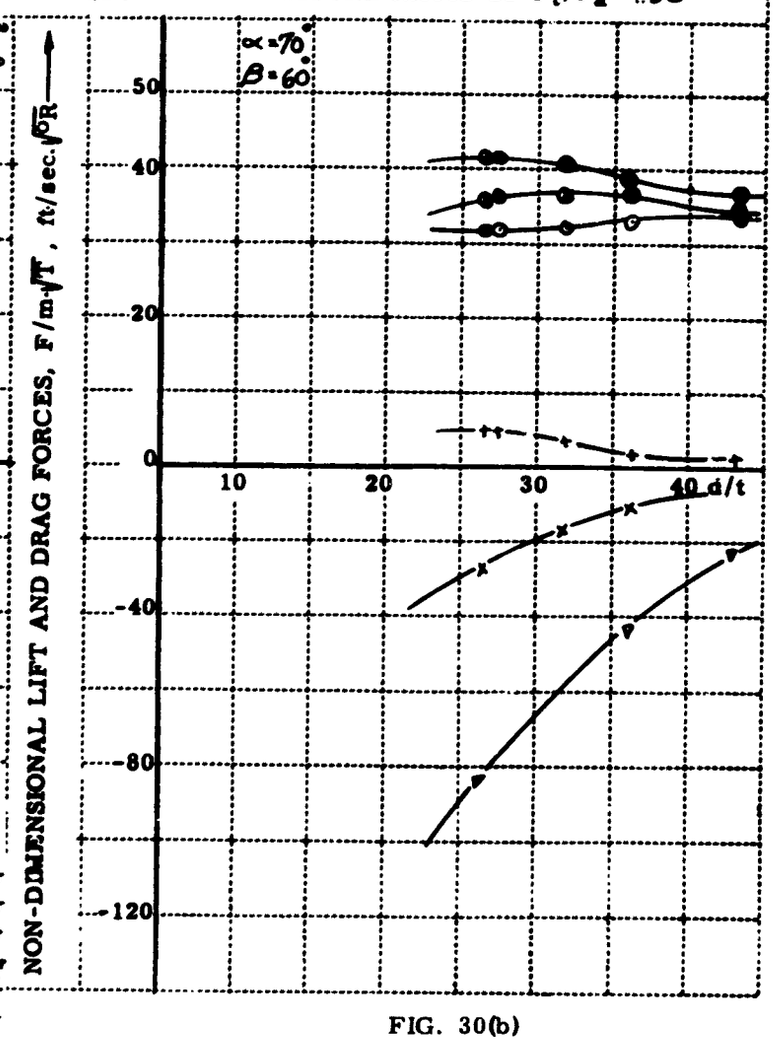

FIG. 30(b)

VARIATION OF THE NON-DIMENSIONAL FORCES, $F/m\cdot\sqrt{T}$, WITH THE NON-DIMENSIONAL CHANNEL WIDTH, d/t, WITH A COANDA SURFACE RADIUS, R = 4.0", FOR A PRESSURE RATIO OF P_t/P_a = 150

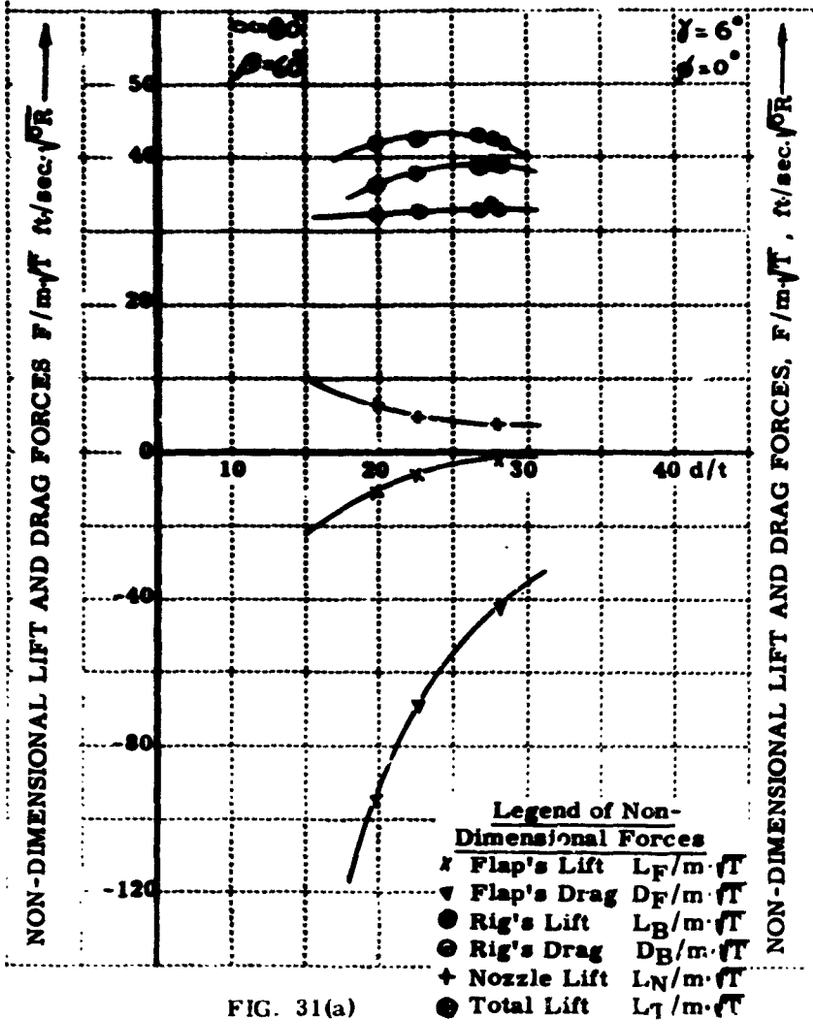

FIG. 31(a)

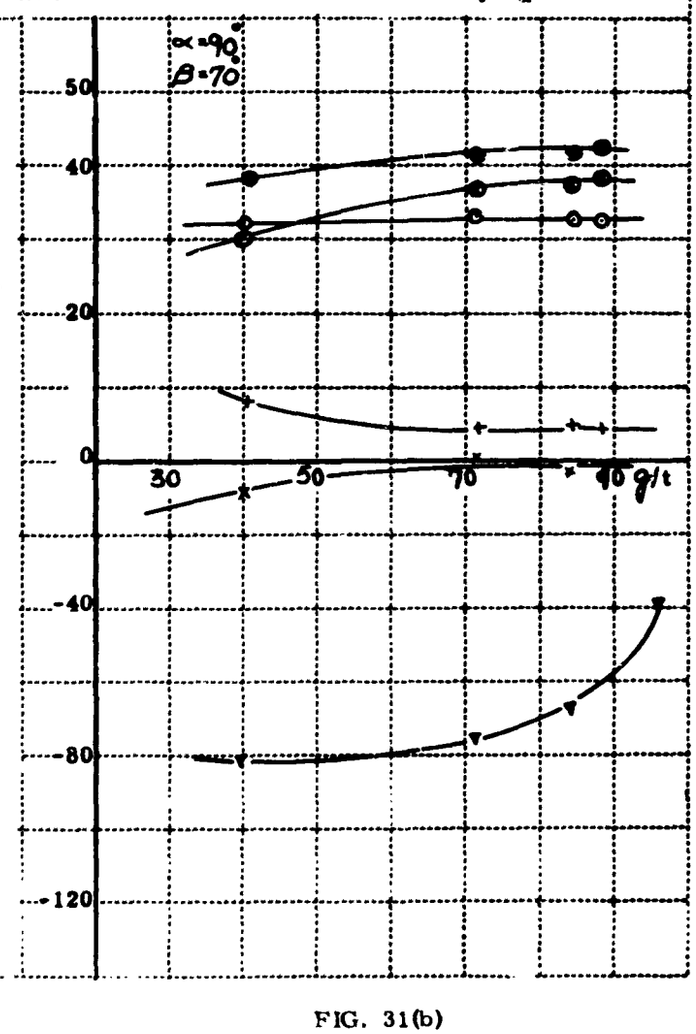

FIG. 31(b)

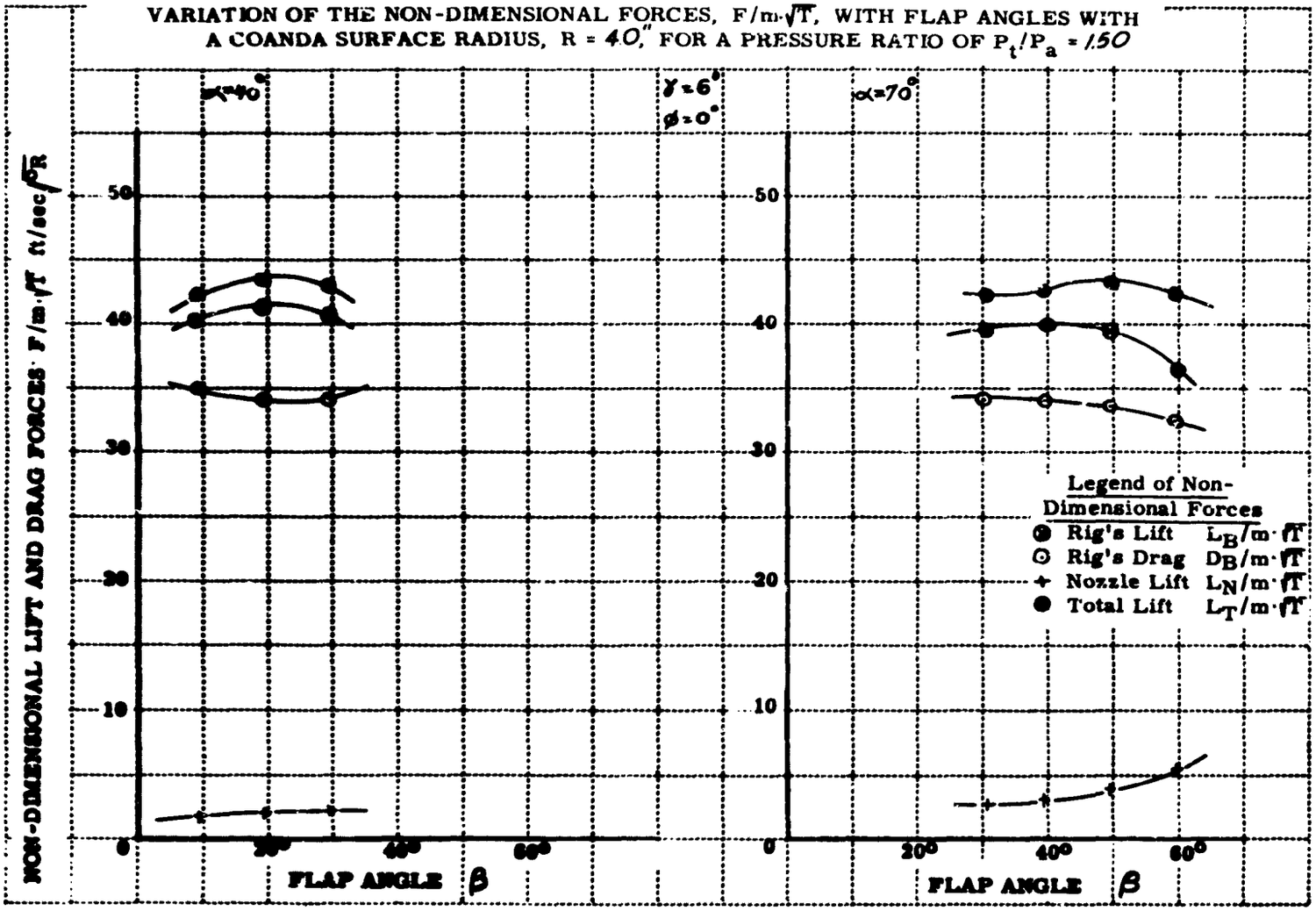

FIG. 32(a)

FIG. 32(b)

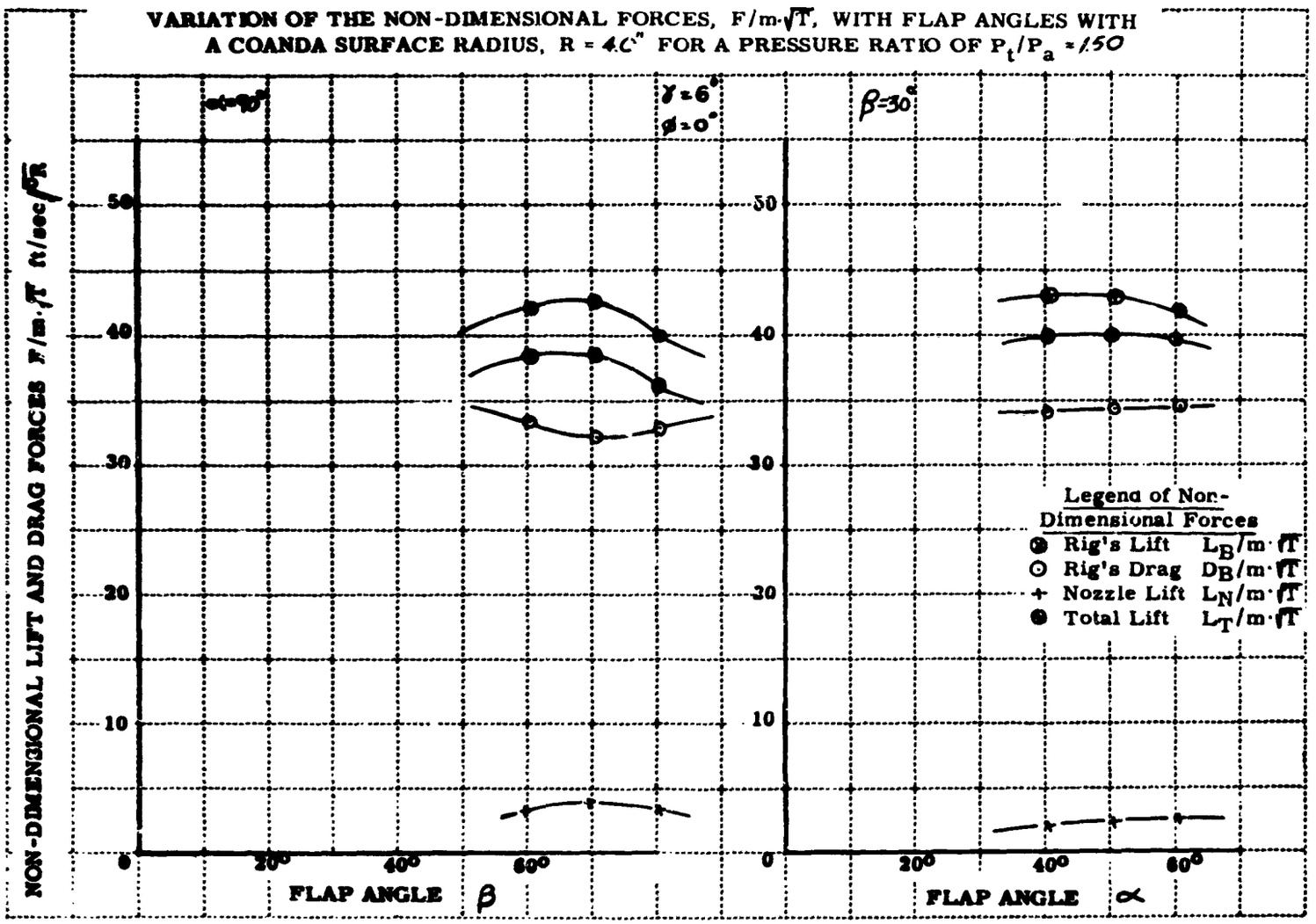

FIG. 33(a)

FIG. 33(b)

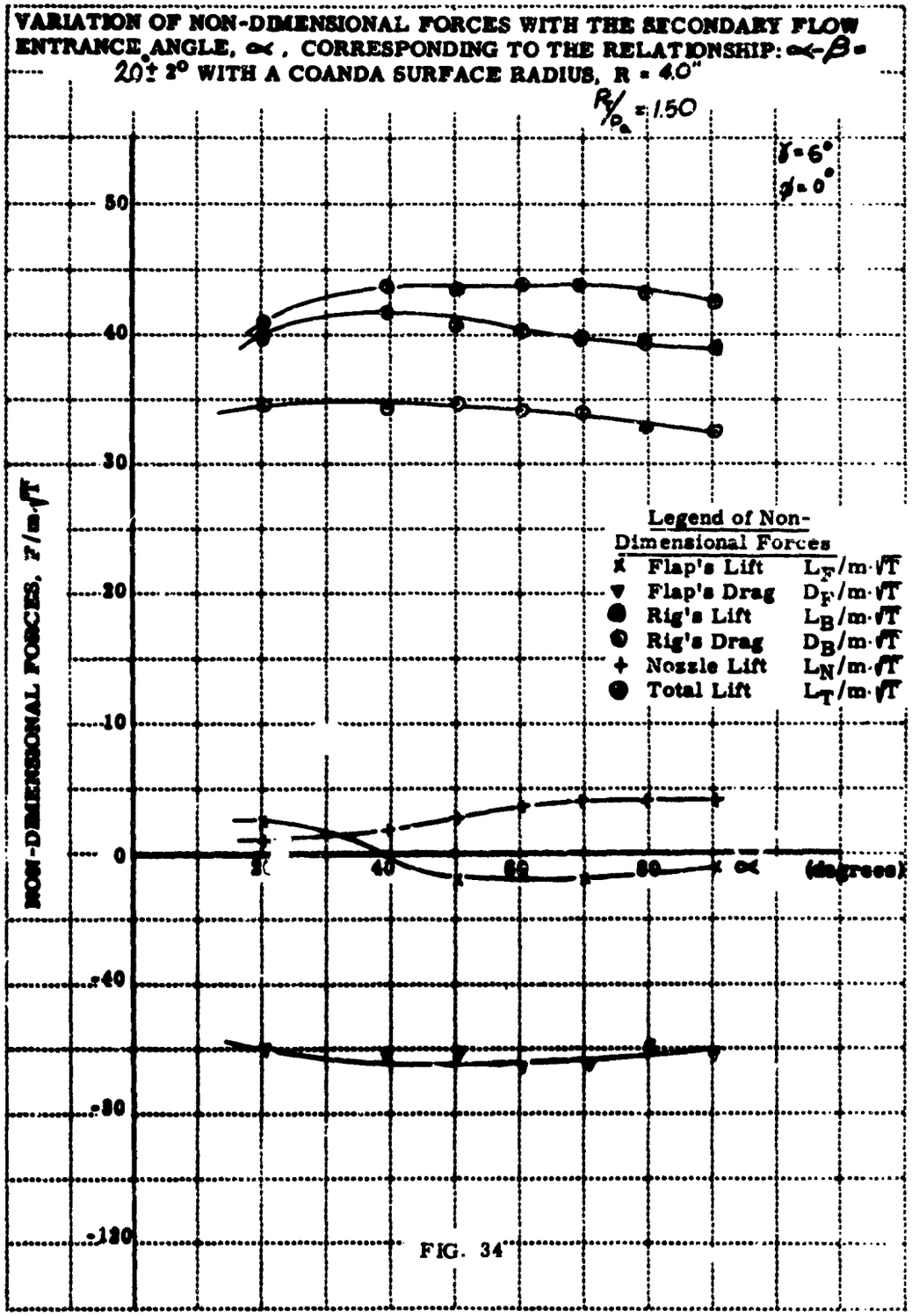
VARIATION OF NON-DIMENSIONAL FORCES WITH THE SECONDARY FLOW ENTRANCE ANGLE, ∝, CORRESPONDING TO THE RELATIONSHIP: ∝-β = 20° ± 2° WITH A COANDA SURFACE RADIUS, R = 4.0"
R/D = 1.50
δ = 6°
φ = 0°
Legend of Non-Dimensional Forces
Flap's Lift L_F/m·√T
Flap's Drag D_F/m·√T
Rig's Lift L_B/m·√T
Rig's Drag D_B/m·√T
Nozzle Lift L_N/m·√T
Total Lift L_T/m·√T
NON-DIMENSIONAL FORCES, F/m·√T
50
40
30
20
10
0
-40
-80
-120
40
60
80
∝ (degrees)

FIG. 34

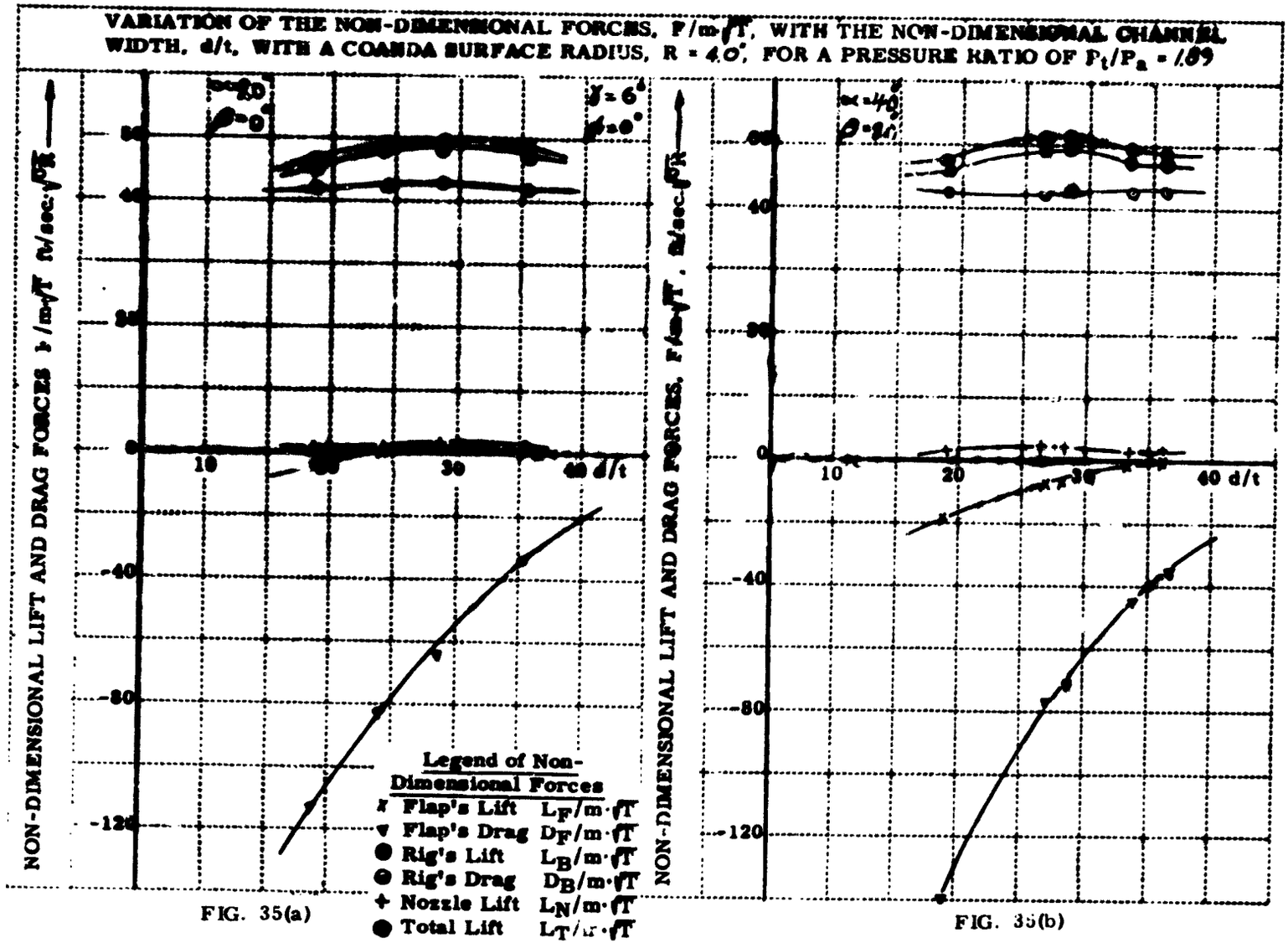

FIG. 35(a)

FIG. 35(b)

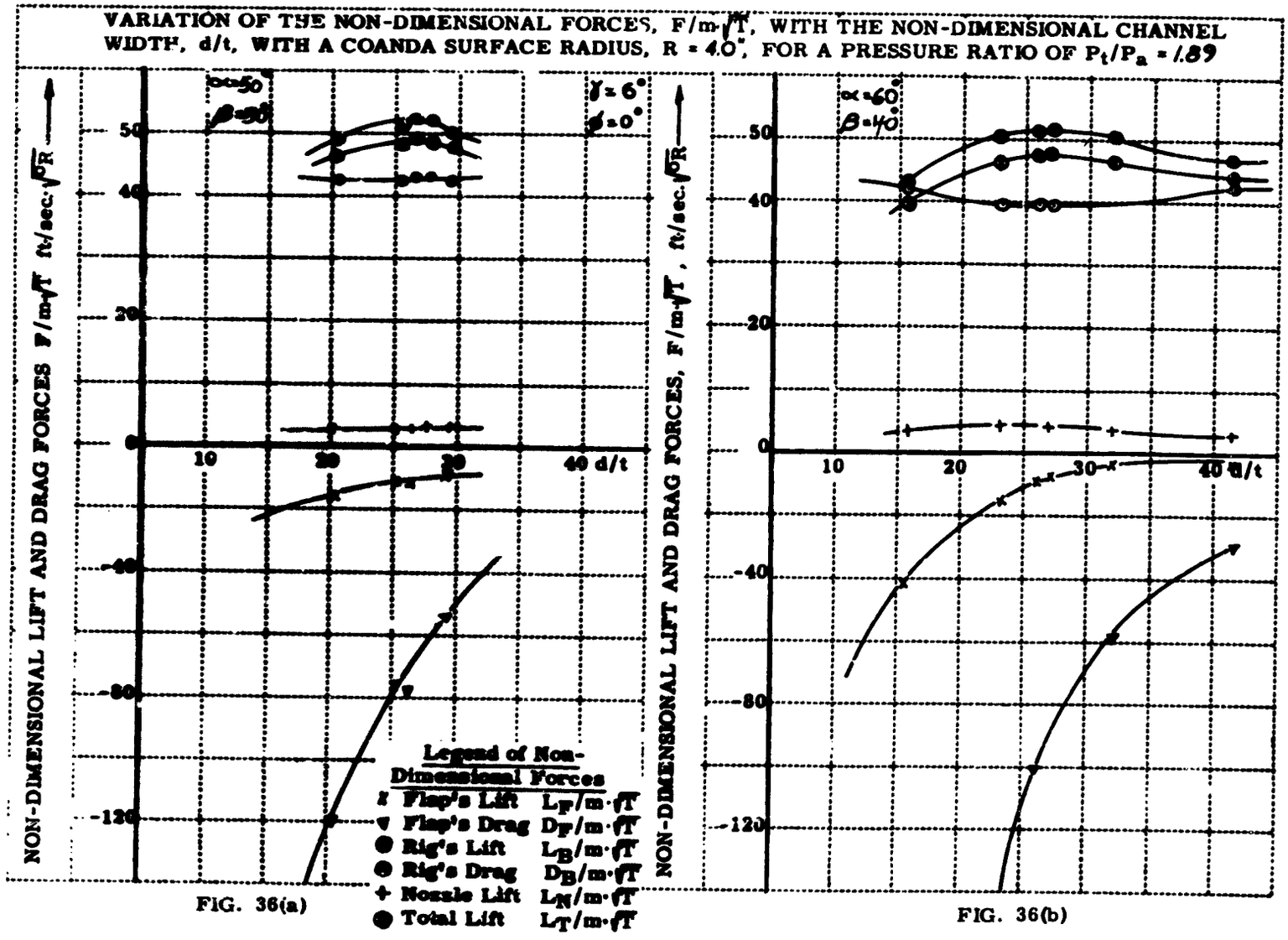

FIG. 36(a)

FIG. 36(b)

VARIATION OF THE NON-DIMENSIONAL FORCES, $F/m\sqrt{T}$, WITH THE NON-DIMENSIONAL CHANNEL WIDTH, d/t, WITH A COANDA SURFACE RADIUS, R = 4.0", FOR A PRESSURE RATIO OF P_t/P_a = 1.89

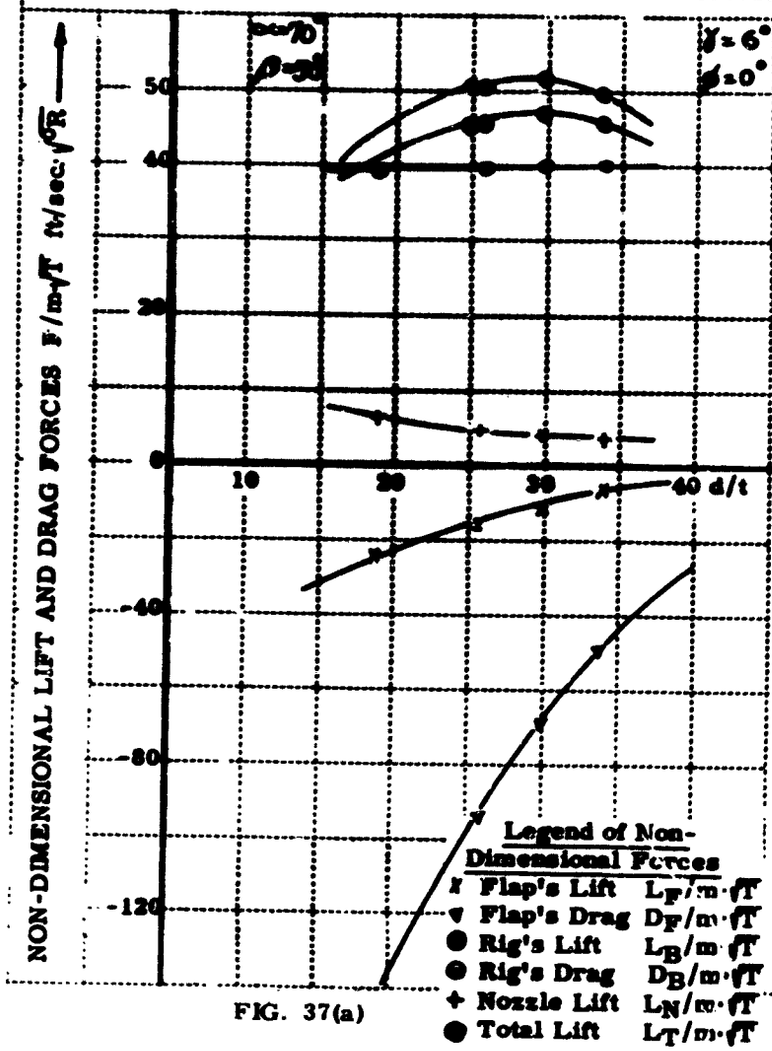

FIG. 37(a)

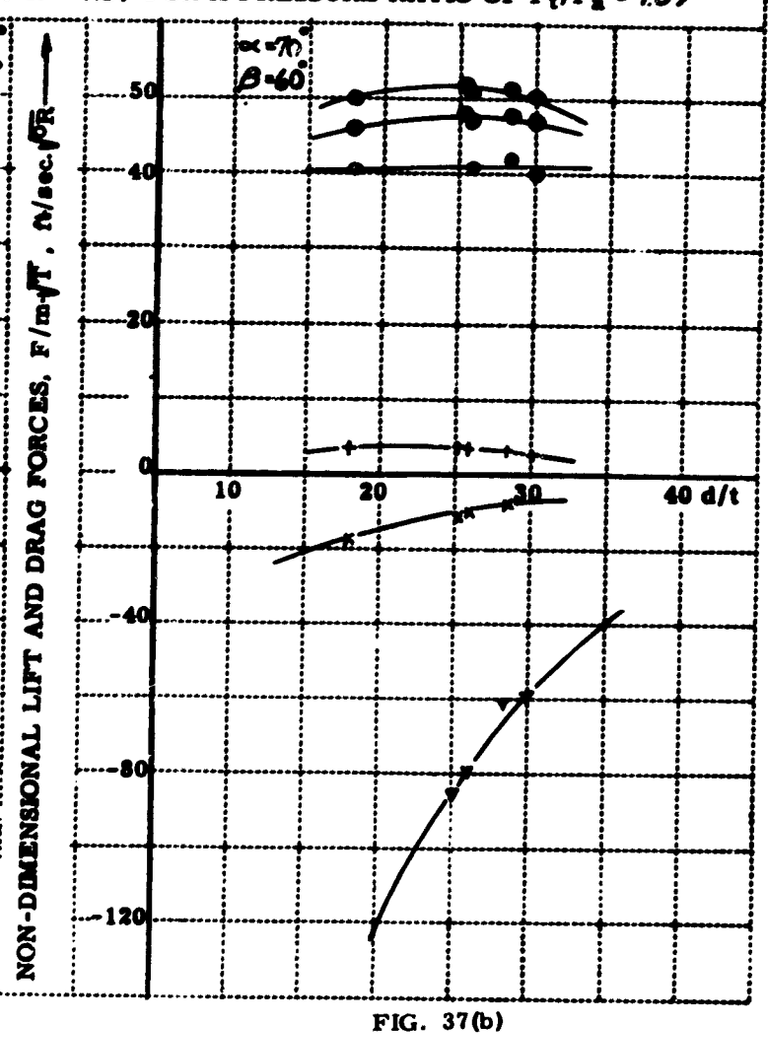

FIG. 37(b)

VARIATION OF THE NON-DIMENSIONAL FORCES, F/m√T, WITH THE NON-DIMENSIONAL CHANNEL WIDTH, d/t, WITH A COANDA SURFACE RADIUS, R = 4.0", FOR A PRESSURE RATIO OF P_t/P_a = 1.89

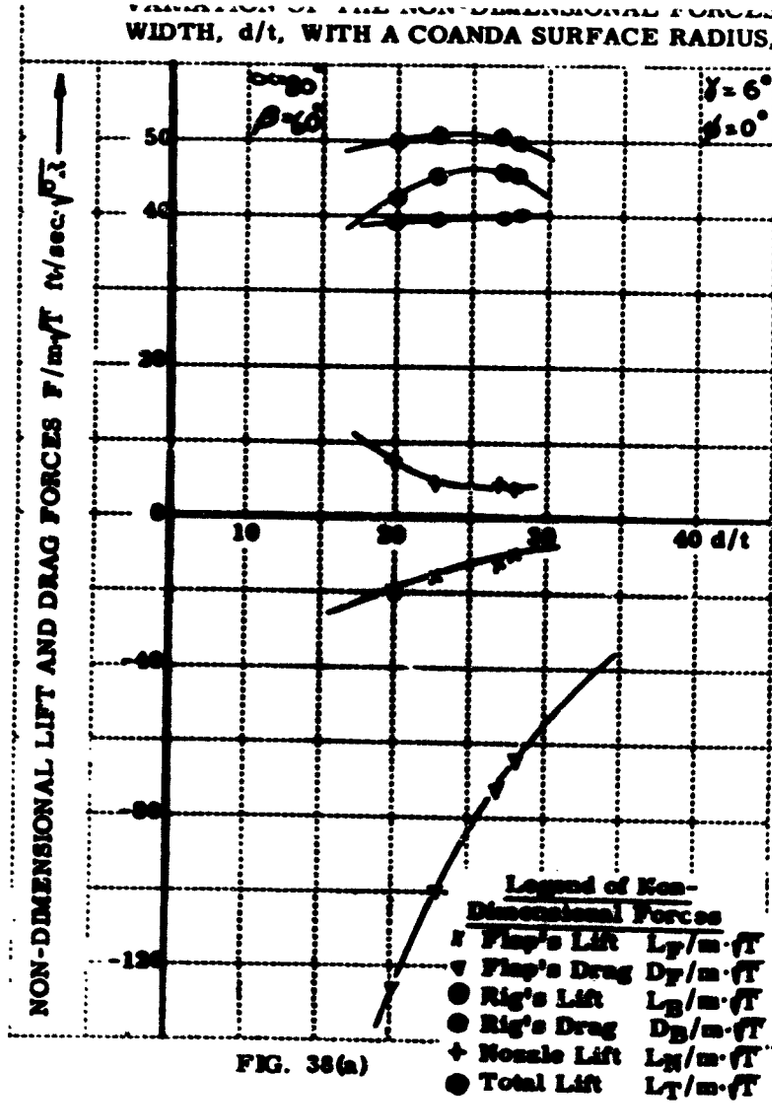

FIG. 38(a)

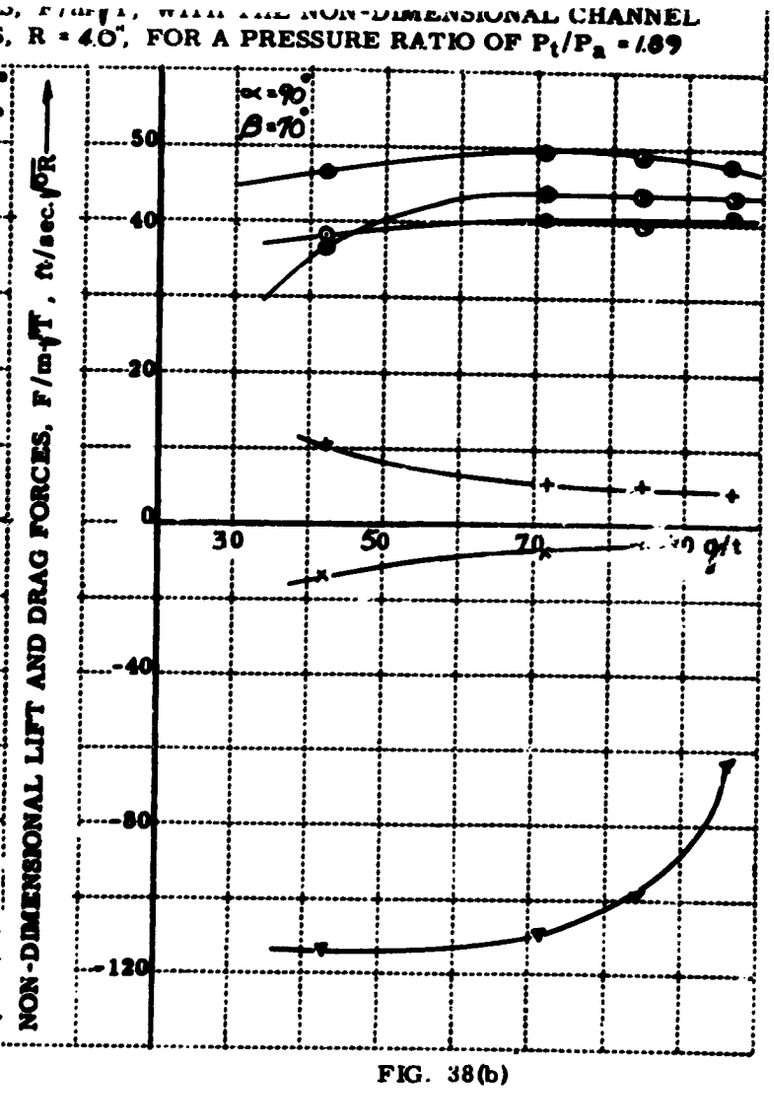

FIG. 38(b)

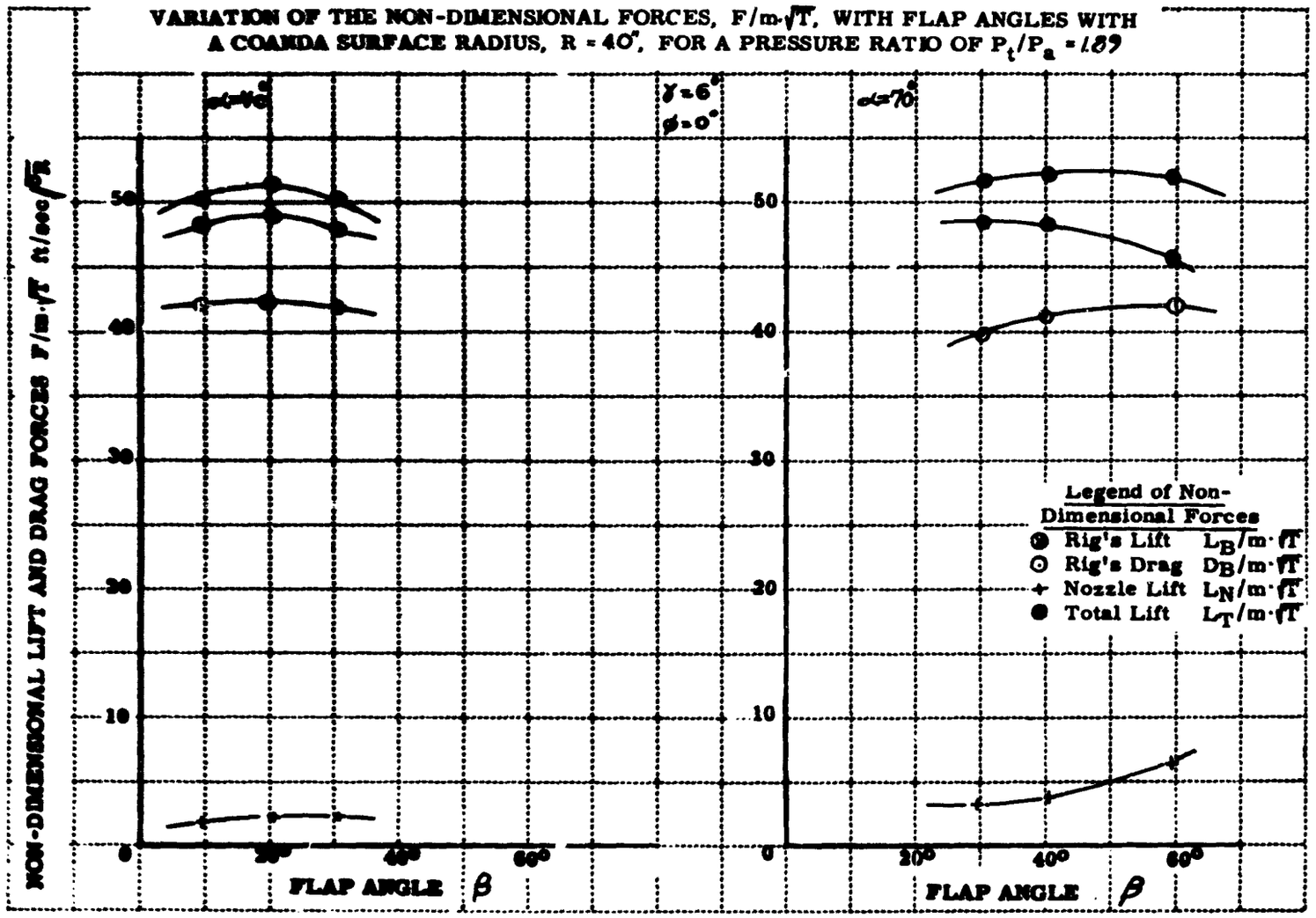

FIG. 39(a)

FIG. 39(b)

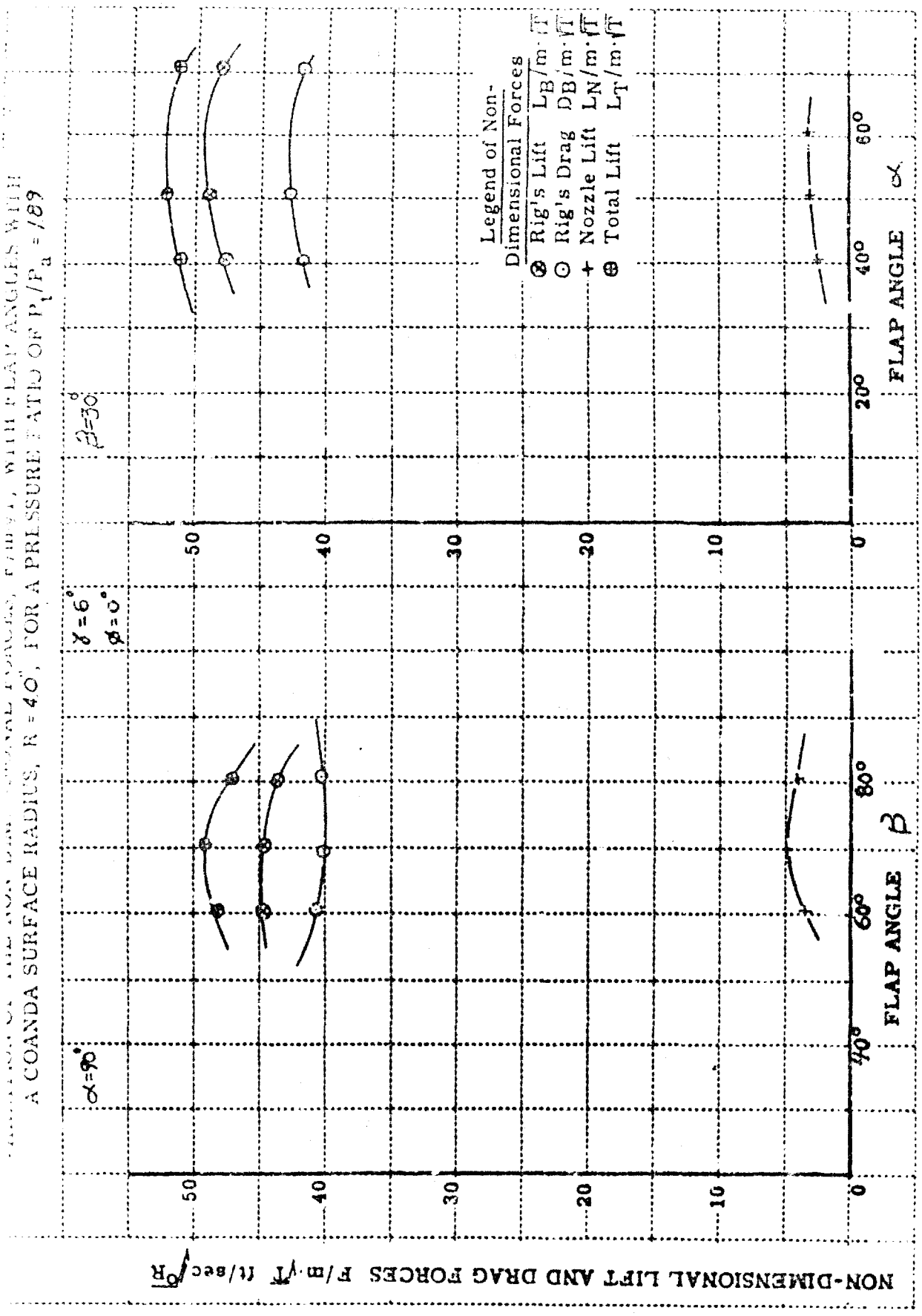

FIG. 40(a)

FIG. 40(b)

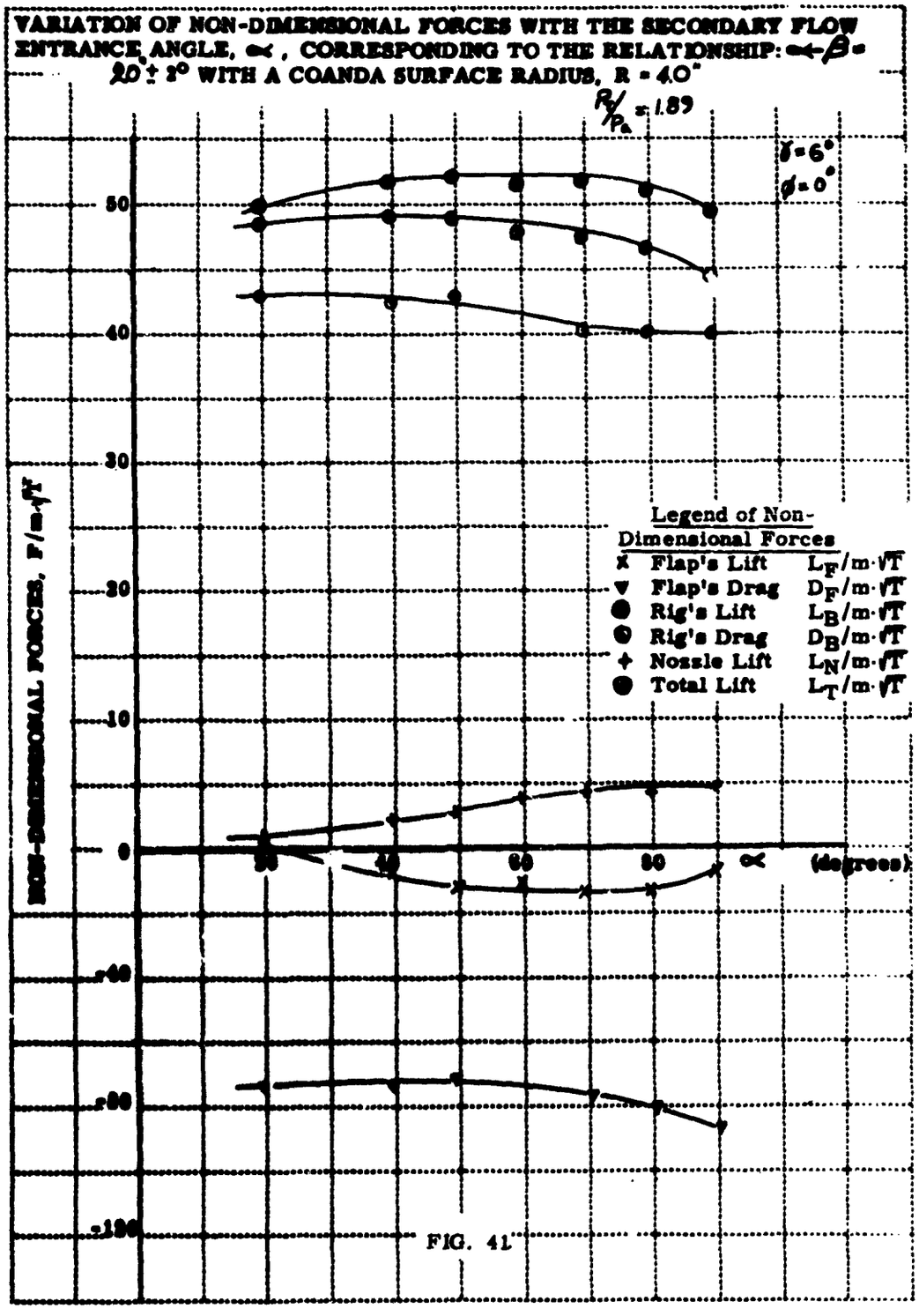
VARIATION OF NON-DIMENSIONAL FORCES WITH THE SECONDARY FLOW ENTRANCE ANGLE, ∝, CORRESPONDING TO THE RELATIONSHIP: ∝+β = 20° ± 3° WITH A COANDA SURFACE RADIUS, R = 4.0"
P_s/P_a = 1.89
γ = 6°
φ = 0°
Legend of Non-Dimensional Forces
Flap's Lift $L_F/m\cdot\sqrt{T}$
Flap's Drag $D_F/m\cdot\sqrt{T}$
Rig's Lift $L_B/m\cdot\sqrt{T}$
Rig's Drag $D_B/m\cdot\sqrt{T}$
Nozzle Lift $L_N/m\cdot\sqrt{T}$
Total Lift $L_T/m\cdot\sqrt{T}$
NON-DIMENSIONAL FORCES, F/m·√T
50
40
30
20
10
0
-40
-80
-120
60
80
∝ (degrees)

FIG. 41

VARIATION OF THE NON-DIMENSIONAL FORCES, $F/m\cdot\sqrt{T}$, WITH THE NON-DIMENSIONAL CHANNEL WIDTH, d/t, WITH A COANDA SURFACE RADIUS, R = 4.0", FOR A PRESSURE RATIO OF P_t/P_a = 200

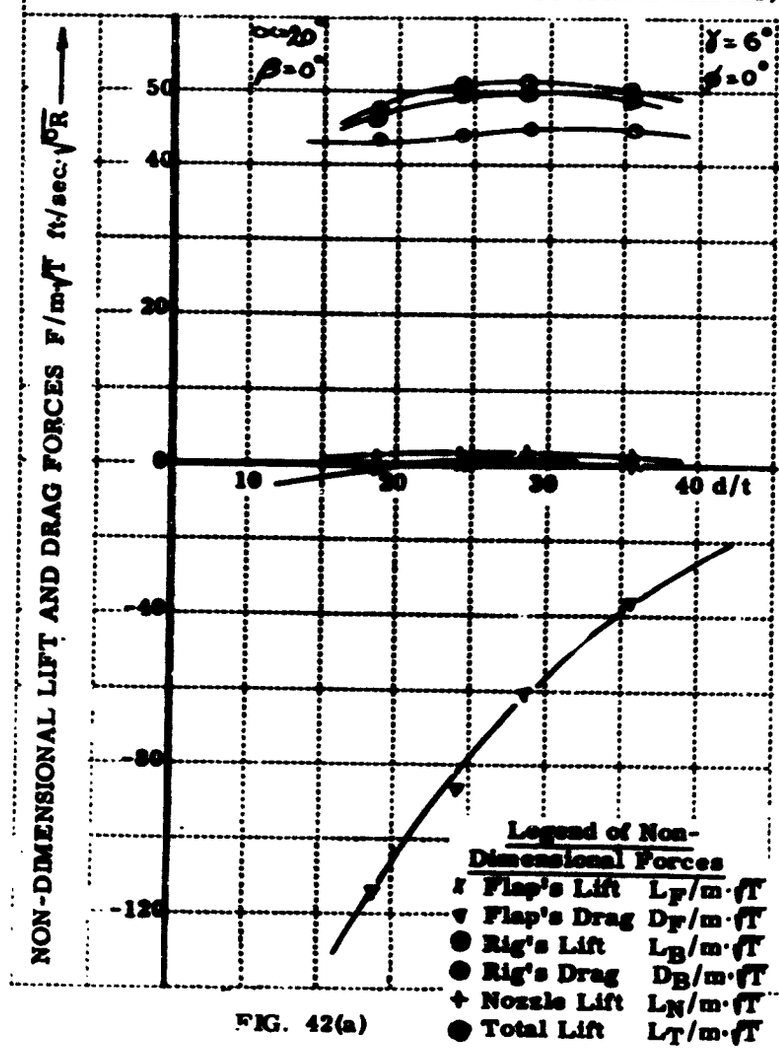

FIG. 42(a)

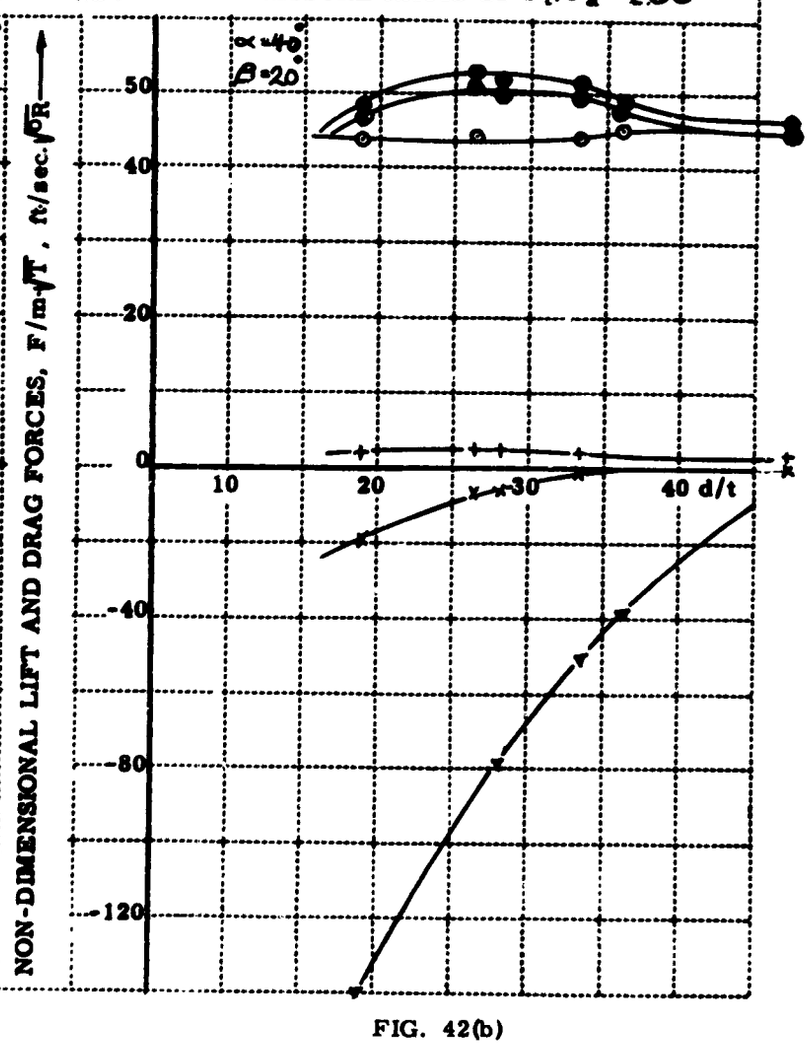

FIG. 42(b)

VARIATION OF THE NON-DIMENSIONAL FORCES, $F/m\cdot\sqrt{T}$, WITH THE NON-DIMENSIONAL CHANNEL WIDTH, d/t, WITH A COANDA SURFACE RADIUS, R = 4.0", FOR A PRESSURE RATIO OF P_t/P_a = 2.00

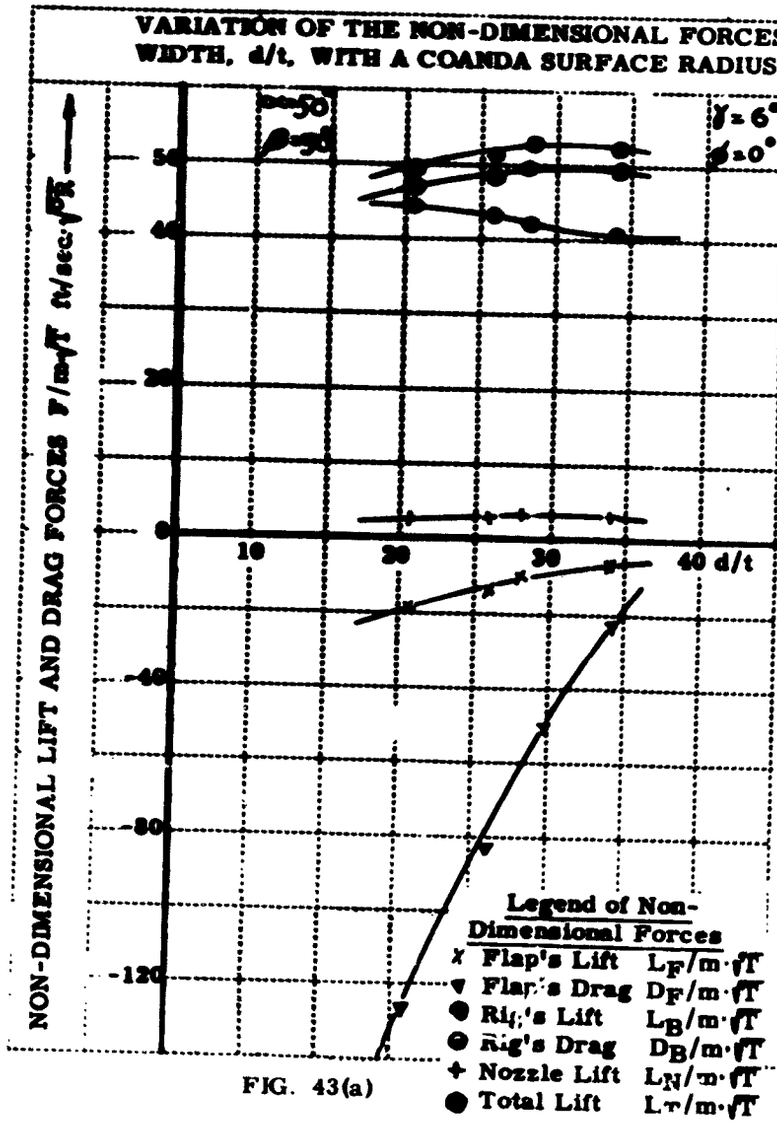

FIG. 43(a)

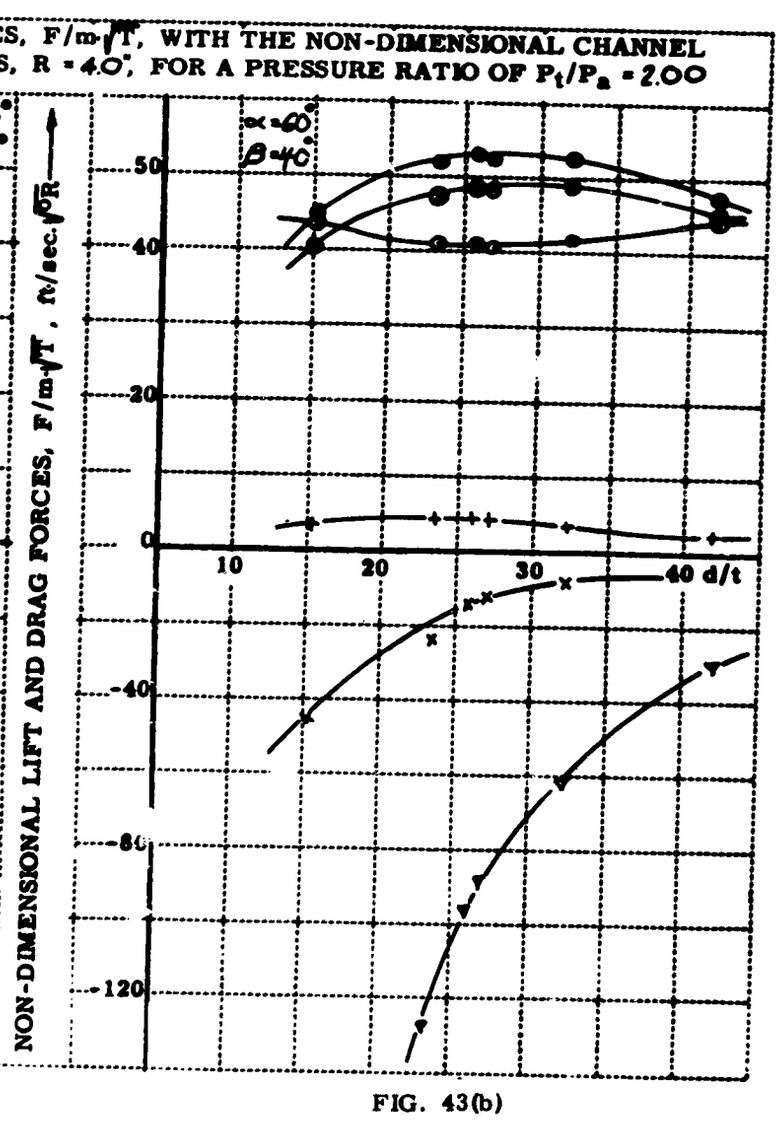

FIG. 43(b)

VARIATION OF THE NON-DIMENSIONAL FORCES, F/m·√T, WITH THE NON-DIMENSIONAL CHANNEL WIDTH, d/t, WITH A COANDA SURFACE RADIUS, R = 4.0", FOR A PRESSURE RATIO OF P_t/P_a = 2.00

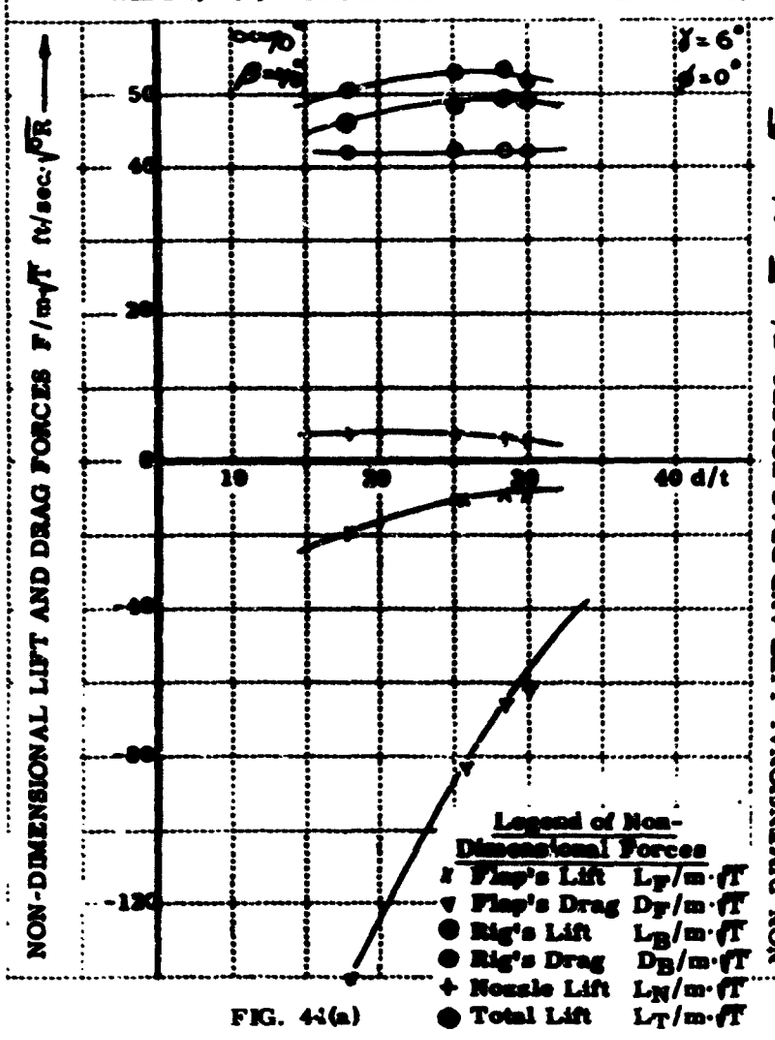

FIG. 44(a)

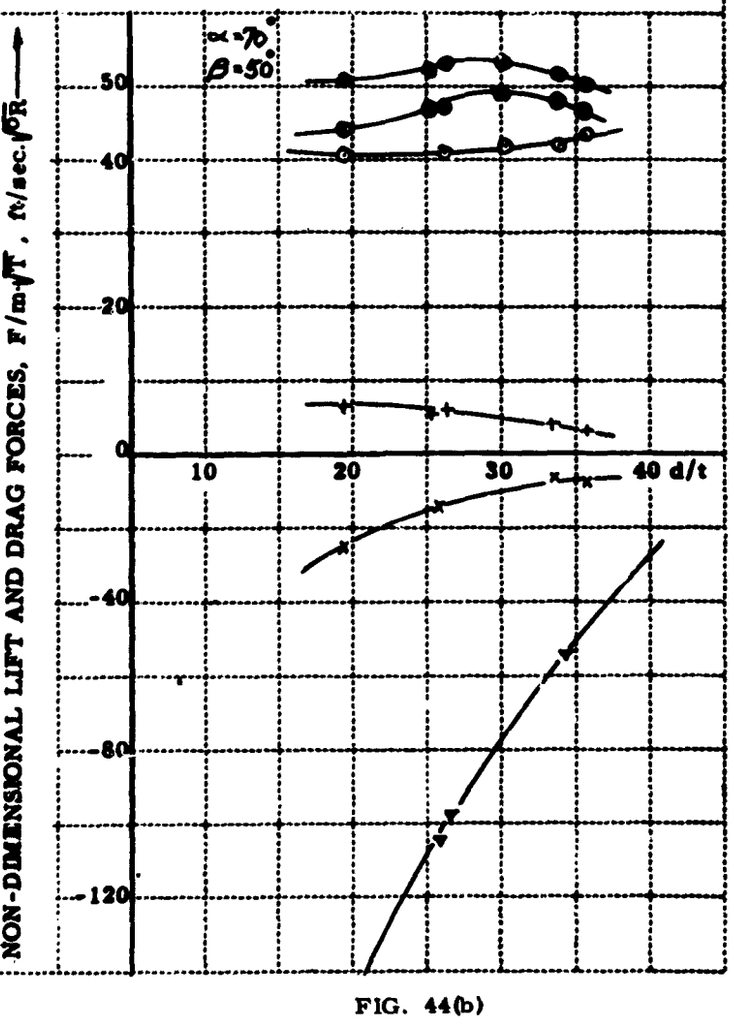

FIG. 44(b)

VARIATION OF THE NON-DIMENSIONAL FORCES, $F/m\sqrt{T}$, WITH THE NON-DIMENSIONAL CHANNEL WIDTH, d/t, WITH A COANDA SURFACE RADIUS, R = 4.0", FOR A PRESSURE RATIO OF P_t/P_a = 2.00

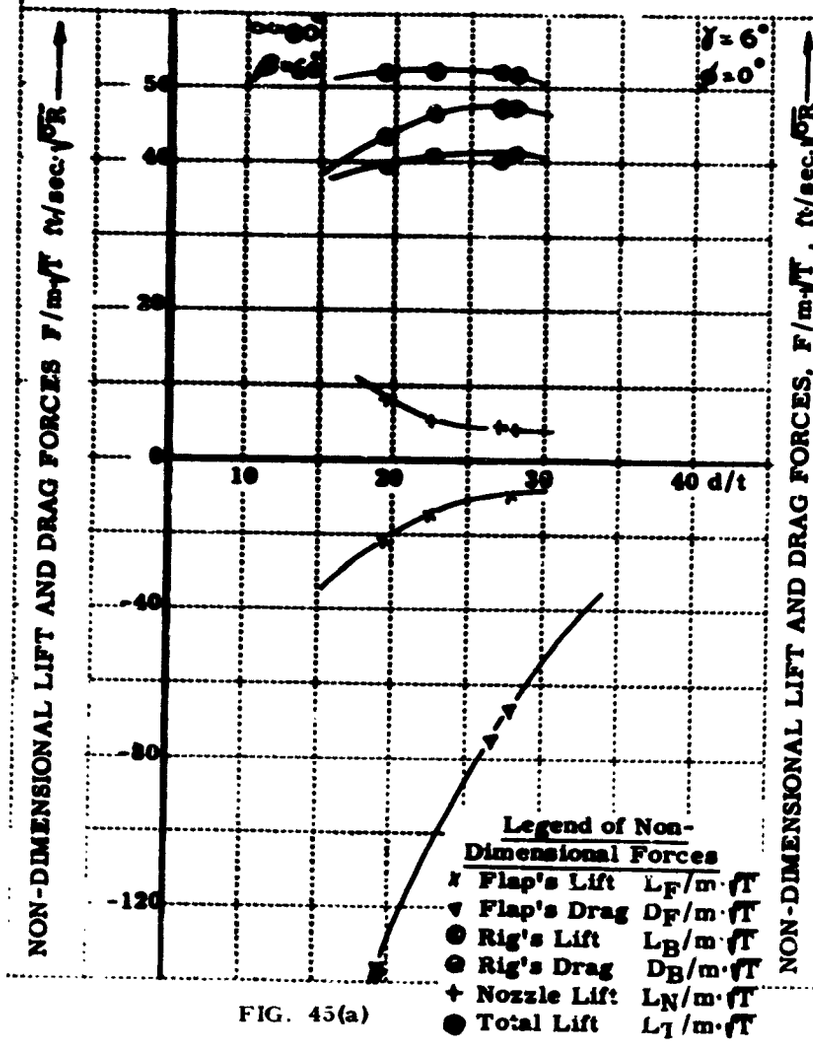

FIG. 45(a)

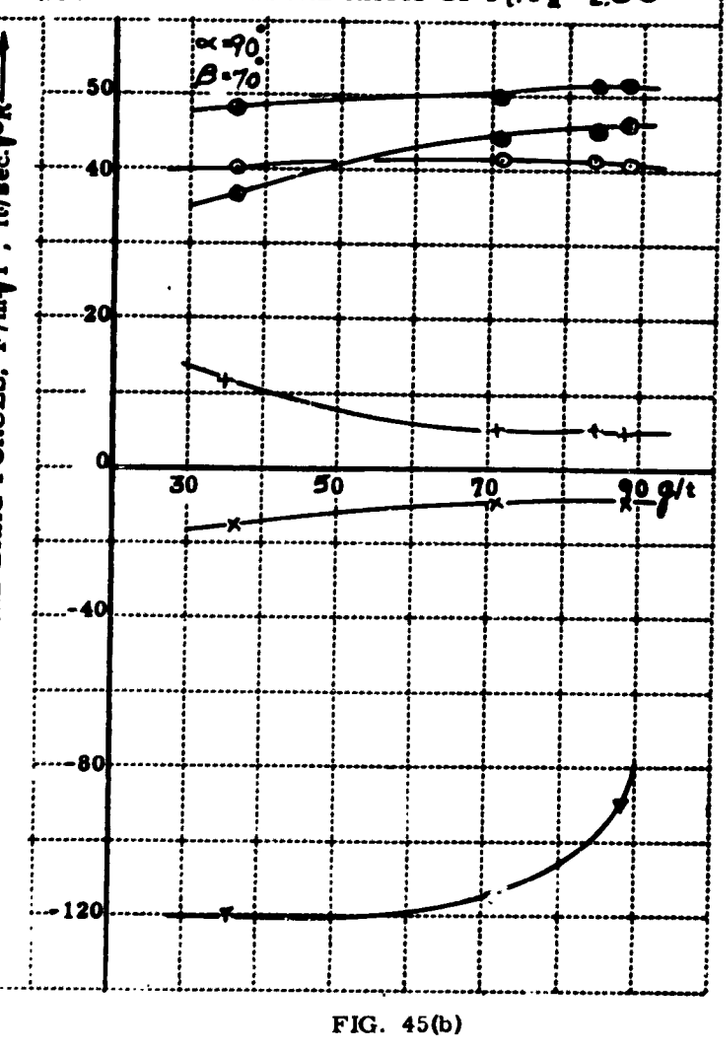

FIG. 45(b)

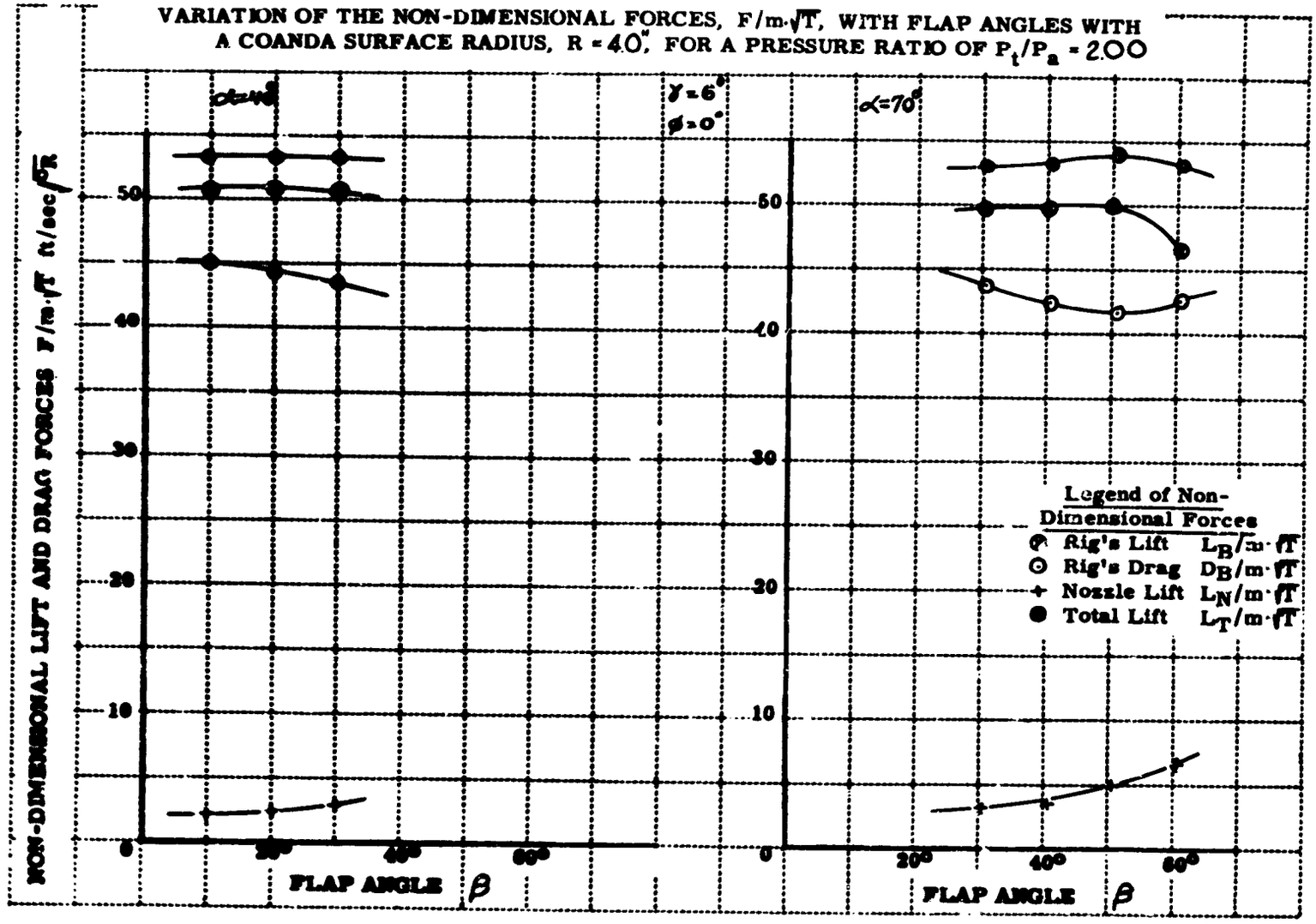

FIG. 46(a)

FIG. 46(b)

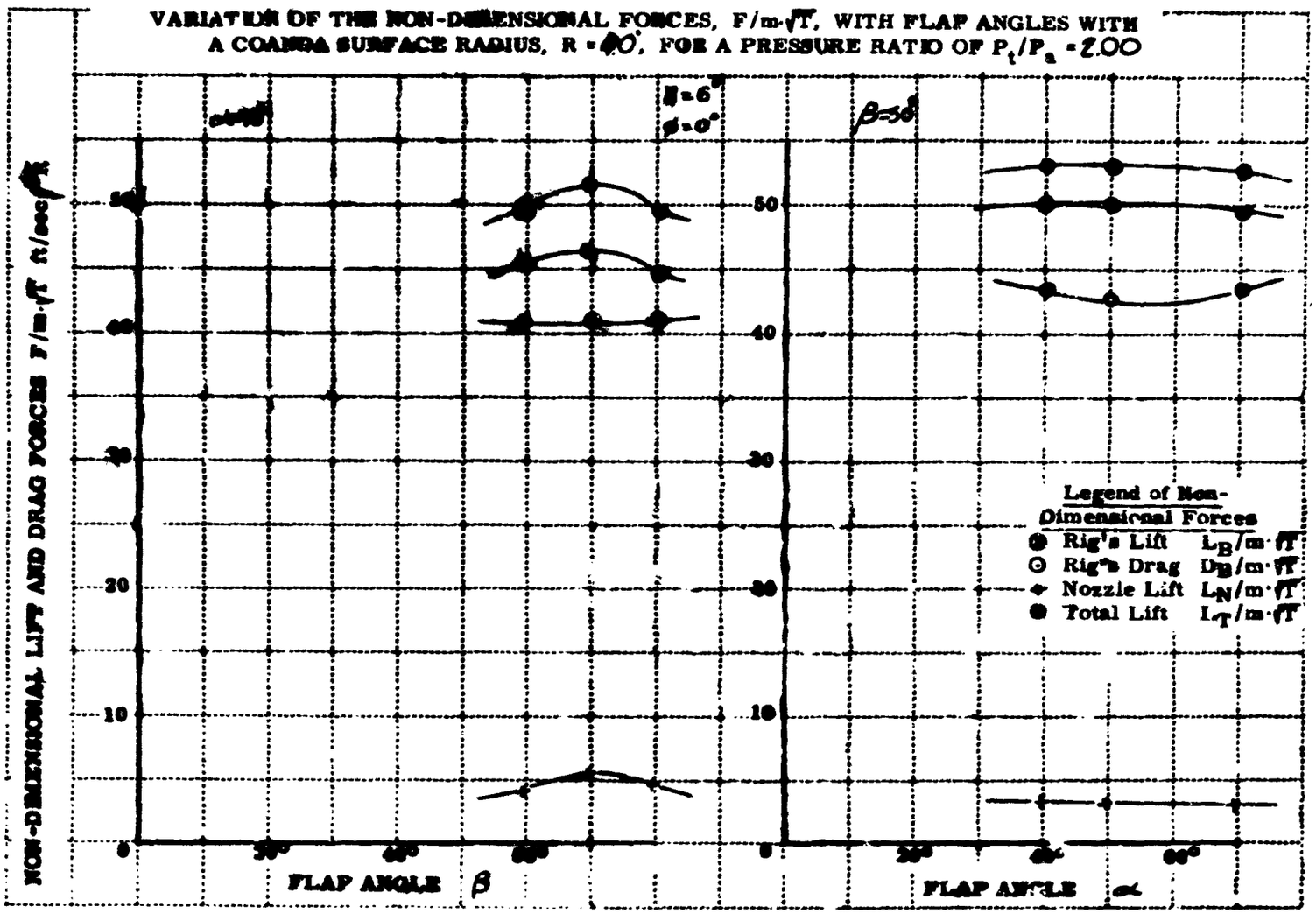
VARIATION OF THE NON-DIMENSIONAL FORCES, F/m·√T, WITH FLAP ANGLES WITH A COANDA SURFACE RADIUS, R = 40, FOR A PRESSURE RATIO OF P_t/P_a = 2.00
NON-DIMENSIONAL LIFT AND DRAG FORCES F/m·√T ft/sec²
β=6°
α=0°
β=36°
50
40
30
20
10
0
FLAP ANGLE β
FLAP ANGLE α
Legend of Non-Dimensional Forces
Rig's Lift L_B/m·√T
Rig's Drag D_B/m·√T
Nozzle Lift L_N/m·√T
Total Lift L_T/m·√T

FIG. 47(a)

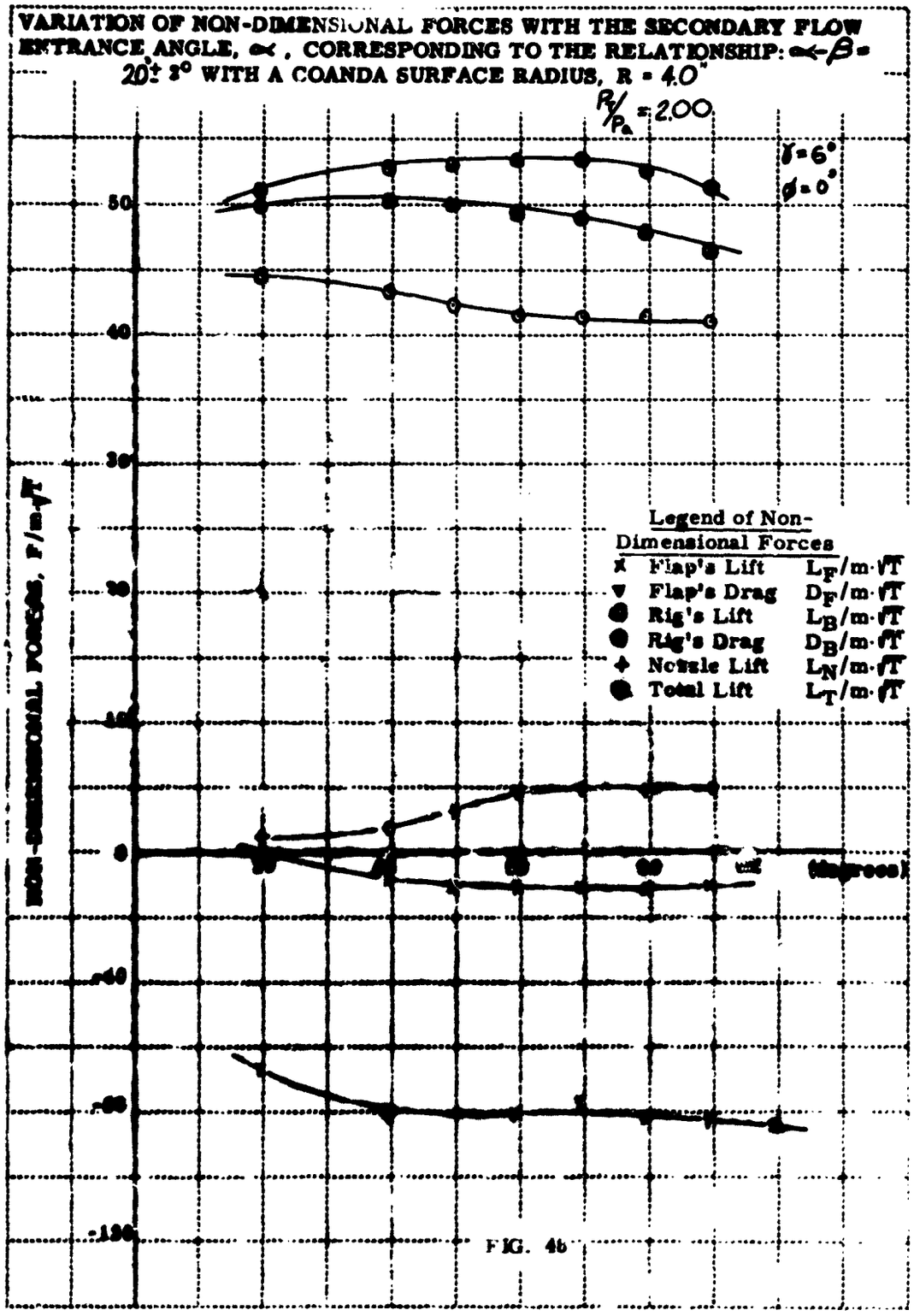
VARIATION OF NON-DIMENSIONAL FORCES WITH THE SECONDARY FLOW ENTRANCE ANGLE, ∝ , CORRESPONDING TO THE RELATIONSHIP: ∝-β = 20° ± 3° WITH A COANDA SURFACE RADIUS, R = 4.0"
P/Pa = 2.00
γ = 6°
ϕ = 0°
50
40
30
20
10
0
-10
-20
-30
-40
NON-DIMENSIONAL FORCES, F/m√T
Legend of Non-Dimensional Forces
Flap's Lift LF/m·√T
Flap's Drag DF/m·√T
Rig's Lift LB/m·√T
Rig's Drag DB/m·√T
Nozzle Lift LN/m·√T
Total Lift LT/m·√T

FIG. 4b

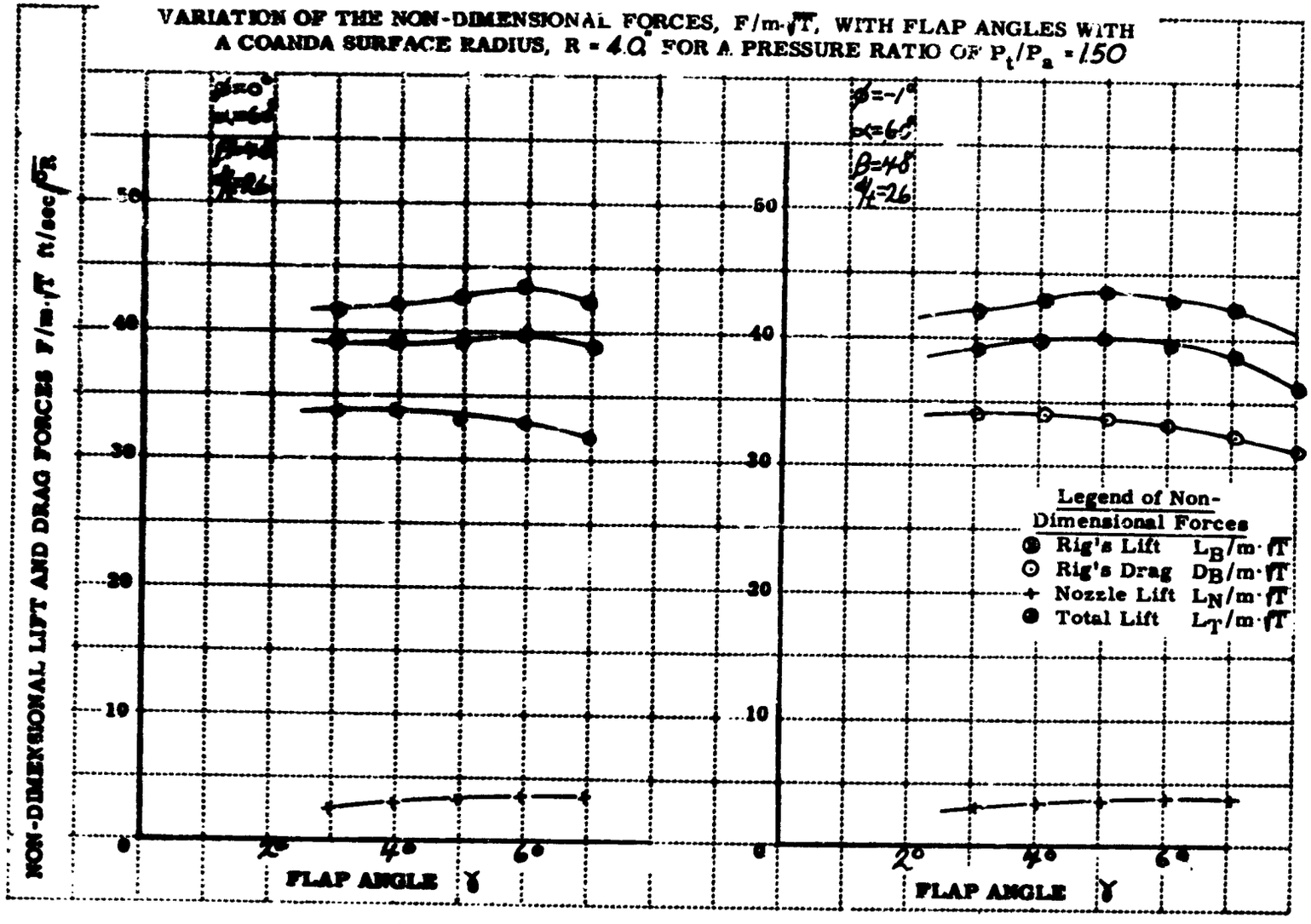

FIG. 49(a)

FIG. 49(b)

VARIATION OF THE NON-DIMENSIONAL FORCES, $F/m\cdot\sqrt{T}$, WITH FLAP ANGLES WITH A COANDA SURFACE RADIUS, R = 4.0", FOR A PRESSURE RATIO OF P_t/P_a = 1.50

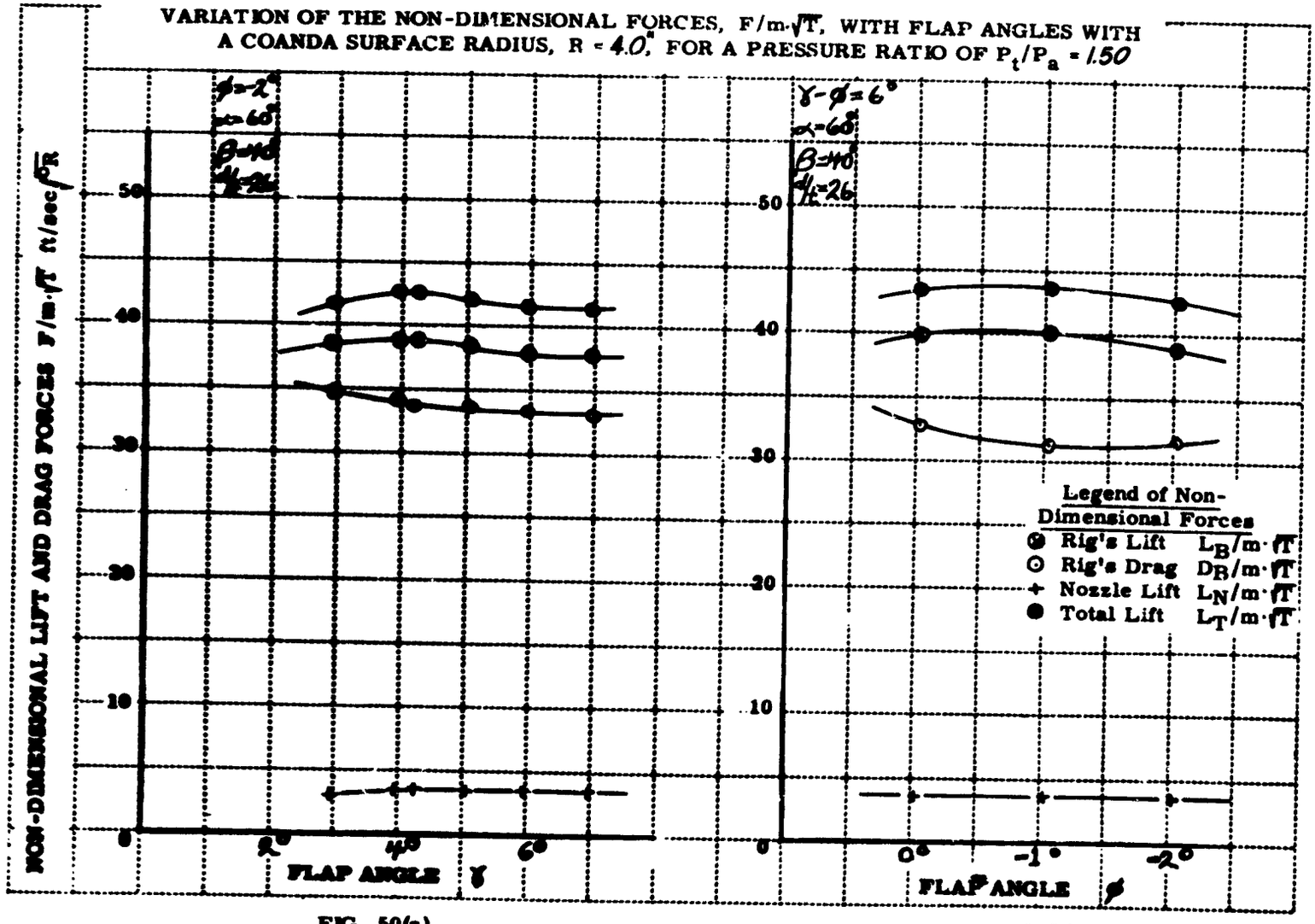

FIG. 50(a)

FIG. 50(b)

SECONDARY FLOW VELOCITY AND PRESSURE PROFILES ACROSS THE ENTRANCE, A_2, WITH $\alpha = 60^o$, $\beta = 40^o$, d/t = .26 AND R = 4.9" FOR A PRESSURE RATIO OF 1.50

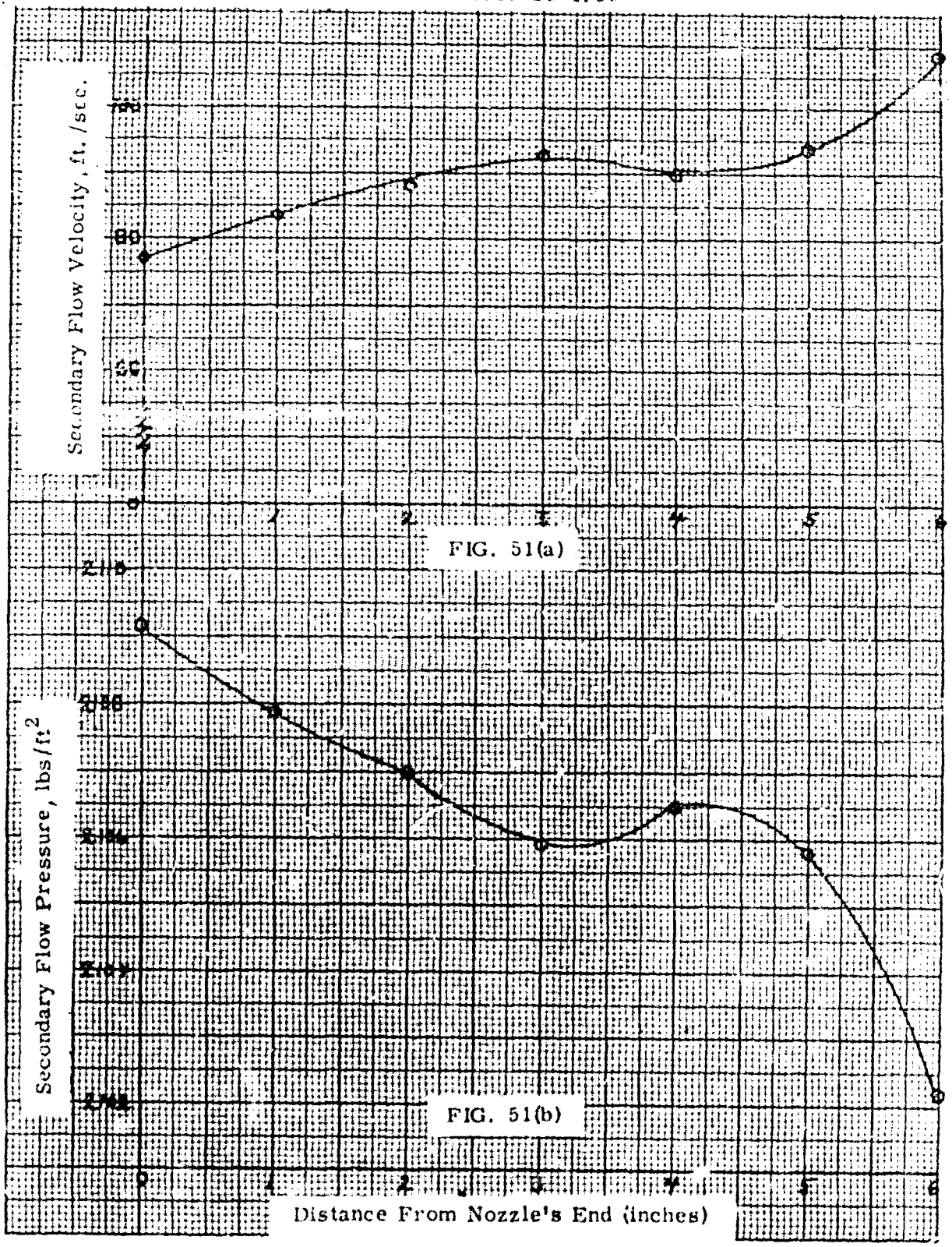

FIG. 51(a)

FIG. 51(b)

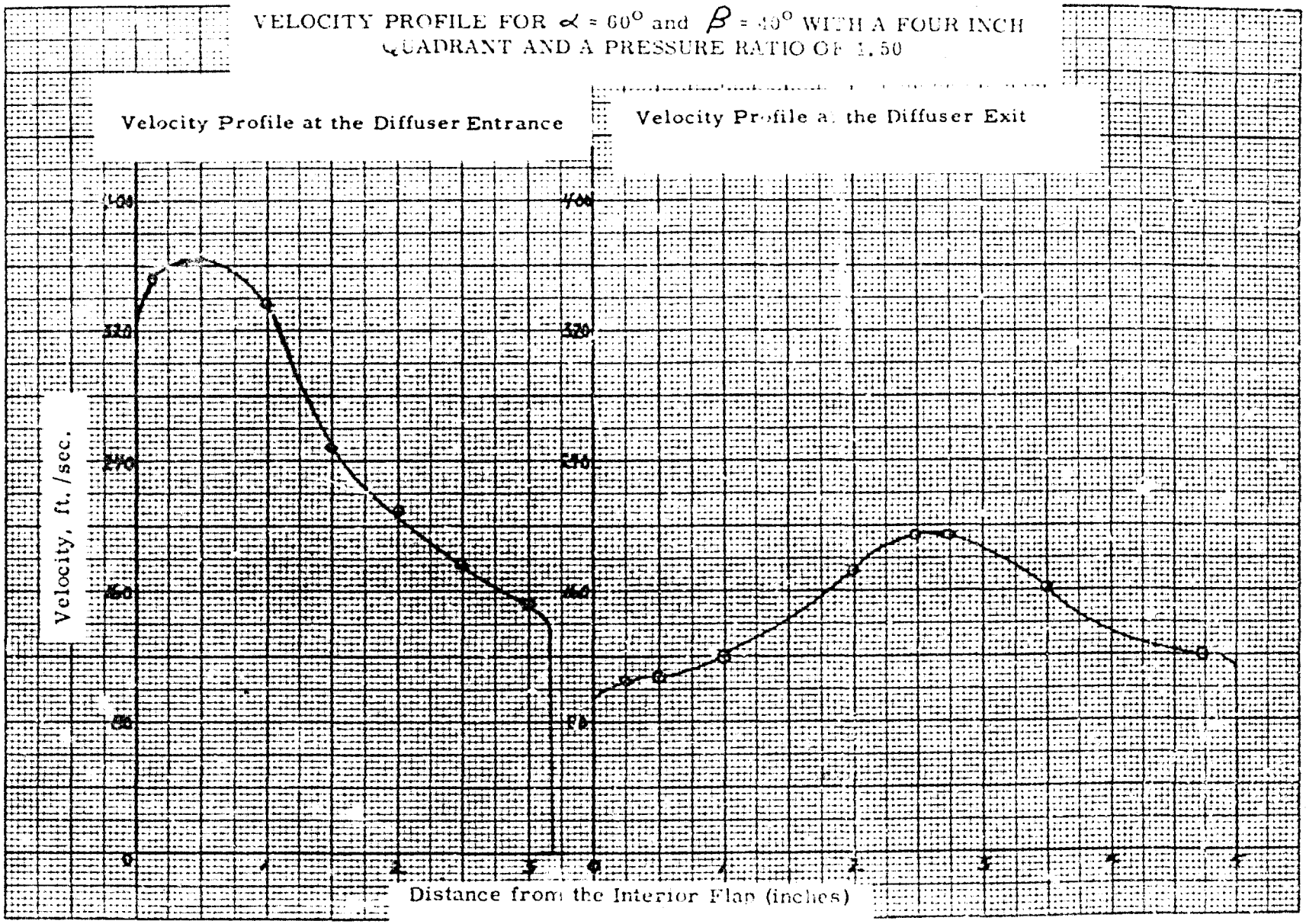

FIG. 52(a)

FIG. 52(b)

DISTRIBUTION

U. S. Army Materiel Command	3
U. S. Army Mobility Command	2
U. S. Army Aviation Materiel Command	5
Chief of R&D, D/A	1
U. S. Army Transportation Research Command	19
U. S. Army Research and Development Group (Europe)	1
U. S. Army Engineer Research and Development Laboratories	2
Army Research Office-Durham	2
U. S. Army Aviation School	1
U. S. Army Aviation Test Activity	1
Air Force Systems Command, Wright-Patterson AFB	2
Air Force Flight Test Center, Edwards AFB	1
Air Proving Ground Center, Eglin AFB	1
Air University Library, Maxwell AFB	1
Office of Naval Research	1
Bureau of Naval Weapons	2
U. S. Naval Postgraduate School	1
Naval Air Test Center	1
David Taylor Model Basin	1
Marine Corps Liaison Officer, U. S. Army Transportation School	1
NASA-LRC, Langley Station	1
Lewis Research Center, NASA	1
NASA Representative, Scientific and Technical Information Facility	2
National Aviation Facilities Experimental Center	1
Canadian Liaison Officer, U. S. Army Transportation School	1
Defense Documentation Center	20

University of Toronto, Institute of Aerophysics, AN EXPERIMENTAL INVESTIGATION INTO THE SHAPE OF THRUST AUGMENTING SURFACES IN CONJUNCTION WITH COANDA-DEFLECTED JET SHEETS (PART I) by C. D. Hope-Gill, TRECOM Tech. Rept. 64-23, December 1964, 90 pp. incl. illus. tables. (Grant DA TC-44-177-G1), Task 1D121401A14224.

UNCLASSIFIED Report

It is known that by means of additional surfaces, the thrust of a jet or jet sheet can be enhanced (thrust

(over)

University of Toronto, Institute of Aerophysics, AN EXPERIMENTAL INVESTIGATION INTO THE SHAPE OF THRUST AUGMENTING SURFACES IN CONJUNCTION WITH COANDA-DEFLECTED JET SHEETS (PART I) by C. D. Hope-Gill, TRECOM Tech. Rept. 64-23, December 1964, 90 pp. incl. illus. tables. (Grant DA TC-44-177-G1), Task 1D121401A14224.

UNCLASSIFIED Report

It is known that by means of additional surfaces, the thrust of a jet or jet sheet can be enhanced (thrust

(over)

University of Toronto, Institute of Aerophysics, AN EXPERIMENTAL INVESTIGATION INTO THE SHAPE OF THRUST AUGMENTING SURFACES IN CONJUNCTION WITH COANDA-DEFLECTED JET SHEETS (PART I) by C. D. Hope-Gill, TRECOM Tech. Rept. 64-23, December 1964, 90 pp. incl. illus. tables. (Grant DA TC-44-177-G1), Task 1D121401A14224.

UNCLASSIFIED Report

It is known that by means of additional surfaces, the thrust of a jet or jet sheet can be enhanced (thrust

(over)

University of Toronto, Institute of Aerophysics, AN EXPERIMENTAL INVESTIGATION INTO THE SHAPE OF THRUST AUGMENTING SURFACES IN CONJUNCTION WITH COANDA-DEFLECTED JET SHEETS (PART I) by C. D. Hope-Gill, TRECOM Tech. Rept. 64-23, December 1964, 90 pp. incl. illus. tables. (Grant DA TC-44-177-G1), Task 1D121401A14224.

UNCLASSIFIED Report

It is known that by means of additional surfaces, the thrust of a jet or jet sheet can be enhanced (thrust

(over)

augmentation). This especially applies to Coanda-deflected jet sheets because of the inherent stronger entrainment into curved flow surfaces. The flow from a two-dimensional subsonic nozzle was deflected by quadrants. A composite thrust-augmenting surface was added, and the effect of its shape on thrust augmentation was studied at various nozzle pressure ratios and radii of the quadrants. This investigation yielded a maximum thrust augmentation of 1.21 for several optimum configurations, which was governed primarily by the relative magnitude and direction of the momentum of the secondary (entrained) flow in relation to the primary (nozzle) flow momentum. Thrust augmentation decreased with increasing nozzle pressure ratio but was independent of quadrant radius. Some of the observed results were predicted theoretically. Suggestions for possibly producing higher thrust augmentation are offered.

augmentation). This especially applies to Coanda-deflected jet sheets because of the inherent stronger entrainment into curved flow surfaces. The flow from a two-dimensional subsonic nozzle was deflected by quadrants. A composite thrust-augmenting surface was added, and the effect of its shape on thrust augmentation was studied at various nozzle pressure ratios and radii of the quadrants. This investigation yielded a maximum thrust augmentation of 1.21 for several optimum configurations, which was governed primarily by the relative magnitude and direction of the momentum of the secondary (entrained) flow in relation to the primary (nozzle) flow momentum. Thrust augmentation decreased with increasing nozzle pressure ratio but was independent of quadrant radius. Some of the observed results were predicted theoretically. Suggestions for possibly producing higher thrust augmentation are offered.

augmentation). This especially applies to Coanda-deflected jet sheets because of the inherent stronger entrainment into curved flow surfaces. The flow from a two-dimensional subsonic nozzle was deflected by quadrants. A composite thrust-augmenting surface was added, and the effect of its shape on thrust augmentation was studied at various nozzle pressure ratios and radii of the quadrants. This investigation yielded a maximum thrust augmentation of 1.21 for several optimum configurations, which was governed primarily by the relative magnitude and direction of the momentum of the secondary (entrained) flow in relation to the primary (nozzle) flow momentum. Thrust augmentation decreased with increasing nozzle pressure ratio but was independent of quadrant radius. Some of the observed results were predicted theoretically. Suggestions for possibly producing higher thrust augmentation are offered.

augmentation). This especially applies to Coanda-deflected jet sheets because of the inherent stronger entrainment into curved flow surfaces. The flow from a two-dimensional subsonic nozzle was deflected by quadrants. A composite thrust-augmenting surface was added, and the effect of its shape on thrust augmentation was studied at various nozzle pressure ratios and radii of the quadrants. This investigation yielded a maximum thrust augmentation of 1.21 for several optimum configurations, which was governed primarily by the relative magnitude and direction of the momentum of the secondary (entrained) flow in relation to the primary (nozzle) flow momentum. Thrust augmentation decreased with increasing nozzle pressure ratio but was independent of quadrant radius. Some of the observed results were predicted theoretically. Suggestions for possibly producing higher thrust augmentation are offered.